Alexandre Lavrov
Malin Torsæter

Physics and Mechanics of Primary Well Cementing

SpringerBriefs in Petroleum Geoscience & Engineering

Series editors

Dorrik Stow, Heriot-Watt University, Edinburgh, UK
Mark Bentley, AGR TRACS Training Ltd, Aberdeen, UK
Jebraeel Gholinezhad, University of Portsmouth, Portsmouth, UK
Lateef Akanji, University of Aberdeen, Aberdeen, UK
Khalik Mohamad Sabil, Heriot-Watt University, Putrajaya, Malaysia
Susan Agar, ARAMCO, Houston, USA

The SpringerBriefs series in Petroleum Geoscience & Engineering promotes and expedites the dissemination of substantive new research results, state-of-the-art subject reviews and tutorial overviews in the field of petroleum exploration, petroleum engineering and production technology. The subject focus is on upstream exploration and production, subsurface geoscience and engineering. These concise summaries (50–125 pages) will include cutting-edge research, analytical methods, advanced modelling techniques and practical applications. Coverage will extend to all theoretical and applied aspects of the field, including traditional drilling, shale-gas fracking, deepwater sedimentology, seismic exploration, pore-flow modelling and petroleum economics. Topics include but are not limited to:

- Petroleum Geology & Geophysics
- Exploration: Conventional and Unconventional
- Seismic Interpretation
- Formation Evaluation (well logging)
- Drilling and Completion
- Hydraulic Fracturing
- Geomechanics
- Reservoir Simulation and Modelling
- Flow in Porous Media: from nano- to field-scale
- Reservoir Engineering
- Production Engineering
- Well Engineering; Design, Decommissioning and Abandonment
- Petroleum Systems; Instrumentation and Control
- Flow Assurance, Mineral Scale & Hydrates
- Reservoir and Well Intervention
- Reservoir Stimulation
- Oilfield Chemistry
- Risk and Uncertainty
- Petroleum Economics and Energy Policy

Contributions to the series can be made by submitting a proposal to the responsible Springer contact, Charlotte Cross at charlotte.cross@springer.com or the Academic Series Editor, Prof Dorrik Stow at dorrik.stow@pet.hw.ac.uk.

More information about this series at http://www.springer.com/series/15391

Alexandre Lavrov · Malin Torsæter

Physics and Mechanics of Primary Well Cementing

Springer

Alexandre Lavrov
SINTEF Petroleum Research
Trondheim
Norway

Malin Torsæter
SINTEF Petroleum Research
Trondheim
Norway

Preface

Primary cementing is one of the most crucial steps in well construction. Poor quality of annular cement is likely to affect the well integrity during the entire subsequent life of the well. Ensuring high quality of well cementing jobs requires a good grasp of physics and mechanics of primary cementing as well as of the subsequent behavior of annular cement when the well is subject to mechanical and thermal loads during its lifetime. Such loads may be induced, e.g., by changes in the casing pressure, by evolution of in situ stresses due to hydrocarbon production, or by injection of cold or hot fluids into the well (water, steam, CO_2, etc.).

Primary cementing and subsequent mechanical or thermal loading involve multiscale and multiphysics processes. For instance, formation temperatures affect the rheological properties of the fluids injected during primary cementing. In situ stresses affect the possible formation fracturing and lost circulation during cement pumping. Cement properties affect the stresses in set cement, which, later on, will affect cement failure during, e.g., casing pressurization.

In this concise monograph, we will make an effort to write the story of well cement from the perspective of physics and mechanics of the basic processes at play. We will follow cement from the time it is pumped down the hole, to the time when it breaks (or does not) under mechanical and thermal loads during well life.

Primary well cementing is a huge area, with technological advances made every year. It would be impossible to cover all the aspects of physics and mechanics of primary cementing in a short text. Therefore, we chose to focus on several selected topics which we believe are most important for both short-term and long-term well integrity.

Chapter 1 covers the basics of primary (annular) well cementing.

In Chap. 2, physical and mechanical properties and behavior of cement are discussed. Familiarity with these properties is essential for understanding the subsequent chapters, where these properties are used.

Chapter 3 covers the physics and mechanics of mud displacement and cement placement during a primary cementing job. The effects of fluid properties (rheology, density), flow regimes, pipe eccentricity and motion, and wellbore cross section

(washouts, breakouts, irregular walls) on the displacement efficiency are summarized.

In Chap. 4, different types of defects inevitably created during cement placement are discussed. These defects may facilitate the leakage and affect the service of the annular cement during the entire life of the well.

Chapter 5 takes a closer look at the cement failure caused by in situ stresses and casing pressure variation. The role of the defects discussed in Chap. 4 becomes clear when we consider debonding at casing–cement and cement–rock interfaces as well as stress concentrations and subsequent failure caused by gas-filled voids and mud channels left in the cement.

Chapter 6 concludes our story of cement by demonstrating the effects of casing heating or cooling on the integrity and failure of the adjacent cement sheath.

Primary cementing is an essential step in drilling and completion of wells in the oil and gas industry. It also plays a crucial role in the geothermal industry by ensuring safe exploitation of geothermal resources. Primary cementing of injection wells during underground storage of greenhouse gases (in particular CO_2) aims to prevent the leakage of the stored gases from the subsurface, also in the long-term perspective. The focus on integrity of geothermal and CO_2 injection wells will only increase in the future. The safety- and environment-related requirements to these wells may be even stricter than those used in the oil and gas industry. In Chap. 7, we discuss the current knowledge gaps and unresolved issues related to the physics and mechanics of primary well cementing.

Trondheim, Norway   Alexandre Lavrov
May 2016   Malin Torsæter

Contents

Chapter 1
Introduction

Abstract Cement is used extensively as a binding material in the petroleum industry today. During the process referred to as primary cementing, it is pumped into the well to fill the annular space between casings, or between casing and formation. After solidification, cement should ideally form a mechanically robust and leakage tight annular seal. This is intended to stabilize the casings and to prevent the influx of formation fluids to the well. Annular seals are not always perfect, and leakage along the well can occur. Different types of well integrity loss are discussed, together with an introduction on how to optimize cement properties by mixing in additives. These are used to adjust either the rheological (flow) properties of cement, its solidification, or its solid-mechanical properties. The chapter aims to provide the reader with the basic information about primary well cementing required to understand the subsequent chapters in the book.

Keywords Drilling · Primary cementing · Leakage · Well integrity · Additives · Remediation · Plugging

In this chapter we introduce basic principles of well cementing, including its objectives, potential leakage pathways, and different types of cementing operations. We provide a summary on well cement chemistry and how it differs from that of regular construction cements. We also define basic terminology that is required to understand the subsequent chapters in the book.

1.1 Why Drill Wells?

It is well known that exploring outer space is an engineering challenge, as it involves overcoming the Earth's gravitational pull and working in environments of low pressure, low temperature and extreme temperature variations. Less discussed, however, are all the challenges related to exploring the "inner space" of our planet. It involves digging kilometer-long holes, referred to as *wells*, into its potentially

boiling hot, highly pressurized interior. Even if they are commonly visualized as thin straws, these wells are actually complex structures of cement and steel that can be compared to inverse skyscrapers. They connect the surface with the subsurface, and thereby allow us to:

- gather scientific data and samples from deep inside the Earth;
- explore for or produce hydrocarbons (oil/gas);
- extract geothermal energy;
- inject gases into underground reservoirs for short- or long-term storage;
- deeply bury nuclear waste or other contaminants.

1.2   The Basics of Well Drilling and Cementing

Being the most critical component in all deep subsurface activities, the well's construction must be extremely robust. A brief description is here made of how wells are drilled and cemented. This is referred to as *primary cementing*, and such operations are the focus of this book.

Drilling is carried out by a rotating drill bit cutting into the Earth, and a *drilling mud* transporting the fragmented rock (drill cuttings) to surface. The drilling mud is pumped through nozzles in the bit, thereby cooling it, and is circulated to surface through the annular space between the drill pipe and the borehole wall. This is illustrated in Fig. 1.1. At the surface, the fragmented rock is separated from the mud before the mud is pumped back down the drill string. The drilling mud has the important task of controlling the pressure inside the well as it is being drilled. It forms a column inside the drilled borehole, and exerts a hydrostatic pressure that can be varied by changing the density of the mud. This is done by mixing in so-called weighting agents, which are heavy particles of e.g. barite. The pressure exerted by the mud column must be lower than the pressure at which the rock formation fractures and higher than the pressure exerted by the fluids in the rock. Drilling with too light a mud can cause formation fluid influx into the well ("kick" or blow-out), while drilling with too heavy a mud can fracture the reservoir and lead

Fig. 1.1 Schematic illustration of the drilling process where the drill bit is grinding the rock into small pieces (*cuttings*) that are transported to surface by mud circulated down the drill string, through nozzles in the drill bit and up along the annular space between the drill string and the formation
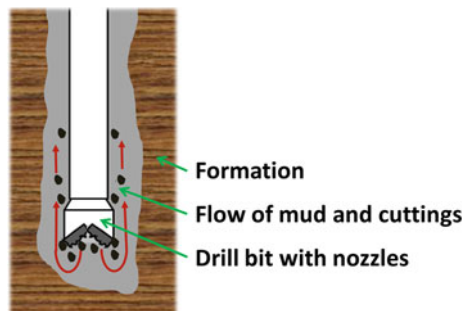
Fig. 1.2 A schematic illustration of **a** how cement is placed into the annular space between casing and rock, and **b** how a finished well looks after all the casings are cemented in place
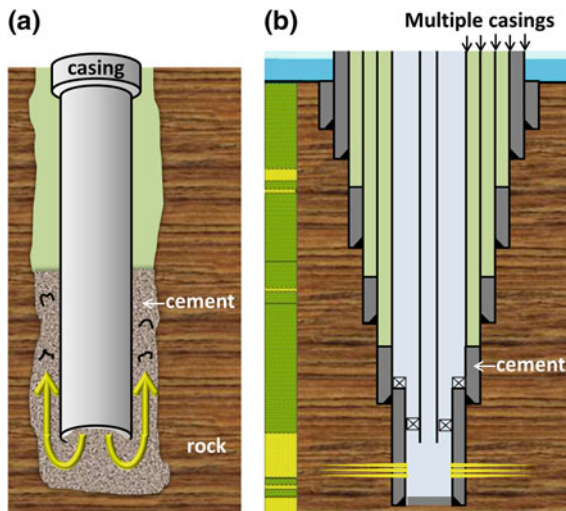
to mud loss into it. This will reduce the height of the hydrostatic mud column, which will again put the well at risk for inflow of formation fluids.

At some point during drilling, it is necessary to "save progress". This is when the pore pressure gradient at the bottom of the well exceeds the fracture gradient (the lost-circulation pressure gradient) higher up in the wellbore. If the mud density is increased, formations higher up in the well will fracture (thereby inducing losses), while if it is not increased, fluids in the deeper formations will be able to flow into the well. These are both situations posing safety- and environmental risks. At this point in the drilling process, a steel casing pipe is lowered into the well and cemented in place.

The cementing operation itself involves first conditioning the hole by circulating mud in it. This is done by pumping mud down the string and up along its sides back to surface. Thereafter, a sequence of preflush fluids is pumped into the well, which is used to clean the hole and separate mud from cement. Finally, the cement slurry is pumped in and placed around the lower part of the casing. It is then given time to harden, to form a robust and tight *annular seal*.

This annular cement sheath has the job of mechanically stabilizing the wellbore and preventing pressurized formation fluids outside the casing from entering the well or flowing between different subsurface zones. Subsequent drilling and casing/cementing operations are performed using casing pipes of progressively smaller diameter until the well obtains a telescopic structure, as illustrated in Fig. 1.2.

1.3 The Importance of Well Cement Integrity

The life cycle of a well stretches from the initial drilling and construction phase, as described above, through its operational phase, and ends with the final abandonment phase. The operational phase includes repairs done to the cement sheath over time, referred to as *remedial cementing*. This requires special techniques that have been outlined e.g. in Ref. [1], and will not be discussed in the following. The abandonment phase is the last phase of the well's life cycle, and involves placing cement plugs in the well to close it down. This is referred to as *plug cementing*, and techniques applied for this operation can also be found in Ref. [1].

The long time spans over which the cemented well needs to retain its integrity is a challenge today. The plugs in an abandoned well, together with annular cement sheaths placed in the well during well construction, need to act as barriers in an eternal perspective. They protect the environment against leakage along the well, either from overburden zones or if pressure builds up again in the reservoir over time. Cement integrity is thus a crucial component of *well integrity*.

Ensuring well integrity essentially means preventing flow of formation fluids along the well throughout its lifetime. This topic has been given increasing importance in recent years, following large accidents like the Macondo blow-out that damaged the Deepwater Horizon rig, killed eleven people and caused a large oil spill in the Gulf of Mexico. Such *acute leakage* incidents (of low probability) are well covered by media and thus receive much attention, but the smaller *chronic leakages* (of higher probability) are also breaches of well integrity. Examples of chronic leakages are various leaks caused by defective well tubulars or damaged cement sheaths in wells. A typical consequence of this type of well integrity loss is *sustained casing pressure*. This essentially means that pressure continues to build up in the annular space between casings, or between casing and formation, even if bled to zero at surface. This is an indication that zonal isolation is imperfect and that flow of formation fluids is occurring between geological strata.

Since well construction materials are prone to degradation with age and upon exposure to downhole fluids, pressures and temperature variations, the number of well integrity problems tends to increase as the wells age. A study of 15,500 wells in the Gulf of Mexico showed that as a well becomes 15 years old, it has a 50 % probability of being affected by sustained casing pressure [2]. The overall percentage of wells suffering from this problem was about 35 % in the Gulf of Mexico [1, 2], and similar numbers have been reported for the North Sea [3].

Leakage along wells is not necessarily caused by breached cement integrity, but this is a major "weak link" in today's well construction [4]. As Fig. 1.3 shows, loss of well integrity can be caused by damage to the downhole tubulars, loss of cement adhesion to casing/rock, flow paths through the cement itself (either as a result of enhanced porosity, cracks/voids/channels or fracturing) or damage to the rock formation during drilling. Most of the problems related to loss of cement integrity can be traced back to improper cement placement [1, 5], but adhesion and

Fig. 1.3 Schematic illustration of the various leakage paths that can be present in a well. Undisplaced mud channels and poor bonding to both casing and rock are seen on the *left-hand side* of the casing, while radial cracking, cement disking, and enhanced porosity are seen on the *right-hand side*
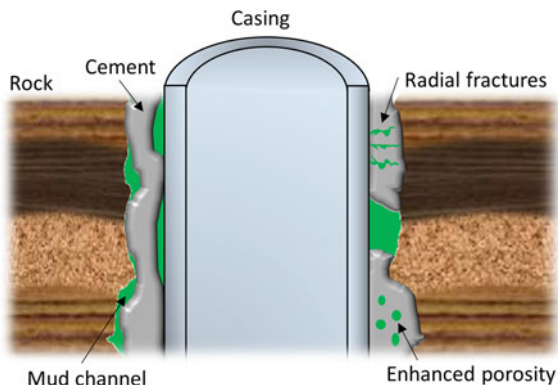
prevention of cement fracturing are also believed to be crucial for ensuring well integrity [6]. There are several types of cement mixtures and additives on the market today that aim to solve these issues, as will be discussed in the next Section.

1.4 Cement Chemistry

Oilwell cement is not the same as concrete used in the construction industry. Concrete is a mixture of cement and aggregate particles (sand or small pieces of rocks), while cement is a pure low-permeability binding material. Dry cement is produced by first pulverizing raw materials (mainly calcium oxide, silica, alumina and iron compounds). The powder is thereafter converted to a clinker by heat treatment in a rotary kiln (typically at 1450 °C), and the finished cement powder is produced by grinding the clinker with gypsum. The latter controls the solidification time and how quickly the cement builds up strength during hardening. The clinker consists of 50–70 % alite (Ca_3SiO_5), 15–30 % belite (Ca_2SiO_4), 5–10 % aluminate ($Ca_3Al_2O_6$) and 5–15 % ferrite (Ca_2AlFeO_5), plus small amounts of other phases [1].

The dry cement powder reacts quickly and strongly with water, and solidifies and develops compressive strength as a result of hydration. This is a process involving complex reactions between water and the cement oxides. A detailed review of the solid phases forming in Portland cement, together with a review of the hydration process can be found in Ref. [7]. When the clinker phases in Portland cement react with water, they release heat to the surroundings. Solidification is, in other words, an exothermic reaction. It can be made more rapid by increasing the alite content, grinding the clinker phases finer or ensuring better mixing of the raw materials. For well construction purposes, the American Petroleum Institute (API) has developed guidelines for how to mix and prepare the cement slurry before pumping it into the well.

Phases in cement are often expressed as sums of oxides, meaning that e.g. Ca_3SiO_5 can be written as $3CaO \cdot SiO_2$. This is further simplified to single letters, C for CaO and S for SiO_2, thus becoming C_3S. Other common abbreviations are H for H_2O and A for Al_2O_3.

A cement slurry is a mixture of cement and water in such proportion that solidification can occur. The *water-to-cement ratio* refers to proportions by mass, and they are typically in the range of 0.3–0.6 for well cement. The solidification starts with *setting*, which is a rapid stiffening without significant strength development, followed by the slower *hardening* process which builds compressive strength.

During hydration, the main cement phase, alite (C3S), reacts and forms two main phases, namely calcium hydroxide (CH) and a nearly amorphous calcium silicate hydrate, C–S–H. These are the main constituents of solidified cement.

Research has so far not managed to come up with one well cement formulation that alone could overcome all the problems associated with primary cementing. Cement slurries are thus optimized with regard to only a few challenges at a time. There are e.g. special cements with resistance towards high temperatures, cements for cold climates, CO_2-restistant cements, etc. To make these, other substances (also referred to as *additives*) are added to the slurry. While ameliorating some properties, these materials often aggravate others. This is exemplified by the so-called *retarders*, which are added in order to delay the setting of cement. They are typically salts, acids, or polymers. Unfortunately, they tend to reduce the annular cement sheath's sealing ability by chemically attacking the casing steel [1].

As several monographs have been produced focusing on the art of mixing the correct cement slurry for the right purpose [1, 7], this will not be the focus of this book. Instead, we will aim to provide the reader with the knowledge of physics and mechanics of primary well cementing necessary for performing cement simulations —both to study cement placement in wells and a cement sheath's resistance towards loads after placement.

1.5   Summary and Discussion

There is extensive use of well cement today. It is used during well construction for stabilizing casings and preventing flow of formation fluids, and it is pumped in order to repair faulty cement or fractured zones in the reservoir (remedial cementing). It is even used for the final close-down phase of the well when it is being plugged and abandoned (plug cementing). Since the latter phase has an eternal perspective, there are high requirements for cement integrity if it is going to last throughout the life of the well. This chapter has outlined the various ways well integrity can be lost, and how problems related to cement integrity are minimized by tailoring the cement slurry composition. Flow properties of cement can be altered to optimize placement as cement is pumped into the well, and additives can be added to the mixture to ensure a reliable solidification and good solid mechanical properties. The chemical

expertise required to tailor cement slurries is high, and several books have already outlined this topic. Instead of going into depth in the special cements and additives available, this book will take a more fundamental approach. The goal is to provide engineers and academics with a brief text on physics and mechanics underlying cement placement and long-term integrity of cement sheaths. It starts out with explaining the basic properties of cement in the next chapter.

References

1. Nelson E, Guillot D (2006) Well cementing, 2nd edn. Schlumberger, Sugar Land
2. Wojtanowicz AK, Nishikawa S, Rong X (2001) Diagnosis and remediation of sustained casing pressure in wells. Technical Report. Louisiana State University
3. Davies RJ, Almond S, Ward RS, Jackson RB, Adams C, Worrall F, Herringshaw LG, Gluyas JG, Whitehead MA (2014) Oil and gas wells and their integrity: Implications for shale and unconventional resource exploitation. Mar Pet Geol 56:239–254
4. Scherer GW, Kutchko B, Thaulow N, Duguid A, Mook B (2011) Characterization of cement from a well at teapot dome oil field: implications for geological sequestration. Int J Greenhouse Gas Control 5(1):115–124
5. Bellabarba M, Bulte-Loyer H, Froelich B, Le Roy-Delage S, van Kuijk R, Zeroug S, Guillot D, Moroni N, Pastor S, Zanchi A (2008) Ensuring zonal isolation beyond the life of the well. Oilfield Rev Spring 18–31
6. Carey JW, Wigand M, Chipera SJ, WoldeGabriel G, Pawar R, Lichtner PC, Wehner SC, Raines MA, Guthrie GD Jr (2007) Analysis and performance of oil well cement with 30 years of CO_2 exposure from the SACROC Unit, West Texas, USA. Int J Greenhouse Gas Control 1 (1):75–85
7. Taylor HFW (1997) Cement chemistry, 2nd edn. Thomas Telford, London

Chapter 2
Properties of Well Cement

Abstract Well cementing involves pumping a sequence of fluids into the well. Often these fluids, such as spacers and cement slurries, have non-Newtonian yield-stress rheology. After the cement slurry has been placed in the annulus, it hardens into a low-permeability annular seal. The complexity of these processes and the multitude of materials involved (drilling fluid, spacer, chemical wash, cement, casing, rocks) call for a sufficiently detailed material characterization in order to design and optimize cement jobs. A review of properties describing cements and other materials used in primary cementing is presented in this chapter. Rheological properties of washes, spacers, and cement slurries that control their flow down the well and up the annulus are discussed. Basics of non-Newtonian fluid rheology required to understand the subsequent chapters are laid out. Transition properties of cement slurry related to its solidification are reviewed. Mechanical, interfacial, hydraulic, and thermal properties of hardened cement that control e.g. response of cement to thermal stresses, vibrations, etc. are introduced, along with laboratory techniques used for their measurement (Brazilian test, uniaxial test, triaxial test, push-out test).

Keywords Cement · Properties · Rheology · Yield stress · Interface · Strength · Measurement

During a cementing job, cement undergoes a transformation from a liquid slurry being pumped down the wellbore to a solid material filling up the annular space between the casing and the borehole. While in the slurry state, the cement is characterized by rheological properties such as yield stress and plastic viscosity. These properties control the slurry flow and determine how cement displaces other fluids as it is placed behind the casing. The transition of cement from the liquid to the solid state is characterized by various properties e.g. volumetric change, rate of strength build-up or how easily formation fluids can enter the not-yet-solid cement. When hardened, cement is characterized by properties that determine how stable and permeable it is, how well it binds to the casing and the rock or how prone it is to fracturing. All of these properties need to be controlled in order to obtain a robust

low-permeability cement sheath in the well. Therefore, we start our journey into the world of well cementing by exploring some important cement properties.

2.1 Properties of the Cement Slurry

When cement is mixed on the surface or platform and is pumped down the well, it is in the liquid state. The flow of cement slurry and the fluid displacement in the well are largely affected by the rheological properties of the fluids and by their densities. From rheological viewpoint, spacers and cement slurries are non-Newtonian fluids. They have a *yield stress*, τ_Y (Pa), which means that a shear stress in excess of a certain threshold value must be applied in order to put the slurry into motion. This implies that in a conduit, such as a well annulus, a finite pressure gradient must be applied in order for flow to commence. When the shear stress in the slurry is above the yield stress, the slurry behaves as a viscous fluid. The simplest rheological model that describes such behavior is the Bingham model. Applied to a simple shear flow, the Bingham model stipulates that the shear stress is a linear function of the shear rate when the shear stress is above the yield stress (Fig. 2.1). The slope of the shear stress versus shear rate curve is called the *plastic viscosity* of the slurry, μ_{pl} (Pa s). The Bingham model is thus a two-parameter model. This is one parameter extra as compared to a *Newtonian* fluid described by only one rheological parameter, i.e. the dynamic viscosity. Applied to a simple shear flow, the Bingham model can be represented as follows:

$$\tau = \tau_Y + \mu_{pl}|\dot{\gamma}| \tag{2.1}$$

where τ is the shear stress (Pa); $\dot{\gamma}$ is the shear rate (s^{-1}). If the yield stress is zero, Eq. (2.1) becomes

$$\tau = \mu_{pl}|\dot{\gamma}| \tag{2.2}$$

which is characteristic of a Newtonian fluid such as water. Newtonian fluids start flowing as soon as a non-zero shear stress is applied to them.

Fig. 2.1 Shear stress versus shear rate (*solid line*) in a simple shear flow of a Bingham fluid
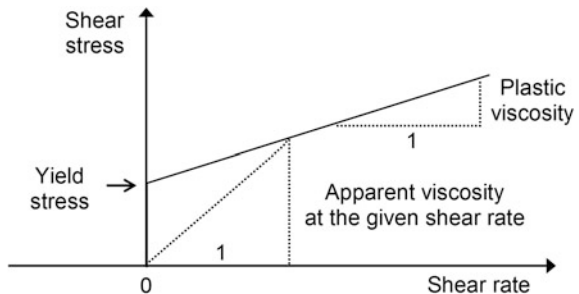
The rheological parameters of the Bingham model, i.e. τ_Y and μ_{pl}, can be measured in a standard rheometric test performed in a rotational viscometer or a rheometer.[1] Different designs of these devices are available. For instance, shear can be applied to a slurry sample placed in the gap between two coaxial cylinders: the static inner cylinder and the rotating outer one. Torque as a function of rotations per minute (rpm) is then used to derive the plastic viscosity and the yield stress of the slurry. Oilwell cement slurries and spacers typically have yield stress on the order of 1–100 Pa, while their plastic viscosity is on the order of 0.01–0.1 Pa s. It should be noted that both τ_Y and μ_{pl} depend on temperature and, to a lesser extent, on pressure. For this reason, rheological measurements should ideally be performed in the range of pressures and temperatures that the fluid will be exposed to as it flows down the well and up the annulus.

Even though the linear model given by Eq. (2.1) only approximately describes the rheological behavior of real yield-stress fluids such as cement, it does capture one essential property of the slurry, namely the existence of a yield stress. As we will see later, this property is crucial for analysis of cement flow in the annulus.

If a more accurate description of cement flow is needed, the assumption of linear dependence of the shear stress on the shear rate above the yield stress should be relaxed. More realistic modelling of yield-stress rheology can then be achieved with e.g. the Herschel-Bulkley model [2] given by

$$\tau = \tau_Y + C|\dot{\gamma}|^n \qquad (2.3)$$

where C is the consistency index; n is the flow behavior index. The consistency index determines the magnitude of the viscous forces at a given shear rate, while the non-dimensional flow behavior index determines whether the fluid becomes less or more viscous as the shear rate increases. If $n > 1$, the fluid thickens (becomes more viscous and difficult to flow) at higher shear rates. If $n < 1$, the fluid exhibits a shear-thinning behavior (becomes less viscous as the shear rate increases). The Bingham model is a specific case of the Herschel-Bulkley model, with $n = 1$. Better representations of cement slurry behavior are obtained using flow behavior indices lower than 1.

The Herschel-Bulkley model is a three-parameter model, and this increases both the complexity of slurry flow calculations and the computing time. In practice, the Bingham model is therefore still often used in the industry to represent the rheology of cement slurries, spacers, and drilling fluids.[2]

---

[1]A rheometer is a more versatile instrument than a viscometer and enables application of oscillatory movement and measurement of viscoelastic properties, in addition to the shear stress versus shear rate curve. The typical shear rate range of a rheometer (10^{-6}–10^5 s^{-1}) is larger than of a typical viscometer (10^{-1}–10^3 s^{-1}). See e.g. [1].

[2]Most fluids used in drilling and cementing have yield-stress rheology. Exceptions are water and air, sometimes used as drilling fluids, and Newtonian washes sometimes used to clean the annulus before pumping spacer and cement in a cementing job.
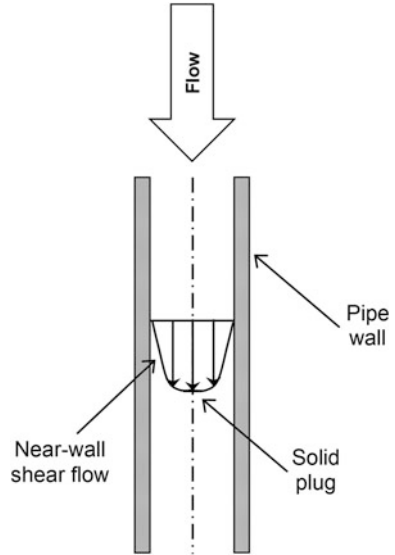
The existence of yield stress has significant implications for fluid flow in pipes
and annuli. In particular, the shear stress is lower than the yield stress around the
axis of the pipe. As a result, a hard core moving as a solid plug rather than a liquid
develops around the axis of the pipe. The fluid thus flows as a liquid near the walls,
where the shear stress is above the yield stress, and moves as a solid plug near the
axis (Fig. 2.2). This can be compared to toothpaste flowing as a plug out of the
tube. A similar flow pattern develops in an annulus, where the fluid flows as a liquid
near the walls and moves as a plug in the middle of the conduit.

The width of the solid plug (core) across the conduit is a function of the pressure
gradient along the direction of flow. As the pressure gradient decreases, the solid
core expands, until it occupies the entire width of the conduit. In annular flow, this
happens when the pressure gradient is equal to [3]:

$$\left|\frac{dP}{dx}\right| = \frac{2\tau_Y}{R_o - R_i} \tag{2.4}$$

where R_i and R_o are the inner and outer radii of the annulus, respectively (m);
x points in the direction of flow. Equation (2.4) assumes that the inner and outer
pipes are concentric, and neither of them is moving. Applying rotating or recip-
rocating motion to one of the pipes, e.g. the inner, increases the total shear rate in
the fluid and thereby facilitates the flow. The threshold pressure gradient may
thereby drop below the value given by Eq. (2.4). This is the principle behind
improving the quality of well cementing by casing rotation or reciprocation.

In addition to the yield stress and plastic viscosity, viscous properties of a
non-Newtonian fluid are sometimes characterized by *apparent viscosity*. This is

what is found by a single viscosity measurement at a constant speed in a viscometer. For a Newtonian fluid, the apparent viscosity is constant (and equal to the dynamic viscosity), but for non-Newtonian fluids the apparent viscosity depends on the shear rate. As a consequence, reporting the apparent viscosity without specifying the shear rate is of limited value. The apparent viscosity is not a material property and is simply the slope of a straight line in the shear stress versus shear rate plot joining the origin with a given point on the rheogram (Fig. 2.1). The apparent viscosity thus describes the flow properties of the fluid at a given shear rate.

The yield stress introduced above characterizes the rheology of a yield-stress fluid as it flows. If the fluid is at rest, its yield stress usually increases over time. *Gel strength* values for cement are typically measured 10 s and 10 min after the fluid was brought to rest. The 10-s gel strength of a "typical" oilwell cement is on the order of 10 Pa. The gel strength builds up because colloidal particles develop a structure as the slurry rests. This is a reversible process, and the structures can be broken if the slurry is again subject to shear. In addition, over a longer time, chemical reactions in cement slurry result in irreversible strength build-up until the slurry solidifies. As pointed out in Ref. [4], ten minutes is too short a time to be representative of static periods that drilling fluid or spacer may experience in the well.

Static *stability* is an important slurry quality that describes how well the slurry maintains homogeneous density while at rest. Solid particles in the slurry tend to settle down, and this can cause a heterogeneous pressure gradient in the annulus whereby the density and the pressure gradient are largest at the bottom of the interval. This may promote the influx of formation fluids into the slurry in the upper parts of the cemented interval where the slurry density is low. If the formation fluid is gas, such influx may create gas channels in the not-yet-hardened cement, which will persist after the cement has hardened.

In laboratory experiments, the static stability of a cement slurry can be evaluated by examining the density distribution in a cement sample that was left to harden in a vertical sedimentation tube. The difference between the density measured at the bottom and at the top of the cement sample divided by the average density provides a quantitative measure of the slurry stability. Slurry segregation may also involve accumulation of *free fluid* (water) in the upper part of the cement column. Free fluid can be measured by placing a sample into a graduated tube [4]. Slurry segregation in horizontal wells may have a particularly detrimental effect on the results of a cement job by creating a channel that runs in the upper part of the cemented annulus [5].

In addition to rheological properties, *density* is an important property of a slurry. Depending on composition, the density of well cement slurries may range from as low as 720 kg/m^3 (foamed cements) to as high as 2400 kg/m^3 (high-density systems). In Chap. 3, we will see how the density and rheological properties of different fluids affect the flow and displacement in the annulus during a primary cementing job.

2.2 From Slurry to Solid: Cement Hardening

Cement powder is mixed with water at the rig site, and the slurry is pumped down the casing. After reaching bottomhole, the cement enters the annulus behind the casing, and pumping continues until an annular cement sheath of a required height is created. Cement is then left in the annulus to harden. The hardening is due to hydration of cement which starts immediately or some time after the cement slurry has been mixed.

Hydration involves changes to both the structure and the properties of cement. In particular, the density of hydration products is higher than that of the original unhydrated phases. In the absence of an extra water supply, this causes neat cement to shrink. Examples of shrinkage-induced reduction of cement bulk volume in the range of 0.5–5 % have been reported [4]. As a result of chemical shrinkage, i.e. shrinkage due to hydration, porosity and pore pressure decrease as setting proceeds [6]. If an external water supply is available, the decline of pore pressure leads to water being sucked into the cement's pore space. Water availability reduces the bulk shrinkage of cement and may even cause bulk expansion. In addition to the decline in porosity and pore pressure, shrinkage may cause fracture growth in cement. It may also lead to the development of a microannulus between the cement and the formation, which is one of the mechanisms behind well leakage [7].

Porosity is defined as the ratio of the pore volume to the total (bulk) volume of the material. If a porous material contains a connected pore system, applying a pressure gradient will put the fluid in the pore space into motion. Flow of a Newtonian fluid through a porous medium, such as a cement slurry undergoing solidification, can be described by Darcy's law. The total discharge Q (m^3/s) can then be calculated as follows:

$$Q = -\frac{kA}{\mu}\frac{\mathrm{d}P}{\mathrm{d}x} \qquad (2.5)$$

where x points in the direction of flow; A is the cross-section area normal to flow (m^2); P is the pore pressure (Pa); μ is the dynamic viscosity of the pore fluid (Pa s). The coefficient k (m^2) in Eq. (2.5) is called the *absolute permeability*. During cement hydration, decreasing porosity results in a significant reduction of permeability [8]. The permeability of a cement slurry is on the order of 1 D, while the permeability of hardened cement is on the order of 1–10 μD. Rapid decline of permeability during setting is mentioned as a key quality of good well cement [6]. It is, however, not easy to measure the exact slurry permeability. Conventional steady-state permeability measurements with water as the flowing fluid show poor reproducibility and significant scatter for cement slurries. Using gas as the flowing fluid encourages cement drying, shrinkage and fracturing [6]. A transient method has been proposed based on analyzing the pore pressure decline in cement during hydration [6].

As cement slurry hydrates, its *tensile strength* and *shear strength* gradually build up. *Tensile strength* (Pa) is defined as the maximum tensile stress that a material can withstand without breaking apart. Tensile strength of a cement slurry undergoing solidification can be measured in laboratory conditions by injecting water at some location inside the slurry [8]. Water is injected at a constant flow rate, and the injection pressure is measured over time. The pressure increases up until a fracture is formed in the slurry. This peak pressure is then used as an estimate of the slurry's tensile strength. Values of the tensile strength as high as 0.5 MPa have been reported for cement slurries [8]. *Shear strength* (Pa) is the maximum shear stress that the slurry can withstand without failing or starting to flow. The shear strength is initially equal to the yield stress of the slurry (i.e. on the order of 1–10 Pa) and gradually increases as the slurry sets.

The pressure that the cement slurry exerts in the annulus is an important factor controlling fluid influx from the formation during cement setting. Laboratory experiments demonstrate that pressure reduction in a slurry column during setting can be quite substantial [9]. Shear stresses between the slurry and the casing or rock (the wall friction) reduce the hydrostatic pressure that the slurry exerts. These stresses are limited by the yield stress of the slurry. Therefore, build-up of cement shear strength reduces the pressure since higher shear stresses can be sustained at the walls. Moreover, the cement pressure can further be reduced if fluid is lost from the slurry into the permeable rock.[3] As the cement hardening proceeds, shrinkage may also causes reduction in the slurry pressure.

Given the detrimental effects of shrinkage, such as fracture development and reduction in the cement column pressure, efforts have been made in the industry to develop well cements that do not shrink or might even expand during setting. This has led to the development of a series of products (*expanding cements*) in which various additives counteract shrinkage. This is achieved either by chemical interaction with Portland cement constituents so as to produce expansion during hydration, or by adding materials that expand themselves and thereby compensate for shrinkage [10]. Other types of shrinkage than chemical shrinkage also exist, e.g. *carbonation shrinkage* if cement reacts with CO_2, or *desiccation shrinkage* if cement dries out.

Cement hydration is an *exothermic reaction*, i.e. heat is released as hydration proceeds. The heat release makes the temperature of cement increase during setting. This causes the casing diameter to be slightly larger than it otherwise would be during cement setting. When the temperature falls back to its regular value, a microannulus can be formed between the cement and the casing. The heat release during hydration also has a detrimental effect when cementing permafrost intervals as it may cause melting of the formation. This may lead to poor bonding and induce subsidence in the near-well region. The heat release is, however, the basis of an evaluation technique for the quality of well cementing, namely the temperature log.

---

[3]Laboratory data about fluid-loss properties of a slurry are obtained in filter-press experiments.

Such logs can be performed after the cement job has been completed, in order to find the *top of cement*, i.e. the height of the cement sheath set in the annulus.

2.3 Properties of Hardened Cement

During the life of a well, the annular cement sheath can be exposed to a variety of forces such as heating/cooling cycles, mechanical stresses, vibrations, formation fluid influx or reactive flows. Properties of hardened cement affect its sealing capacity, and understanding them is therefore crucial for maintaining well integrity. Properties of solid cement can be subdivided into mechanical, interfacial, hydraulic, and thermal.

Mechanical properties characterize the response of cement to mechanical loads and deformations. These can further be subdivided into *elastic properties* and *strength properties*. We have already come across strength properties of cement slurries in Sect. 2.2 (tensile and shear strength).

(i) *Elastic properties*. The most commonly used elastic properties are *Young's modulus* and *Poisson's ratio*. Both of these parameters can be obtained from stress-strain curves recorded in a uniaxial compressive test. In this test, a cylindrical cement specimen is loaded by applying compressive load at its top and bottom faces (Fig. 2.3). The specimen geometry with the height-to-diameter ratio of 2–3 is most common in rock mechanics since it reduces the effect of friction between the specimen and the loading platens on the test results. However, in cement testing, using cubic specimens is not uncommon [4]. In a uniaxial test, Young's modulus is
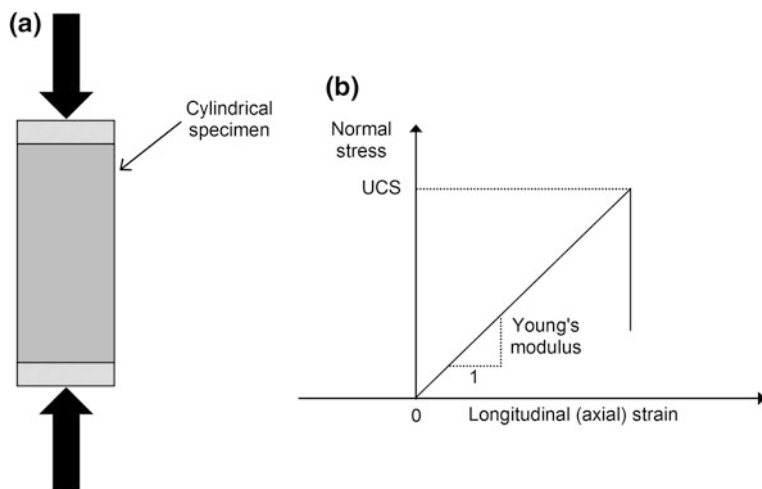
Fig. 2.3 Schematic illustration of a uniaxial compressive test (**a**) and stress-strain *curve* obtained in a such test (**b**). UCS is unconfined compressive strength

the slope of the axial stress versus axial strain curve. Poisson's ratio is the ratio of the transverse strain to the axial strain.

The elastic parameters evaluated from stress-strain curves are called *static moduli*. Alternatively, both parameters can be evaluated from the velocities of longitudinal and shear acoustic waves propagating through cement. Moduli obtained in this way are called *dynamic moduli*. The dynamic Young's modulus is higher than the static modulus. The static Young's modulus is typically on the order of 1–10 GPa for oilwell cements, while Poisson's ratio is on the order of 0.1–0.25.

The perfectly linear stress-strain curve shown in Fig. 2.3 is an idealization. Real curves are nonlinear, and Young's modulus can be estimated as the slope of the curve at the stress equal to 50 % of peak stress (stress at failure). Inelastic deformation of cement grains, irreversible slip at grain boundaries, closing of microcracks and intergranular pores, and generation of new microcracks may all contribute to inelastic deformation of cement during loading.

(ii) *Strength properties*. When the stress in the uniaxial test reaches a certain value, the specimen breaks down. The stress value at which this happens is called the *unconfined compressive strength* (UCS). It describes the ability of cement to carry load under compression. UCS is on the order of megapascals or tens of MPa for oilwell cements, depending on their structure and composition. It should be remembered, however, that cement set in the annulus is, in general, in a triaxial stress state. *Triaxial tests* can be used for a more detailed characterization of cement strength in compressive conditions. In a triaxial test, stresses are applied not only at the top and bottom, but also on the side surface of a cylindrical specimen. The stress applied on the side surface is known as the *confining stress*. Confining and axial stresses on the specimen are first increased simultaneously to the same level. Then, the confining stress is held constant while the axial stress is increased to failure. Several tests at different confining stresses are usually performed to fully characterize cement in triaxial conditions.

The material strength in triaxial stress state is commonly described using one of the so-called failure criteria. A *failure criterion* defines a combination of stresses at which the material fails. In stress space, the failure criterion defines a surface (the *failure surface*). Several failure criteria have been proposed for hardened cement, differing in their degree of detail and complexity. Higher accuracy usually increases the number of parameters that need to be determined from triaxial tests. One of the simplest criteria routinely used for cement, concrete, and some rocks is the *Mohr-Coulomb failure criterion*. In terms of principal stresses ($\sigma_1 \geq \sigma_3$), it can be expressed as follows:

$$\sigma_1 = \sigma_{\mathrm{UCS}} + \tan^2\left(\frac{\pi}{4} + \frac{\varphi}{2}\right)\sigma_3 \qquad (2.6)$$

where σ_1 and σ_3 are the maximum and minimum principal stresses (Pa; positive in compression); σ_{UCS} is the unconfined compressive strength (Pa); φ is the *angle of*
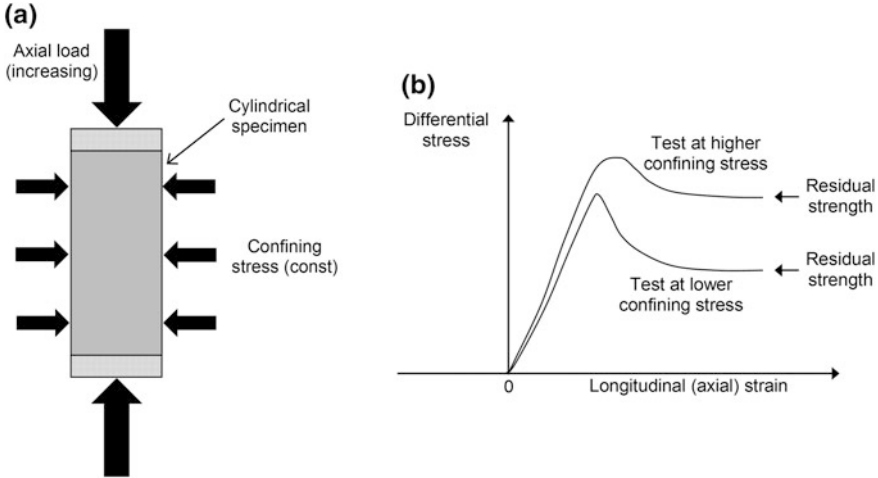
Fig. 2.4 Schematic illustration of a triaxial compressive test (**a**) and stress-strain curves obtained in such a test (**b**). Differential stress is axial minus confining stress. Higher confining results in more ductile (less brittle) behavior

internal friction (°). Hence, the Mohr-Coulomb criterion makes use of two constitutive parameters, σ_{UCS} and φ, meaning that a minimum of two triaxial tests (or a triaxial test and a uniaxial test) are required in order to characterize cement with this criterion. As evident from Eq. (2.6), the Mohr-Coulomb criterion does not account for a possible effect of the intermediate principal stress, σ_2, on cement failure. More elaborate failure criteria may include σ_2. Poromechanical models of well cements, based on Biot theory of poroelasticity/poroelastoplasticity, have been introduced recently [11].

According to Eq. (2.6), confining stress increases the triaxial strength. It also makes the mechanical response of cement more ductile: as the confining stress increases, the post-failure part of the stress-strain curve becomes less steep, and the residual strength increases (Fig. 2.4).

The Mohr-Coulomb criterion describes failure in compression. It needs to be supplemented with a tensile failure criterion to completely describe the strength of cement. This is usually done by specifying the *tensile strength*, i.e. the maximum magnitude of a tensile stress that the material can sustain without breaking apart. This can be measured in a direct tension test, in which a cylindrical specimen is pulled in opposite directions at its ends (imagine the reverse of the uniaxial compressive test shown in Fig. 2.3). It turns out, however, that performing a direct tension test is more cumbersome and may require specially shaped specimens (e.g. "dog bone" shape). An alternative often employed in testing of brittle materials is the so-called Brazilian test (Fig. 2.5). *Brazilian test* is an indirect tensile test in which a specimen shaped as a circular cylinder is loaded in compression along the straight lines on its curved side surface. This creates a nonuniform stress state even if the material is perfectly homogeneous. In particular, tensile stress normal to the

Fig. 2.5 Schematic illustration of Brazilian test. The *dashed line* indicates the loading diameter
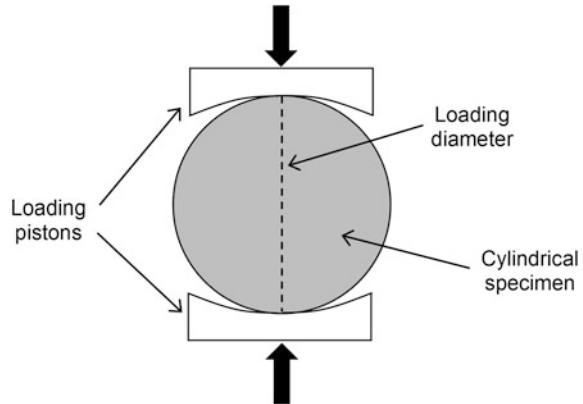
loading diameter is produced along a significant part of that diameter. The tensile stress is largest near the cylinder's axis and tends to split the cylinder into two halves. Compressive load is increased during the test up until the specimen breaks down. The maximum load, F_m, recorded during the test is then used to obtain the tensile strength of the material, T_0 [12]:

$$T_0 = \frac{2F_m}{\pi DL} \tag{2.7}$$

where D and L are the diameter and length of the cylinder (m).

Compressive and tensile strength values are important characteristics of cement's load-bearing capacity. For instance, fracture nucleation and propagation in cement when the casing diameter increases as a result of casing pressurization is controlled by the cement's tensile strength, amongst other parameters. It should, however, be remembered that annular cement can be subject to complicated stress paths and loading/unloading cycles during its lifetime. Annular cement is confined between the casing and the formation, and its deformation is therefore strongly influenced by deformations of the casing and the rock. The coupled deformation of casing, cement and rock can be studied in specially-designed laboratory tests such as the one described in [13]. In this test, a complex structural test of a casing-cement-rock assembly was performed. The assembly was composed of a central core (a cylinder representing the casing), a cement sheath around it, and an outer metal hollow cylinder representing the formation. The cement sheath could be loaded/unloaded and brought to failure by expanding/contracting the core. Permeability measurements of cement were performed during the test. It should be noted that these kinds of tests are not standardized. Therefore, it can be difficult to compare results obtained with such specially-designed tests in different laboratories.

An important aspect of cement's mechanical behavior is that cement is a brittle material, i.e. it fails with very little preceding plastic deformation. Similarly to other brittle materials, such as crystalline rocks or consolidated sandstones, cement has much larger compressive strength (UCS) than tensile strength (often by an order of magnitude). Brittleness of cement is often estimated indirectly by means of its Young's modulus. Lower Young's modulus indicates a less brittle cement. Low Young's modulus improves the ability to deform without stresses becoming so high that they would exceed the strength of cement. Unfortunately, lowering the Young's modulus by means of additives may degrade other properties of cement, in particular strength. Improving mechanical stability of solid cement by changing its composition is therefore an optimization exercise.

Interfacial properties In addition to failure in the bulk cement, there are other mechanisms that control cement failure in wells. In particular, interfaces between cement and casing, and between cement and rock are known as potential weak spots. Local lack of bonding can be discovered by performing a cement bond log after the cement job is finished. However, even when bonding is good, the *interface bonding strength* can be lower than the bulk cement strength. The bonding strength can be estimated by means of laboratory tests, e.g. push-out experiments [14–16]. The setup is schematically shown in Fig. 2.6. It includes a compound specimen with a steel pipe or a rock cylinder in the middle and cement around it. During the test, the steel pipe or rock is pushed downwards so as to induce failure at the cement interface. The interfacial bonding strength is calculated as the peak load divided by the area of contact between the steel (rock) and the surrounding cement. The shear bond strength evaluated this way is typically on the order of 0.1–1.0 MPa.

The interfacial bonding strength evaluated in a push-out test is the shear strength. During the lifetime of a well, tensile stresses acting in the cement in the radial direction can be induced as we will see in Chaps. 5 and 6. Such stresses are likely to promote *tensile* failure at the interface. Development of a commonly-accepted test for tensile interface strength is still an outstanding task.

Fig. 2.6 Principle of push-out testing for interfacial bond strength
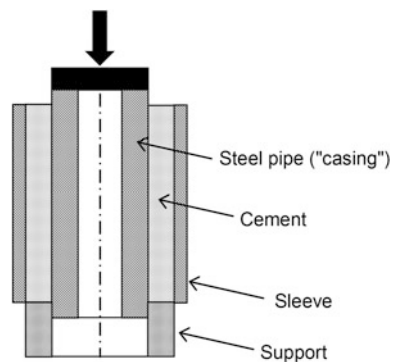
In addition to the bonding strength, *hydraulic bonding* properties of an interface can provide a valuable estimate of the bond quality with respect to possible leakage. Laboratory tests have been designed that quantify hydraulic bonding by applying fluid pressure at the interface in a compound cement-steel or cement-rock specimen [4].

It should be noted that the terms "interface failure" and "interface strength" may suggest that the cement-steel or cement-rock systems fail at the very interface. Experiments show, however, that interface failure is a much more complex phenomenon. In particular, as we will see in Chap. 4, a so-called *interfacial transition zone* (*ITZ*) forms in cement along cement-steel interfaces. The strength of cement in this zone is lower than in the bulk cement or at the very wall. As a result, fractures often develop not at the very contact between cement and steel, but inside the ITZ, i.e. at some distance from the wall [17].

Hydraulic properties Mechanical properties determine one important function of cement, namely its resistance to mechanical loads. Hydraulic properties determine the other, i.e. the ability to create a leak along the well or the rate with which the cement sheath will be chemically degraded. Leakage along the annulus may create communication between geological horizons or even bring formation fluids to the surface. The leakage can, in particular, be due to microannulus, gas channels, and fractures in cement. If cement is free of these flaws, the leakage capacity is determined by cement's *permeability*, the parameter introduced in Sect. 2.2. Permeability of currently used well cements is considered sufficiently low to prevent leakage if the cement remains intact. We will see in later chapters how microannuli, fractures, and gas channels develop in cemented wells. We will see, in particular, how imperfect slurry flow and displacement may produce gas channels and how the mechanical properties introduced above control the formation of fractures during a well's life.

Thermal properties One of the mechanisms of fracture development in well cement is linked to heating and cooling. In this case, in addition to mechanical properties, thermal properties of cement play a crucial role, in particular the *coefficient of thermal expansion* and the contrast between casing, cement and formation with regard to it. A sample of some "typical" values of this parameter for steel, cement and sandstone is given in Table 2.1. Other thermal properties include the *thermal conductivity* and the *specific heat capacity*.

Table 2.1 Example values of the coefficient of thermal expansion for steel, cement and rocks

Material	Coefficient of thermal expansion ($\times 10^{-6}$ K^{-1})
Steel	10–16
Cement	10–12
Sandstone	10–12

2.4   Summary and Discussion

Well cementing involves pumping a sequence of fluids into the well. At least some of these fluids, such as spacers and cement slurries, have non-Newtonian yield-stress rheology. After the cement slurry has been placed in the annulus, it hardens into a low-permeability annular seal. The complexity of all these processes and the multitude of materials involved (drilling fluid, spacer, chemical wash, cement, casing, rocks) call for a sufficiently detailed material characterization in order to design and optimize cement jobs. A review of cement properties presented in this chapter shows that these properties can largely be grouped into three classes:

- rheological properties of washes, spacers, and cement slurries that control their flow down the well and up the annulus;
- transition properties of cement slurry related to its solidification;
- mechanical, interfacial, hydraulic, and thermal properties of hardened cement that control e.g. response of the cement to thermal stresses, vibrations, etc.

Well-established testing procedures can be used to obtain some of these parameters. They are described in e.g. API Recommended Practices[4] and ASTM Standards.[5] Measurements of other parameters, such as the gel strength, are standardized to a much lesser extent.

In later chapters, we will see how the material properties introduced in this chapter affect the quality of cement jobs and the performance of an annular cement sheath during a well's lifetime from drilling to plugging and abandonment.

References

1. Carrington S, Langridge J (2005) Viscometer or rheometer? Making the decision, Laboratory News (August)
2. Kelessidis VC, Dalamarinis P, Maglione R (2011) Experimental study and predictions of pressure losses of fluids modeled as Herschel-Bulkley in concentric and eccentric annuli in laminar, transitional and turbulent flows. J Petrol Sci Eng 77(3–4):305–312
3. Laird WM (1957) Slurry and suspension transport—basic flow studies on bingham plastic fluids. Ind Eng Chem 49(1):138–141
4. Nelson EB, Guillot D (eds) (2006) Well cementing. Schlumberger
5. Watters J (2012) RPSEA Task 2.0 Technology status Assessment. 10122-19.02. Lowering drilling cost, improving operational safety, and reducing environmental impact through zonal isolation improvements for horizontal wells drilled in the Marcellus shale 10122-19. Houston
6. Appleby S, Wilson A (1996) Permeability and suction in setting cement. Chem Eng Sci 51(2):251–267

---

[4]www.api.org.

[5]http://www.astm.org/Standard/.

7. Dusseault MB, Gray MN, Nawrocki PA (2000) Why oilwells leak: cement behavior and long-term consequences. In: SPE paper 64733 presented at the SPE international oil and gas conference and exhibition in china held in Beijing, China, 7–10 Nov 2000
8. Backe KR, Lile OB, Lyomov SK, Elvebakk H, Skalle P (1999) Characterizing curing-cement slurries by permeability, tensile strength, and shrinkage. SPE Drill Completion 14(3):162–167
9. Chenevert ME, Shrestha BK (1991) Chemical shrinkage properties of oilfield cements. SPE Dril Eng 37–43
10. Goboncan VC, Dillenbeck RL (2003) Real-time cement expansion/shrinkage testing under downhole conditions for enhanced annular isolation. In: SPE/IADC paper 79911 presented at the SPE/IADC drilling conference held in Amsterdam, The Netherlands, 19–21 Feb 2003
11. Bois A-P, Garnier A, Rodot F, Saint-Marc J, Aimard N (2011) How to prevent loss of zonal isolation through a comprehensive analysis of microannulus formation. SPE Drill Completion 26(1):13–31
12. Fjær E, Holt RM, Horsrud P, Raaen AM, Risnes R (2008) Petroleum related rock mechanics, 2nd edn. Elsevier, Amsterdam
13. Boukhelifa L, Moroni N, james SG, Le Roy-Delage S, RThiercelin MJ, Lemaire G (2005) Evaluation of cement systems for oil- and gas-well zonal isolation in a full-scale annular geometry. SPE Drill Completion 20(1):44–53
14. Liu H, Bu Y, Guo S (2013) Improvement of aluminium powder application measure based on influence of gas hole on strength properties of oil well cement. Constr Build Mater 47: 480–488
15. Opedal N, Todorovic J, Torsaeter M, Vralstad T, Mushtaq W (2014) Experimental study on the cement-formation bonding. In: SPE paper presented at the SPE international symposium and exhibition on formation damage control held in Lafayette, Louisiana, USA, 26–28 Feb 2014
16. Ladva HKJ, Craster B, Jones TGJ, Goldsmith G, Scott D (2004) The cement-to-formation interface in zonal isolation. IADC/SPE paper 88016 presented at the IADC/SPE Asia Pacific drilling technology conference and exhibition held in Kuala Lumpur, Malaysia, 13–15 Sept 2004
17. Torsæter M, Todorovic J, Lavrov A (2015) Structure and debonding at cement–steel and cement–rock interfaces: effect of geometry and materials. Constr Build Mater 96:164–171

Chapter 3
Fluid Flow and Displacement in the Annulus

Abstract During a primary cementing job, a sequence of fluids is pumped into the annulus in order to displace the mud and prepare the annulus for cement placement. The factors affecting the mud displacement efficiency are discussed in this chapter. The effects of pipe eccentricity, breakouts, and irregular wellbore cross-section on the displacement efficiency are demonstrated using a simple kinematic model of annular cementing. In particular, it is shown that breakouts may have a substantial detrimental effect on the displacement efficiency since the displacing fluids might be flowing only in the breakouts. Channelization is also shown to occur when the wellbore has neither breakouts nor washouts, but rather a slightly irregular cross-section, like real wells normally do in sedimentary formations. In this case, viscous instabilities occur for unfavorable mobility ratios. Channelization may in this case be prevented most effectively by increasing the yield stress of the displacing fluid. The effects of well inclination, pipe movement and flow regime are discussed. A brief overview of numerical models of well cementing is provided. Unresolved issues in modelling are summarized.

During primary cementing, a sequence of fluids is injected into the annulus in order to displace the drilling mud and prepare the annulus for cement placement. After the interval has been drilled, the well is first circulated in order to bring drill cuttings to surface. The drill string is then pulled out of the hole, while the circulation may continue. Circulation is then stopped, the well is logged, the casing string is run in hole, and the mud circulation is resumed. Mud circulation before logging and after running casing in hole is usually called *mud conditioning*. It serves to remove gas and solids (cuttings, settled weighting agents such as barite, and filter cake possibly deposited against a permeable formation). Moreover, mud conditioning is intended to break gel if the mud has been static in the well for a long time. According to current industrial recommendations, mud circulation should be carried on as long as it takes to remove solids and gelled mud from the well [1]. Moreover,

mud conditioning aims to replace the thicker, heavier mud used while drilling the well, with a lighter, thinner mud that is easier to displace during subsequent cementing. Since solids can be scraped off the wellbore walls by running the casing pipe, it may be wise to perform mud conditioning also at intermediate depths as the casing is being run in hole. Thinning the mud during conditioning should, however, not jeopardize its ability to hold the weighting agent and solids in suspension [2]. Circulation of at least two annular volumes with the highest possible rate during mud conditioning is recommended, according to the current industrial practices [2].

After the casing has been set and the mud has been conditioned, a sequence of *preflushes* is pumped into the hole. Preflushes prepare the annulus for the upcoming cement placement and should therefore satisfy a set of requirements [2–4]:

- preflushes must leave the casing and formation water-wet, in order to improve the subsequent bonding of cement;
- preflushes should, ideally, be pumped in turbulent regime to improve the efficiency of mud removal, but at the same time without fracturing the formation (which may happen if the pump rate, and thus the bottomhole pressure, become excessively high) and without causing unacceptable formation damage;
- a sufficient contact time between a preflush and the surfaces exposed in the annulus should be allowed in order to improve mud removal and clean the walls from the mud film and mud cake;
- all in all, the sequence of preflushes must ensure the most efficient mud displacement from the annulus;
- preflush fluids should be easily removable from the annulus by subsequent cement pumping.

The effect of using preflushes increases with the contact time between the preflush and the walls exposed in the annulus. According to some industrial practices, a minimum contact time of 10 min is recommended for preflushes. Other sources recommend 4, 5, or 8 min [2]. Shorter times (e.g. 4 or 5 min) usually mean that the preflush is pumped in turbulent regime.

Preflushes are normally subdivided into washes (non-weighted fluids) and spacers (weighted fluids) (Fig. 3.1). Washes have Newtonian rheology, relatively low density, and low viscosity, and can be pumped in turbulent regime. The purpose of a wash is to clean the surfaces exposed in the annulus (formation and casing). Washes can be either oil-based or water-based. Examples are fresh water,

Fig. 3.1 Classification of preflushes
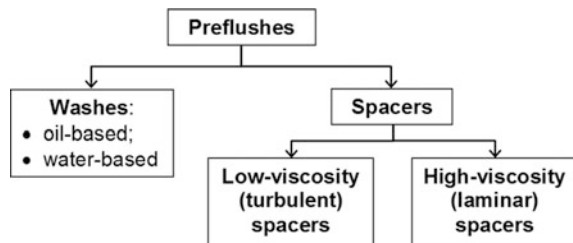
base oil, or a chemical solution. Fresh water can be used, e.g., in a wellbore drilled with water-base mud. Washes may contain dispersants and surfactants for more effective cleaning, in which case they are known as *chemical washes*. Diesel oil or a mixture of water, mutual solvents, and surfactants can be used in a well drilled with a non-aqueous fluid (oil- or synthetic-base mud) [2].

The upside of using washes is high cleaning capability in turbulent flow. There might, however, be a risk of formation fluid influx when circulation is stopped, due to the low density of the wash. The pumping schedules should be designed so that the hydrostatic pressure in the annulus does not fall below the formation pore pressure or the borehole-stability limit at any location along the open hole.

Weighting may be necessary in order to increase the bottomhole hydrostatic pressure and thus prevent borehole instabilities. According to Sauer [3], weighted preflushes (spacers) are typically heavier than the mud by 60 kg/m^3. According to Khalilova et al. [5], weighted spacers are optimally 10 %, yet less than 2 ppg (240 kg/m^3), heavier than the mud. Weighting agents such as barite, hematite and calcium carbonate are commonly used in spacers. The purpose of a spacer is to separate incompatible fluids and to displace mud and solids from the annulus. In order to prevent sedimentation of weighting solids, viscosifiers (typically, bentonite or polymers) can be made part of the spacer composition. While improving the displacement efficiency, weighting of spacers increases the bottomhole pressure during the subsequent cement placement, thereby increasing the risk of formation fracturing. Spacers can be pumped either in turbulent regime (low-viscosity spacers) or in laminar regime [4]. Surfactants are added to spacers and washes in order to water-wet the casing and formation surfaces exposed in the annulus, and thereby improve the subsequent cement bonding.

Here are a few examples of possible fluid trains pumped during primary cementing [2, 3]:

- In a wellbore drilled with oil-base mud: mud conditioning (cleaning and thinning), then pumping base oil, followed by viscous spacer to displace the mud, then seawater and chemical wash to clean and water-wet the surfaces exposed in the annulus, then viscous spacer to displace the dirty fluids from the annulus, and finally lead cement and tail cement slurries;
- In a wellbore drilled with water-base mud: mud conditioning (cleaning and thinning), then pumping viscous spacer to displace the mud, followed by seawater (or fresh water) and chemical wash to clean the surfaces exposed in the annulus, then viscous spacer to displace the dirty fluids from the annulus, and finally lead cement and tail cement slurries.

One of the targeted properties of a preflush is its *compatibility* with both cement and drilling mud. Compatibility of two fluids means that the rheological properties of their mixture are between those of the individual fluids [1]. When mixed together, two incompatible fluids (e.g., cement and oil-base mud) may result in solids settling, flocculation, fluid separation, etc. Oil-base muds are typically less compatible with cement than water-base muds are [2]. If cement gets in contact with an

incompatible fluid, the thickening time may be increased, the development of compressive strength of set cement may be delayed, and the final compressive strength is lowered [5]. If two preflushes are incompatible with each other, they may build a solid mass, and cement will channel through it during subsequent cement pumping [2]. All these scenarios result in poor quality of annular cement.

Flow and displacement of fluids in the annulus during a cement job are the key factors that determine integrity of the cement sheath during the subsequent life of the well. If mud channels are left in the annulus, or if gas channels are introduced in the cement by gas migration during cement setting, these channels may affect all subsequent history of the well. Other consequences of poorly executed primary cementing jobs can be casing corrosion and failure, well control issues, and, eventually, the economic costs associated with remedial cementing. Therefore, improving the quality of mud displacement from the annulus and of cement placement in the annulus during primary cementing is of paramount importance in well construction.

Perfect cement placement in the annulus implies that all the fluids that were originally present there (drilling fluid with cuttings; formation fluids) are completely replaced by cement, and cement fills all the annulus. Such perfect displacement is rarely achievable. For instance, pockets of undisplaced mud may remain in washouts created in the borehole wall during drilling. Washouts may contain dehydrated mud that is difficult to remove by pumping preflushes. Such gelled mud may later contaminate the cement slurry.

The main factors affecting the fluid flow and displacement in primary cementing are as follows:

- borehole shape (breakouts, washouts)
- eccentric positioning of casing in the wellbore (eccentric annulus);
- rheological properties of the drilling fluid, cement, and preflushes;
- densities of the drilling fluid, cement, and preflushes;
- injection schedule (pump rates, pumping time);
- well inclination (vertical, deviated, or horizontal)
- flow regimes (laminar, turbulent, mixed);
- lost circulation, whereby cement escapes into the formation via natural or induced fractures (or into vugs and cavities, e.g. in carbonate rocks);
- fluid loss to the formation (fluid loss from the cement slurry builds a filter cake in the annulus, which changes the displacement regime, makes the slurry more viscous, reduces the annular gap, and thus may increase the circulating bottomhole pressure during cement placement).

Effective scheduling of injection in primary cementing can be achieved by optimizing the flow rates, densities, rheology, and chemistry of the fluids. In this chapter, we will take a look at various factors affecting the flow and displacement in the annulus during primary cementing.

3.1 Forces Acting on Mud During Mud Displacement

Forces driving mud out of the annulus during primary well cementing are as follows:

- pressure gradient in the annulus;
- drag force imposed on the mud by the faster-moving displacing fluid (preflush or cement);
- buoyancy (if the mud is lighter than the displacing fluid);
- forces applied to the mud by the casing pipe movement.

  Forces resisting the mud flow in the annulus are as follows:

- yield stress and, possibly, gel strength of the mud;
- viscosity of the mud;
- friction between the mud and the walls (wellbore wall and casing pipe.)

Some of these forces can be enhanced under certain circumstances. For instance, the gel strength may increase over time and at elevated downhole temperatures; filter cake build-up on the borehole wall can make it more difficult to remove the mud during subsequent cementing.

The outcome of a primary cementing job is determined by the interplay between the driving and the resisting forces.

3.2 Kinematic Model of Annular Cementing

Throughout this chapter, we will use a simple kinematic model of annular flow and displacement to illustrate some basic physics of primary cementing [6]. In this model, the annulus is discretized into slices along the well (Fig. 3.2). Each slice is then discretized into a finite number of sectors. The inner boundary of each sector is centered at the casing axis (Fig. 3.3, left-hand panel). The outer boundary of each

Fig. 3.2 Annulus discretized into slices along the well
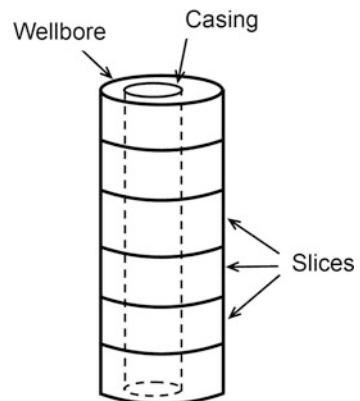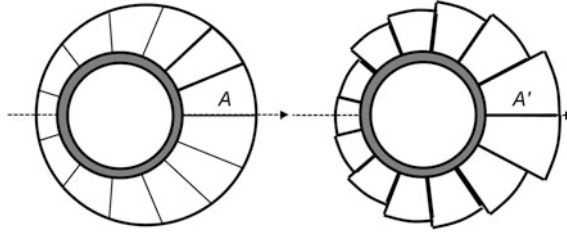
Fig. 3.3 Slice of annulus discretized into sectors (*left-hand panel*) and equivalent sectors replacing the original sectors (*right-hand panel*). The equivalent sector A' has same area and the same inner radius as the original sector, A

sector is determined by the wellbore geometry. This can be, e.g., circular, as in Fig. 3.3 (left-hand panel), or irregular, representing washouts in the wellbore. Each sector is then replaced with an *equivalent sector*. Each such equivalent sector is a sector with the inner and outer boundaries being concentric, unlike the original sector, the inner and outer boundaries of which were not necessarily concentric (and the outer boundary did not even have to be circular). The equivalent sector has the same inner radius as the original sector; it is equal to the casing radius. The outer radius of the equivalent sector is calculated so that the areas of the equivalent and the original sectors are equal. A sequence of equivalent sectors arranged one above another along the wellbore axis forms a "tube".

The representation of the annulus by a finite number of equivalent sectors is due to McLean et al. [7]. In a subsequent work by Luo and Peden, an eccentric annulus was discretized into an infinite number of equivalent sectors, with subsequent integration along the azimuth [8]. The approach of Luo and Peden was recently employed by Erge et al. [9].

For a Bingham fluid of plastic viscosity μ_{p1} and yield stress τ_Y, the flow rate through an equivalent sector is given by [10]

$$
\begin{aligned}
Q^{(\text{sector})} = {} & \frac{\Delta\theta}{\mu_{pl}}\frac{\Delta P}{16h}\left[R_o^4 - R_i^4 - b^4 + a^4\right] + \frac{\Delta\theta}{\mu_{pl}}\tau_Y\left[\frac{a^3+b^3}{6} - \frac{R_i^3 - R_o^3}{6}\right] \\
& + \frac{\Delta\theta}{\mu_{pl}\ln\frac{aR_o}{bR_i}}\left[-\frac{\Delta P}{16h}\left(R_o^2 - R_i^2\right)^2 + \frac{\tau_Y}{8}(b+a)\left(b^2 - a^2\right)\right. \\
& \left. + \frac{\tau_Y}{4}(R_i + R_o)\left(R_o^2 - R_i^2\right) - \frac{\tau_Y}{4}(R_i + R_o)\left(b^2 - a^2\right)\right]
\end{aligned}
\tag{3.1}
$$

with a and b obtained from

$$
\begin{aligned}
b - a &= \frac{2\tau_Y h}{\Delta P}, \\
ab &= \frac{\frac{R_o^2 - R_i^2}{2} + \frac{b^2 - a^2}{2} - (b-a)(R_i + R_o)}{\ln\frac{aR_o}{bR_i}}
\end{aligned}
\tag{3.2}
$$

where R_o and R_i are the external and internal radii of the equivalent sector (R_i is the outer radius of the casing); h is the height of the sector, i.e., its dimension along the well and in the direction normal to page in Fig. 3.3; ΔP is the frictional pressure loss on h; $\Delta\theta$ is the angle of the sector apex. [Note that a typo made in the expression for ab in Ref. [10] has been remediated in our Eq. (3.2).]

Initially, some fluid (called "fluid in place" in this text) resides in all sectors. The fluid in place can be, e.g., the drilling mud. Another fluid is pumped into the annulus from the bottom, starting at time $t = 0$. This fluid (called "injected fluid" or "displacing fluid" in this text) can be, e.g., spacer. The mass and momentum conservation equations are solved using Eq. (3.1), and the position of the interface between the fluid in place and the injected fluid is updated at each time step. Both fluids are assumed to be incompressible, to have the same density and to be described by the Bingham rheological model. Only laminar flow is considered in our kinematic model. The effects of turbulence will be discussed in Sect. 3.8.

Two major simplifications in this kinematic model are (1) the absence of momentum transfer between the tubes and (2) the absence of azimuthal flows.

Momentum transfer caused by friction between the fluids in adjacent tubes would normally facilitate the mud displacement since the displacing fluid would drag the static fluid (mud) in the adjacent tube. Without this friction force, the mud flow can only be initiated by the pressure gradient created over the interval by the flowing fluid. Azimuthal flows would normally contribute to facilitate the mud displacement, too, as we shall see later in this chapter.

In a cement job, the efficiency of fluid displacement from the annulus *at a given location along the wellbore* can be quantified by the *displacement efficiency*, η_{area}, defined as [11]

$$\eta_{area} = A_i/A_a \qquad (3.3)$$

where A_i and A_a are the area occupied by the displacing fluid and the full area of the annulus, respectively.

Displacement efficiency can also be defined for the entire cemented interval as follows [2]:

$$\eta_{vol} = V_i/V_a \qquad (3.4)$$

where V_i and V_a are the volume occupied by the displacing fluid and the full volume of the annulus, respectively.

As mud displacement proceeds, the mud displacement efficiency gradually increases from 0 towards some asymptotic value (Fig. 3.4). There are several reasons for gradual (rather than instantaneous) increase of displacement efficiency. The fluid velocity varies in the radial direction. It is zero at the walls (casing and formation) and has a maximum at some distance from the walls. Therefore, the fluid is displaced first in the middle of the annulus. At a given location, this effectively means that the displacement efficiency increases gradually as the displacing fluid passes that location. A film of the original fluid may remain on the walls until it is

Fig. 3.4 Schematic plot of
displacement efficiency
[defined in Eq. (3.4)] versus
injected fluid volume for a
centered annulus (*solid line*)
and eccentric annulus with
some immobile mud (*dashed
line*)
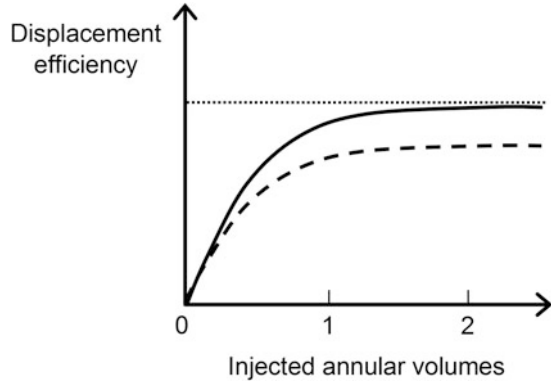
removed e.g. by means of a chemical wash. Removing a mud cake built on the
formation wall may require significant effort, e.g. erosion by turbulent flow.
Therefore, even with a perfectly circular wellbore and centered casing, displace-
ment efficiency equal to 1 might not be achievable. Eccentric positioning of the
casing string makes displacement efficiency of 1 even less likely, as we shall see in
the next section.

As pointed out in Ref. [2], there are circumstances when the displacement
efficiency is not a very good measure of the displacement quality. For instance, a
very thin mud film left on the casing surface may only slightly reduce the efficiency
defined by Eqs. (3.4), but may have a significant effect on the results of the cement
job by creating a microannulus. As another example, a mud channel remaining on
the narrower side of an eccentric annulus might not reduce the efficiency dramat-
ically, but may provide a continuous flow path along the well, compromising zonal
isolation.

3.3   Effect of Eccentric Annulus

In this and subsequent sections, we shall consider different factors affecting mud
displacement in primary cementing. Each of these factors is considered in isolation.
For instance, the effect of casing string eccentricity is studied in this section for the
simplest case: a vertical well with a perfectly circular cross-section. The effect of
irregular wellbore shape is discussed in Sect. 3.4, and the effect of well inclination
in Sect. 3.6.

When the casing pipe is positioned eccentrically in the annulus, it is easier for
preflush or cement to flow along the wider part of the annulus. As a result, the mud
(and other fluids) may remain undisplaced in the narrow part of the annulus
(Fig. 3.5). The reason for this is the *nonzero yield stress* of the mud (or other fluids
residing in the annulus). As we saw in Chap. 2, a finite pressure gradient needs to
be applied along the annulus in order to make a Bingham fluid flow.

Fig. 3.5 Undisplaced mud
left in the narrow part of the
annulus after the cement job is
completed
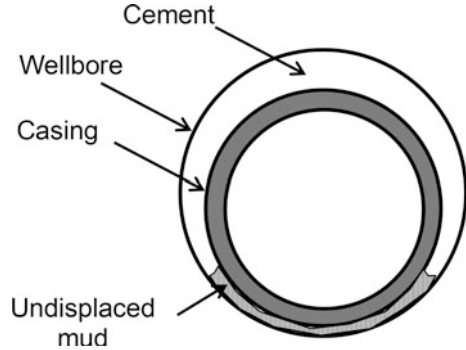
The degree of casing eccentricity in the wellbore is usually described by the
standoff. Standoff is defined as follows:

$$\text{Standoff} = \frac{w_{\min}}{R_w - R_c} \cdot 100\,\% \tag{3.5}$$

where $w_{\min}$ is the minimum distance between the borehole wall and the casing; R_w
and R_c are the radii of the well and of the casing, respectively. Standoff 100 %
means that the casing is perfectly centered in the wellbore. Standoff 0 % means that
the casing stands against the borehole wall.

For the sake of brevity, we will call the fluid in place "mud" and the injected
fluid "spacer" in this section. It should be remembered, however, that many dif-
ferent fluids may be pumped in a cementing job.

The displacement efficiency of mud from the narrow part of an eccentric annulus
is determined, in the first place, by the following factors.

- the geometry of the annulus (i.e., the standoff);
- the yield stress and the plastic viscosity of the injected fluid as compared to the
  yield stress and plastic viscosity of the fluid in place;
- the density of the injected fluid as compared to the density of the fluid in place;
- the injection flow rate.

Reducing the standoff and making the mud thicker (or spacer thinner) will result
in poorer mud displacement, all the rest being equal. The effect of standoff and
rheology can be quantified through the *mobility ratio* defined as follows [7]:

$$\text{Mobility ratio} = \frac{w_{\max}\tau_Y^{(\text{mud})}}{w_{\min}\tau_Y^{(\text{sp})}} \tag{3.6}$$

where $w_{\min}$ and $w_{\max}$ are the minimum and the maximum distances between the
borehole wall and the casing, respectively; $\tau_Y^{(\text{mud})}$ and $\tau_Y^{(\text{sp})}$ are the yield stress values
of mud and spacer, respectively. The smaller the mobility ratio, the more efficient
the mud displacement will be.

Fig. 3.6 Fluid distribution in the annulus in simulation A (Table 3.1) after pumping 1275 L of spacer. Mobility ratio 3.74; flow rate 15 L/s. A 100-m interval is simulated. The annulus is shown unwrapped. Mud (fluid in place) is shown in *grey*. Spacer (injected fluid) is shown in *black*. The flow direction is upwards
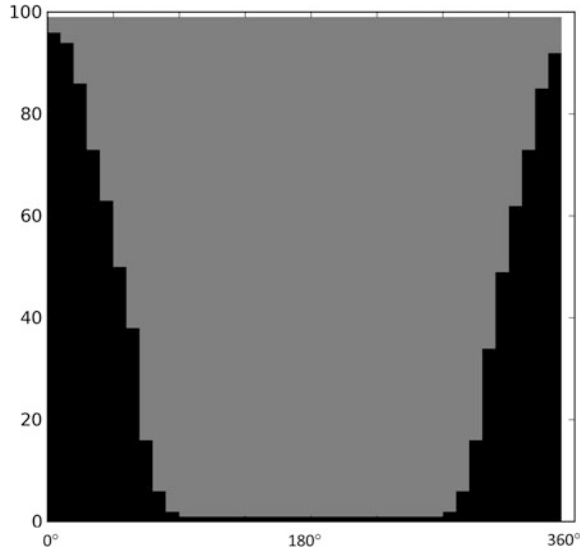
The effect of mobility ratio on mud displacement is illustrated in Figs. 3.6, 3.7, 3.8, 3.9, 3.10 and 3.11 using our simple kinematic model. Spacer is injected with the same flow rate of 15 L/s in these simulations (simulations A through F in Table 3.1). The plots in Figs. 3.6, 3.7, 3.8, 3.9, 3.10 and 3.11 show the fluid distribution in the annulus after 85 s of injection, i.e. after 1275 L of spacer has been pumped. The wider part of the annulus is located at the azimuth of 0°/360°. The narrow part of the annulus is at 180°. Channelization of spacer along the wider part of the annulus is evident in Figs. 3.6, 3.7, 3.8, 3.9, 3.10 and 3.11.

Fig. 3.7 Fluid distribution in the annulus in simulation B (Table 3.1) after pumping 1275 L of spacer. Mobility ratio 1.87; flow rate 15 L/s. A 100-m interval is simulated. The annulus is shown unwrapped. Mud (fluid in place) is shown in *grey*. Spacer (injected fluid) is shown in *black*. The flow direction is upwards
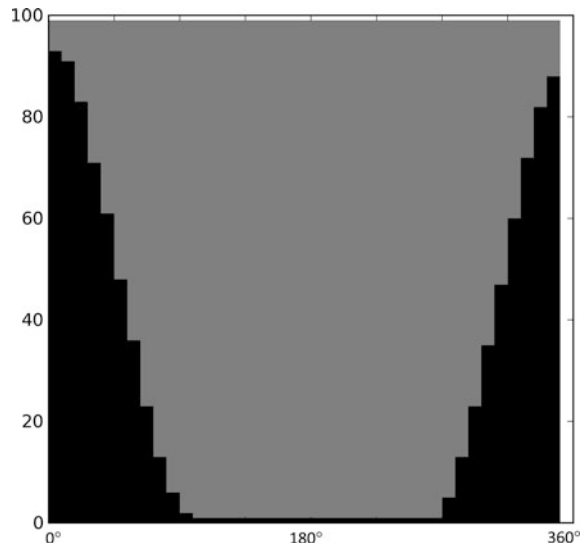
Fig. 3.8 Fluid distribution in the annulus in simulation C (Table 3.1) after pumping 1275 L of spacer. Mobility ratio 0.94; flow rate 15 L/s. A 100-m interval is simulated. The annulus is shown unwrapped. Mud (fluid in place) is shown in *grey*. Spacer (injected fluid) is shown in *black*. The flow direction is upwards

Fig. 3.9 Fluid distribution in the annulus in simulation D (Table 3.1) after pumping 1275 L of spacer. Mobility ratio 1.87; flow rate 15 L/s. A 100-m interval is simulated. The annulus is shown unwrapped. Mud (fluid in place) is shown in *grey*. Spacer (injected fluid) is shown in *black*. The flow direction is upwards
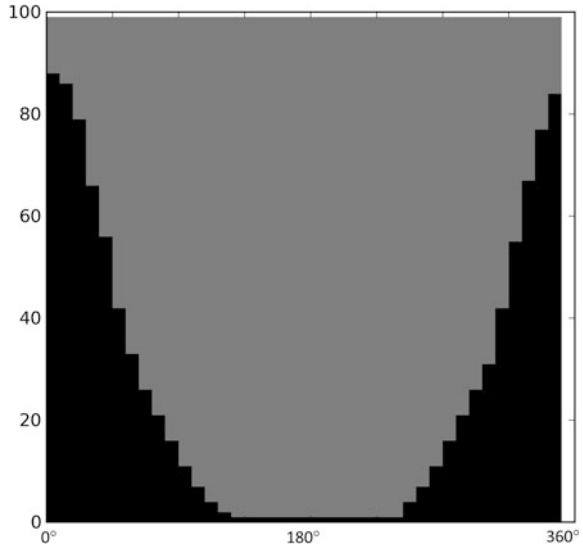

Increasing the yield stress of spacer (by a factor of two), while keeping the yield stress of the mud and the plastic viscosity of both the mud and the spacer unchanged, improves the displacement (compare Figs. 3.7 and 3.8). On the other hand, *increasing the plastic viscosity of the spacer* (by a factor of two), while keeping the plastic viscosity of mud and the yield stress of both the mud and the spacer unchanged, brings about only a marginal improvement (compare Figs. 3.7 and 3.9). This is one of the reasons why only yield stresses enter the mobility ratio
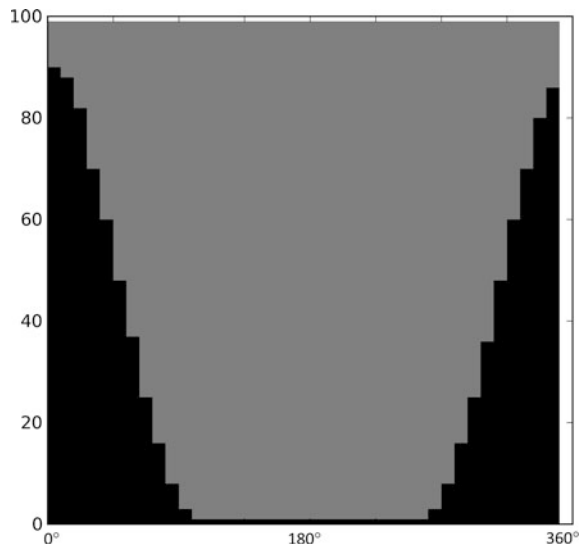
Fig. 3.10 Fluid distribution
in the annulus in simulation E
(Table 3.1) after pumping
1275 L of spacer. Mobility
ratio 0.94; flow rate 15 L/s.
A 100-m interval is simulated.
The annulus is shown
unwrapped. Mud (fluid in
place) is shown in *grey*.
Spacer (injected fluid) is
shown in *black*. The flow
direction is upwards

Fig. 3.11 Fluid distribution
in the annulus in simulation F
(Table 3.1) after pumping
1275 L of spacer. Mobility
ratio 0.47; flow rate 15 L/s.
A 100-m interval is simulated.
The annulus is shown
unwrapped. Mud (fluid in
place) is shown in *grey*.
Spacer (injected fluid) is
shown in *black*. The flow
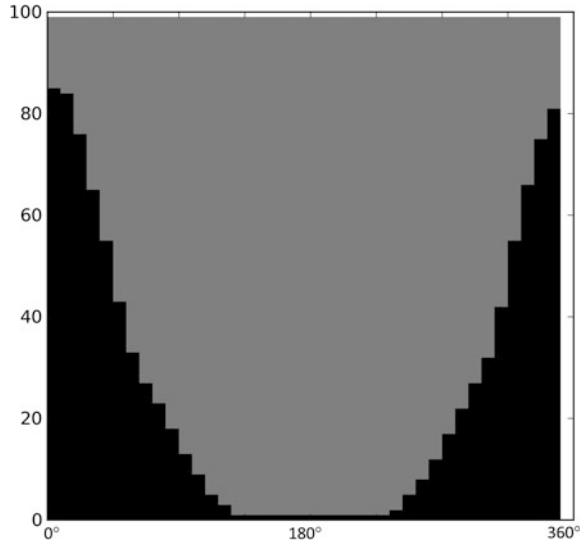direction is upwards
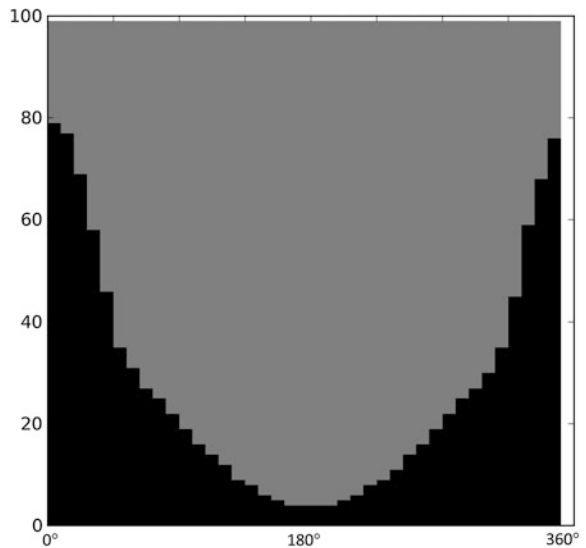
[Eq. (3.6)]: the mobility ratios in Figs. 3.7 and 3.9 are equal, while in Figs. 3.7 and
3.8 they differ by a factor of two (Table 3.1).

Out of the six simulations, A though F, only in F flow has been initiated in the
entire mud (Fig. 3.11). This is the simulation with the lowest mobility ratio, 0.47.

The effect of mobility ratio on mud displacement has also been observed in
laboratory experiments [11]. Because of the mobility effect, it is recommended that
cement has higher yield stress and plastic viscosity than mud, in order to ensure

Table 3.1 Simulations with standoff 70 % (casing diameter 0.34 m, wellbore diameter 0.406 m, $w_{\min} = 0.023$ m, $w_{\max} = 0.043$ m)

Simulation ID	Fluid in place (mud)		Pumped fluid (spacer)		Mobility ratio	Pumping rate (L/s)	Snapshot after pumping 1275 L
	Yield stress (Pa)	Plastic viscosity (cP)	Yield stress (Pa)	Plastic viscosity (cP)			
A	20	20	10	10	3.74	15	Figure 3.6
B	10	10	10	10	1.87	15	Figure 3.7
C	10	10	20	10	0.94	15	Figure 3.8
D	10	10	10	20	1.87	15	Figure 3.9
E	10	10	20	20	0.94	15	Figure 3.10
F	10	10	40	10	0.47	15	Figure 3.11
G	10	10	10	10	1.87	300	Figure 3.12

effective mud displacement and to minimize bypassing. This can be achieved either by thickening the cement or by thinning the mud. As stressed by Clark and Carter, having a thin, well-conditioned mud in the annulus before starting the cementing job is essential for high-quality well cementing [11].

As pointed out by McLean et al. [7], the mobility ratio provides only an approximate indicator of whether mud will be bypassed by spacer or not. Pumping with a higher flow rate at the given mobility ratio produces higher pressure differential along the flowing part of the annulus. The same higher pressure differential acts on the non-flowing fluid (mud in the narrowest part of the annulus). As a result, the critical pressure gradient required to initiate flow of the mud can be overcome in narrower parts of the annulus than it would otherwise be at a lower flow rate. This will increase the displacement efficiency.

The effect of the flow rate is illustrated in Fig. 3.12 (simulation G in Table 3.1). The mobility ratio in this simulation is 1.87, which would result in spacer bypassing mud when the flow rate was 15 L/s (see Fig. 3.7). With the flow rate of 300 L/s, mud is displaced in the entire annulus, including the narrowest part of it. It should be remarked that the flow would most likely be turbulent at such high flow rate. However, since our purpose is demonstration only, the same model of laminar flow was used to perform simulation G as the other simulations listed in Table 3.1.

The improved displacement efficiency observed with higher flow rate in an eccentric annulus (Figs. 3.12 vs. 3.7) is easy to grasp: Higher flow rate generates higher frictional pressure loss in the wider part of the annulus. The same pressure gradient acts on the fluids in the narrow part of the annulus as in the wider part. Thus, the higher pressure gradient is applied also on the narrow part. This improves the mud displacement in the narrow part as well. The frictional drag force between the "tubes", neglected in the simulations, will be higher with high flow rates, too, which will additionally contribute to improved displacement at higher rates.

On the other hand, for yield stress fluids such as spacer or cement, a lower flow rate leads to a flatter velocity profile across the annular gap. Such velocity profiles

Fig. 3.12 Fluid distribution in the annulus in simulation G (Table 3.1) after pumping 1275 L of spacer. Mobility ratio 1.87; flow rate 300 L/s. A 100-m interval is simulated. The annulus is shown unwrapped. Mud (fluid in place) is shown in *grey*. Spacer (injected fluid) is shown in *black*. The flow direction is upwards
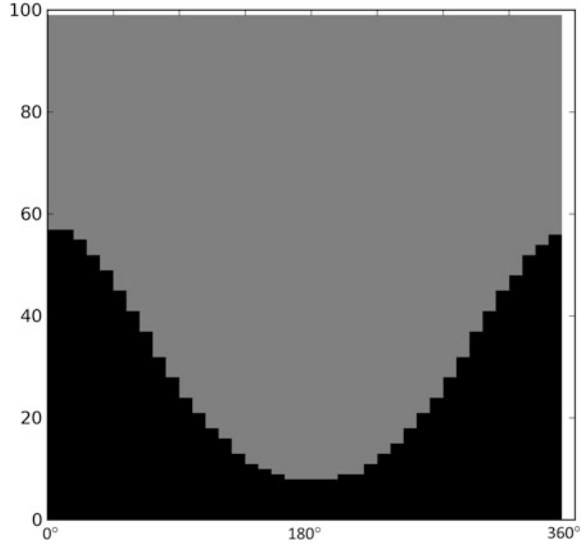

might be beneficial for removing mud from the walls in the annulus [2]. This effect cannot be captured in our essentially two-dimensional kinematic model.

In addition to affecting the displacement efficiency, eccentric positioning of the casing pipe results in lower annular pressure loss than what would be the case with a centered casing. In Fig. 3.13, the annular pressure loss obtained in simulation C is compared to the annular pressure loss obtained in a simulation in which the fluids and the pumping rate were the same as in simulation C, but the casing was centered (standoff 100 %). The annular pressure loss is lower with the standoff of 70 % as compared to the standoff of 100 %.

Experiments by Kelessidis et al. [12] show that the reduction in the annular frictional pressure loss caused by eccentricity are more pronounced for yield-stress fluids than they are for Newtonian fluids.

Increasing the density of the displacing fluid should have a similar effect to increasing its rheological properties, i.e., mud displacement should become more efficient as the spacer-to-mud density ratio increases (Fig. 3.14). Experiments show, however, that at downhole conditions the effect of density (buoyancy) on mud displacement might be less significant than the effect of rheology [11]. The effect of density contrast between spacer and mud is reduced by mud gelation and by fluid loss from the mud into permeable formations.

It was mentioned in Sect. 3.2 that azimuthal flows were neglected in our kinematic model. In reality, such flows may contribute to better distribution of the displacing fluid in the annulus, also in its narrow part [2, 7]. This is schematically illustrated in Fig. 3.15 where arrows indicate the flow paths the spacer might take in a well, namely from the wider side towards the narrower side of the annulus. Such flows, observed experimentally by Tehrani et al. [13], can facilitate the mud displacement.
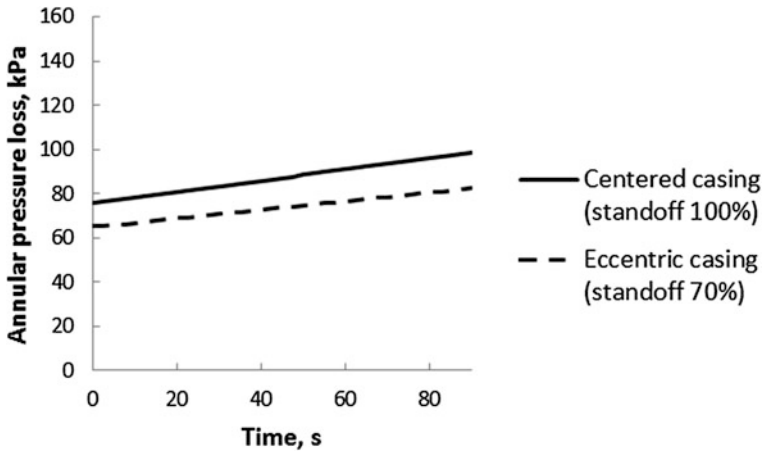
Fig. 3.13 Annular pressure loss over a 100-m interval versus time in simulation C (Table 3.1, standoff 70 %) and a simulation with the same fluid properties and flow rate but a standoff of 100 % (centered casing)

Fig. 3.14 Schematic plot of displacement efficiency in an eccentric annulus as a function of flow rate for spacers of different densities. The mud density is the same for both *curves*. The spacer density is greater for the *solid curve*. Based on the results of laboratory experiments reported in Ref. [7]
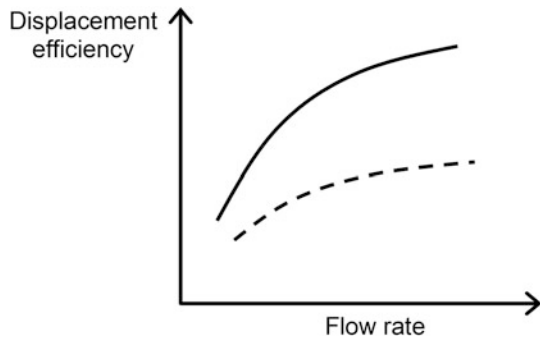
The relative strength of the azimuthal flows, as compared to the flow along the wellbore, can be estimated by dividing the gravity-induced driving force by the inertia-induced driving force. The gravity-induced driving force is given by $\left[\rho^{(\mathrm{sp})} - \rho^{(\mathrm{mud})}\right]gL$, where L is the length of the interval being cemented, g is the acceleration of gravity, and $\rho^{(\mathrm{mud})}, \rho^{(\mathrm{sp})}$ are the densities of mud and spacer, respectively. The inertia-induced driving force is given by $\rho^{(\mathrm{sp})}\bar{v}^2/2$, where $\bar{v}$ is the average fluid velocity in the annulus, i.e. the flow rate divided by the annulus cross-section area. The non-dimensional group that characterizes the strength of azimuthal flows is then given by $2\left[\rho^{(\mathrm{sp})} - \rho^{(\mathrm{mud})}\right]gL/\rho^{(\mathrm{sp})}\bar{v}^2$ [13].

In summary, mud displacement is improved by centering the pipe (Fig. 3.16). According to some industrial guidelines, a minimum standoff of 67 % (80 % for cementing liners) should be maintained in order to obtain good quality of cementing

Fig. 3.15 Azimuthal flows (indicated by *white arrows*) in an eccentric annulus
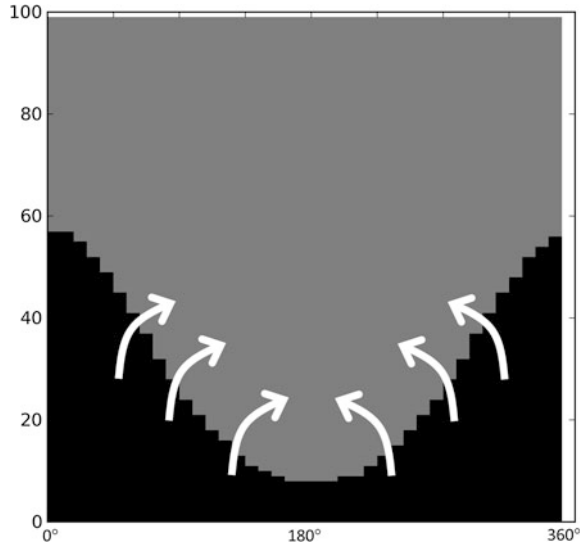

Fig. 3.16 Schematic plot of displacement efficiency in an eccentric annulus as a function of time for different standoffs. The fluid properties are the same for *both curves*. The standoff is greater for the *solid curve*. Based on the results reported in Ref. [2]
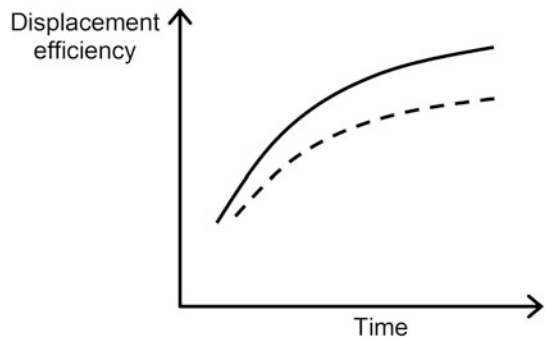
[14]. Others recommend a minimum standoff of 75 % [2]. Maintaining sufficient standoff is more difficult to achieve in deviated and horizontal wells than in vertical wells. Better mud displacement from an eccentric annulus can be achieved by the following measures:

- increasing the yield stress, the plastic viscosity, and the density of spacer and cement;
- thinning the mud;
- increasing the pump rate;
- moving the casing pipe (Sect. 3.9).

3.4 Effect of Borehole Shape

The cross-section of a borehole is rarely circular. The borehole wall can be damaged by the drillstring action during drilling. The wellbore will thereby acquire an irregular shape. The resulting local enlargements of the borehole are known as *washouts* and can be identified from caliper logs. Another type of borehole enlargement is *breakouts*. Breakouts usually appear as two more or less symmetric enlargements of the borehole on the opposite sides of the borehole cross-section [15]. Breakouts are often caused by in situ stress anisotropy (Fig. 3.17), but may also appear under isotropic stress conditions.

In this section, we will use our kinematic model to explore the effects of three kinds of borehole cross-section irregularities on primary cementing of a vertical well:

- a slightly irregular cross-section;
- washouts;
- breakouts.

The casing is assumed to be centered with regard to the original (perfectly circular) wellbore in all cases considered in this section.

A slightly irregular cross-section is introduced by slightly varying, at random, the areas of the equivalent sectors. The standard deviation of the sector area is set equal to 4.1 % of the average sector area in our example. Five simulations with different rheological parameters are performed (Table 3.2). The pumping rate is the same in all simulations (15 L/s). The densities of mud and cement are equal in all simulations.

The displacement results after 10 and 150 s of pumping are shown in Figs. 3.18, 3.19, 3.20, 3.21 and 3.22 for simulations 1 through 5, respectively. The results suggest that an irregular borehole cross-section may lead to viscous fingering, if the

Fig. 3.17 Borehole breakouts in a *vertical well*. The directions of the minimum (S_{min}) and maximum (S_{max}) horizontal in situ stresses are indicated by *arrows*
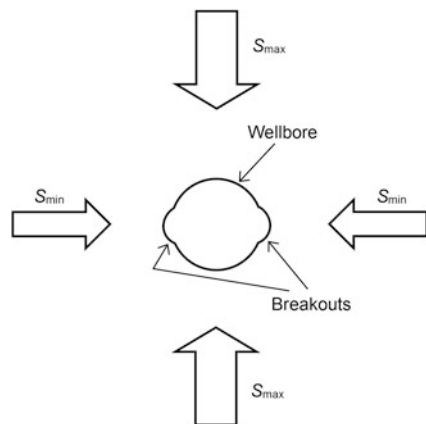
Table 3.2 Simulations with centered casing and slightly irregular wellbore (casing diameter 0.34 m, wellbore diameter 0.403 m)

Simulation ID	Fluid in place (mud)		Pumped fluid (spacer)		Pumping rate (L/s)	Results
	Yield stress (Pa)	Plastic viscosity (cP)	Yield stress (Pa)	Plastic viscosity (cP)		
1	20	20	10	10	15	Figure 3.18
2	20	20	10	20	15	Figure 3.19
3	20	20	20	10	15	Figure 3.20
4	20	20	20	20	15	Figure 3.21
5	10	10	20	20	15	Figure 3.22

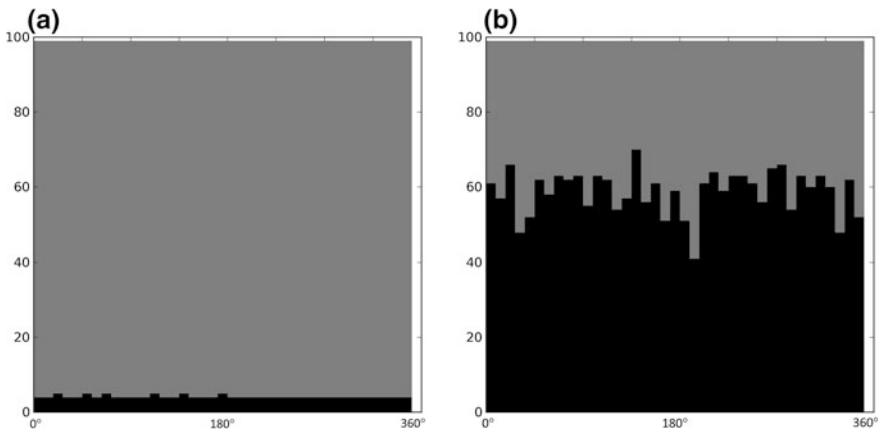**Fig. 3.18** Fluid distribution in the annulus in simulation 1 (Table 3.2) after pumping 150 L (**a**) and 2250 L (**b**) of spacer. Flow rate 15 L/s. A 100-m interval is simulated. The annulus is shown unwrapped. Mud (fluid in place) is shown in *grey*. Spacer (injected fluid) is shown in *black*. The flow direction is upwards

injected fluid has sufficiently lower rheological properties than the fluid in place (simulations 1 and 2, Figs. 3.18 and 3.19).

In order to estimate the extent of fingering in Simulations 1 through 5, it is instructive to quantitatively describe the shape of the mud-spacer interface, and its evolution during the injection. We choose the standard deviation of the interface's vertical position as the measure of interface variability. As the displacement proceeds, the standard deviation increases for all five simulations (Fig. 3.23). The greatest increase is observed in simulation 1, i.e., when both the plastic viscosity and the yield stress of the injected fluid (spacer) are lower than those of the fluid in place (mud). The variation in the interface position is the least in simulation 5, i.e. when both the plastic viscosity and the yield stress of the injected fluid (spacer) are higher than those of the fluid in place (mud). Still, the standard deviation is nonzero and is increasing over time even in the case of the most favorable mobility ratio
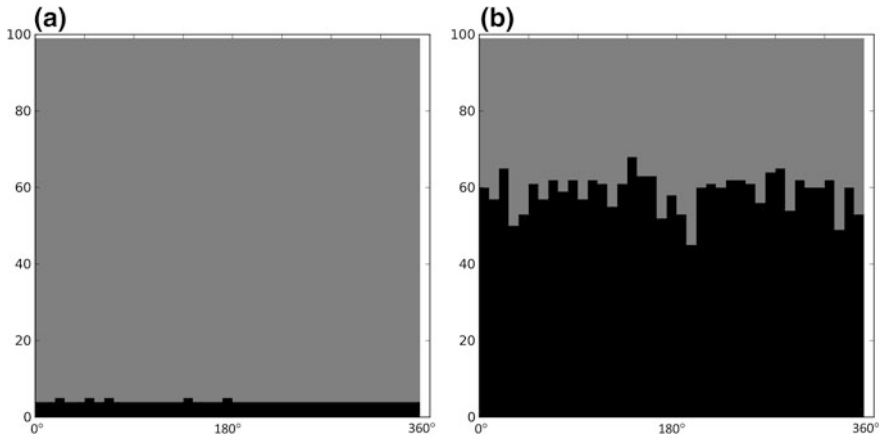
Fig. 3.19 Fluid distribution in the annulus in simulation 2 (Table 3.2) after pumping 150 L (**a**) and 2250 L (**b**) of spacer. Flow rate 15 L/s. A 100-m interval is simulated. The annulus is shown unwrapped. Mud (fluid in place) is shown in *grey*. Spacer (injected fluid) is shown in *black*. The flow direction is upwards
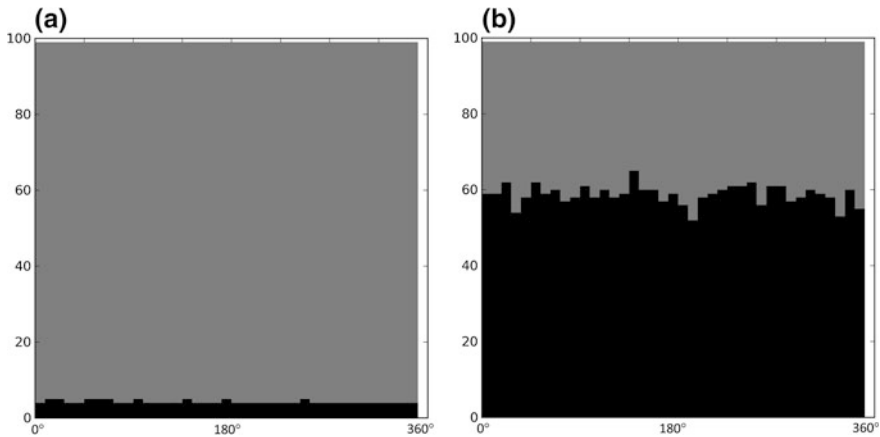

Fig. 3.20 Fluid distribution in the annulus in simulation 3 (Table 3.2) after pumping 150 L (**a**) and 2250 L (**b**) of spacer. Flow rate 15 L/s. A 100-m interval is simulated. The annulus is shown unwrapped. Mud (fluid in place) is shown in *grey*. Spacer (injected fluid) is shown in *black*. The flow direction is upwards

(simulation 5). This suggests that we should rather use the normalized standard deviation, i.e. the standard deviation divided by the average propagation distance of the interface (which is determined by the pumping rate and the pumping time). This quantity is plotted in Fig. 3.24. The normalized standard deviation remains unchanged (after some initial fluctuations) in simulation 4, i.e. when the rheological properties of the fluid in place and of the injected fluid are identical. The normalized

Fig. 3.21 Fluid distribution in the annulus in simulation 4 (Table 3.2) after pumping 150 L (**a**) and 2250 L (**b**) of spacer. Flow rate 15 L/s. A 100-m interval is simulated. The annulus is shown unwrapped. Mud (fluid in place) is shown in *grey*. Spacer (injected fluid) is shown in *black*. The flow direction is upwards
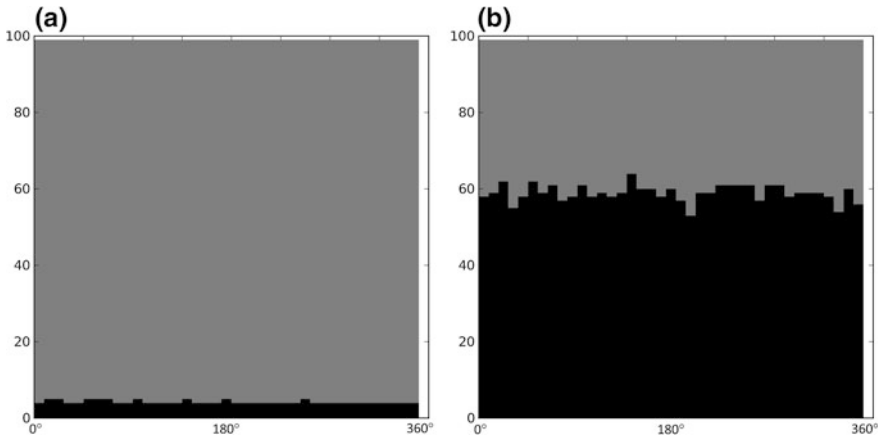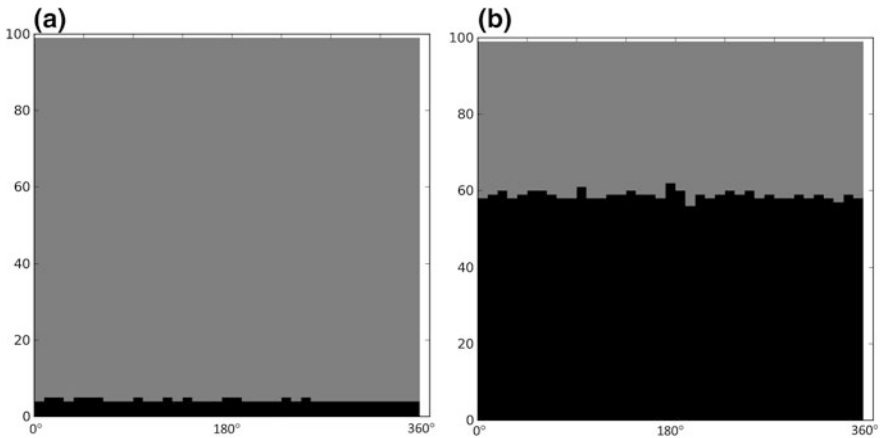

Fig. 3.22 Fluid distribution in the annulus in simulation 5 (Table 3.2) after pumping 150 L (**a**) and 2250 L (**b**) of spacer. Flow rate 15 L/s. A 100-m interval is simulated. The annulus is shown unwrapped. Mud (fluid in place) is shown in *grey*. Spacer (injected fluid) is shown in *black*. The flow direction is upwards

standard deviation decreases in simulation 5 (favorable mobility ratio) and increases in simulations 1, 2, and 3 (unfavorable mobility ratios).

The phenomenon evident in Figs. 3.18 and 3.19 is *viscous instability* (also known as *Rayleigh-Taylor instability*). Let us find out why viscous instability develops with unfavorable mobility ratio, and why it does not do so with favorable mobility ratio. We assume for now that the densities of the two fluids are equal.

Fig. 3.23 Standard deviation of mud-spacer interface position along the wellbore axis versus pumping time. Settings of simulations 1 through 5 are given in Table 3.2
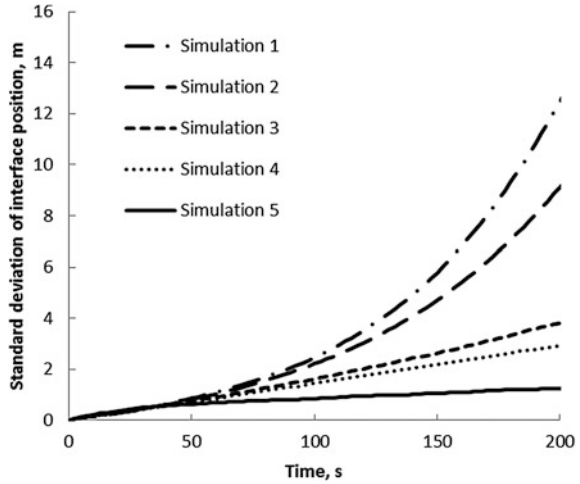
Fig. 3.24 Standard deviation of mud-spacer interface position along the wellbore axis normalized by the average interface propagation distance versus pumping time. Settings of simulations 1 through 5 are given in Table 3.2
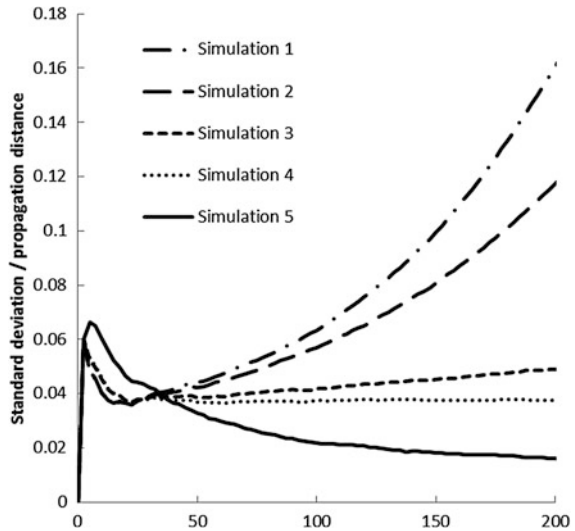
Consider first the case where the displacing fluid has lower yield stress and lower plastic viscosity than the fluid in place does. The mobility ratio is thus unfavorable. Consider two tubes in our kinematic model, with different positions of the interface (Fig. 3.25). The difference in the interface position can be due to e.g. fluctuations caused by irregular wellbore cross-section. Since the two tubes in Fig. 3.25 are parts of the same annulus, the same fluid-pressure differential acts between the ends of both tubes. Since the less viscous fluid occupies a larger part of tube B than of tube A ($L_4 > L_2$), the flow resistance in tube B is smaller than in tube A. The fluid velocity in tube B will therefore be greater than in tube A. Thus, the interface between the two fluids is moving upwards faster in tube B than it is in tube A.

Fig. 3.25 Illustration of annular displacement with unfavorable mobility ratio: a less viscous fluid displaces a more viscous one. The flow direction is shown with an *arrow*. The interface between the fluids has advanced farther up in the *right-hand* tube than in the *left-hand* tube, e.g. because of perturbations caused by irregular wellbore shape
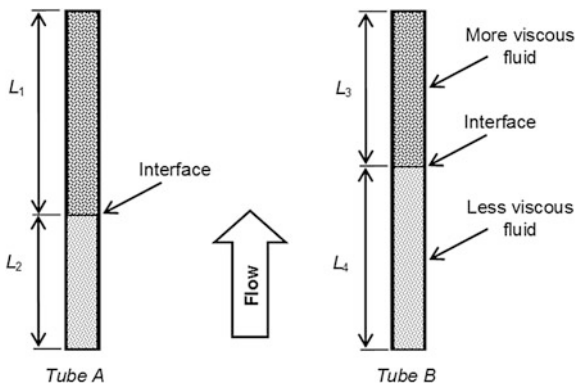
Fig. 3.26 Illustration of annular displacement with favorable mobility ratio: a more viscous fluid displaces a less viscous one. The flow direction is shown with an *arrow*. The interface between the fluids has advanced farther up in the *right-hand* tube than in the *left-hand* tube, e.g. because of perturbations caused by irregular *wellbore shape*
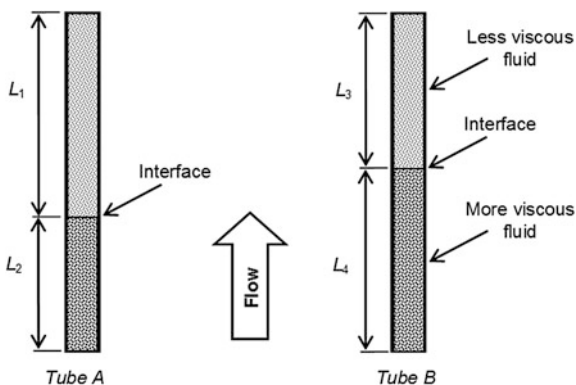
Hence, a small difference in the interface positions in the tubes, once created by e.g. irregular wellbore profile, will be increasing as the flow continues. The annular flow is thus unstable in this case since a small fluctuation in the shape of the mud-spacer interface will increase over time.

Consider now the case where a more viscous fluid is displacing a less viscous fluid (Fig. 3.26). In this case, if, by some fluctuation, the interface in tube B gets ahead of the interface in tube A, the flow resistance in tube B will increase ($L_4 > L_2$). The fluid velocity in tube B will therefore decrease. This will slow down the interface advancement in tube B. Thus, favorable mobility ratio has a stabilizing effect on the flow.

The physics illustrated in Figs. 3.25 and 3.26 explains why it is more advantageous to pump fluids of progressively higher rheology during well cementing jobs. Exceptions are, or course, possible, if e.g. one intends to clean the mud from pockets or from the walls by using turbulent flow. Creating turbulent flow with a higher-rheology fluid may violate the lost-circulation pressure of the formation and may thereby jeopardize the entire cementing job.

Current industrial practices stipulate that the frictional pressure loss of the displacing fluid should be at least 20 % higher than that of the fluid being displaced, in order to prevent mud by-passing [1]. In addition, the frictional pressure loss of the displacing fluid should be sufficiently large to break the gel of the fluid in place. In an eccentric annulus, this imposes the following condition on the frictional pressure gradient of the displacing fluid, $(dP_{fr}/dz)^{(sp)}$ [1]:

$$\left(\frac{dP_{fr}}{dz}\right)^{(sp)} = \frac{2\tau_{gel}^{(mud)}}{(R_o - R_i)s} - \left[\rho^{(sp)} - \rho^{(mud)}\right]g \cos i \qquad (3.7)$$

where superscripts "mud" and "sp" refer to the fluid in place and the displacing fluid, respectively; τ_{gel} is the gel strength; ρ is the fluid density; R_i and R_o are the inner and the outer annular radii, respectively; s is the standoff factor (1 for standoff 100 %; 0 for the casing touching the wellbore wall); i is the angle of well inclination; g is the acceleration of gravity.

Even though mud having lower yield stress is easier to displace during a well cementing job, low yield stress facilitates solids settling in the mud. In a deviated or horizontal well, this may lead to the increase of mud density and rheology at the lower side of the annulus, as discussed later in this chapter. There is, thus, a trade-off between lowering the mud rheological properties (to facilitate mud displacement) and keeping them (in particular, the yield stress and the gel strength) sufficiently high to prevent solids settling.

Densities of both fluids were assumed to be equal so far in this section. What happens if they are different? Similarly to the viscous instability considered above, a *gravity instability* may develop if the displacing fluid is lighter than the fluid in place.

Consider again two tubes (Fig. 3.27). Assume now that the two fluids have the same rheological properties, but different densities. Assume again that, by virtue of some fluctuation in the system, the interface in tube B advanced somewhat ahead of the interface in tube A. The difference in the interface position can be due e.g. to

Fig. 3.27 Illustration of annular displacement with unfavorable density ratio: a lighter fluid displaces a heavier one. The flow direction is shown with an *arrow*. The interface between the fluids has advanced farther up in the *right-hand* tube than in the *left-hand* tube, e.g. because of perturbations caused by irregular *wellbore shape*
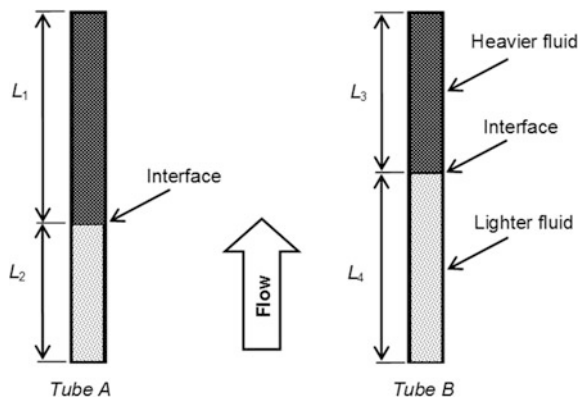
fluctuations caused by irregular wellbore cross-section. Since the two tubes in Fig. 3.27 are parts of the same annulus, the same fluid-pressure differential exists between the ends of both tubes. This pressure differential is a sum of two components: the one due to gravity (hydrostatic component) and the one due to the frictional pressure loss. Since the heavier fluid occupies a larger part of tube A than of tube B ($L_1 > L_3$), the hydrostatic component of the pressure differential is greater in tube A than in tube B. Since the total pressure differentials are equal in the two tubes, the frictional pressure loss must be smaller in tube A than in tube B. This can only be achieved if the fluid velocity in tube A is smaller than in tube B since the rheological properties of the fluids are assumed to be identical. The fluid velocity in tube B will therefore be greater than in tube A. Thus, the interface between the two fluids will be moving upwards faster in tube B than in tube A. Hence, a small difference in the interface positions in the tubes, once created by e.g. irregular wellbore profile, will be increasing as the flow continues. The annular flow is thus unstable in this case since a small fluctuation in the shape of the mud-spacer interface will increase over time.

The opposite happens if the density of the displacing fluid is greater than that of the fluid in place (Fig. 3.28). The pressure differential is again equal in both tubes, but the hydrostatic component of the pressure differential is now greater in tube B. As a result, the frictional pressure loss in tube B is smaller than in tube A. The fluid velocity is therefore lower in tube B, and so is the propagation speed of the interface. Thus, the head start that the interface might have in tube B will be reduced. The favorable density ratio, with the displacing fluid being heavier than the fluid in place, thus acts as a stabilizing factor. It prevents the gravity instability.

Laboratory experiments carried out at downhole conditions suggest that the effect of gravity may be less important downhole [11]. As pointed out by Clark and Carter [11], in order for the buoyancy to have an effect on the annular flow and displacement, the fluid in place must be mobile. Mud is likely to have a reduced mobility at downhole conditions because of two mechanisms: (i) fluid loss into the permeable formation increases the mud yield stress; (ii) elevated downhole temperatures increase the mud yield stress. Therefore, the first priority must be to design the displacing fluids so that their mobility is lower than that of the mud. Making the

Fig. 3.28 Illustration of annular displacement with favorable density ratio: a heavier fluid displaces a lighter one. The flow direction is shown with an *arrow*. The interface between the fluids has advanced farther up in the *right-hand* tube than in the *left-hand* tube, e.g. because of perturbations caused by irregular *wellbore shape*
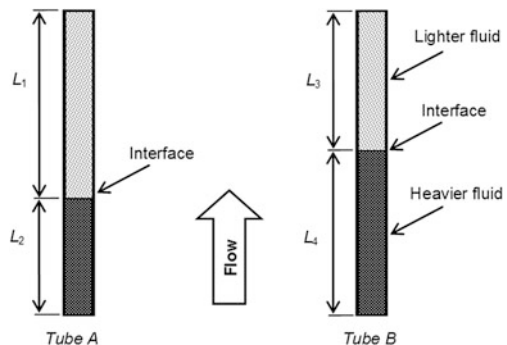
Table 3.3 Simulations with borehole breakouts (casing diameter 0.34 m, wellbore diameter 0.406 m, standoff 100 %, $w_{min} = 0.033$ m, $w_{max} = 0.1142$ m)

Simulation ID	Fluid in place (mud)		Pumped fluid (cement)		Mobility ratio	Pumping rate (L/s)
	Yield stress (Pa)	Plastic viscosity (cP)	Yield stress (Pa)	Plastic viscosity (cP)		
B1	20	20	10	10	6.92	15
B2	10	10	20	20	1.73	15
B3	10	10	40	40	0.87	15

displacing fluid much less buoyant than the fluid in place is unlikely to improve the displacement significantly if the mobility of the former is still higher than that of the latter. The displacing fluid should, however, be sufficiently dense to avoid gravity instabilities. According to current industrial practices, the displacing fluid should be at least 10 % heavier than the fluid in place for a stable displacement [1].

Borehole breakouts may cause substantial channelization of the annular flow during well cementing, even with favorable mobility ratios. To illustrate this point, we run three simulations with the fluid properties listed in Table 3.3.

The mobility ratio in Table 3.3 was calculated based on Eq. (3.6), with w_{min} being the annular gap in the well without breakouts, and w_{max} being the annular gap at the maximum depth of breakouts. Breakouts were created as two symmetrical grooves running along the entire 100-m-long interval and located at azimuths 90° and 270°.

The position of the displacement front after 50 s of injection is shown in Figs. 3.29, 3.30 and 3.31 for simulations B1, B2 and B3, respectively. It is evident from these Figures that most of the displacing fluid flows in the breakouts, even in

Fig. 3.29 Fluid distribution in the annulus in simulation B1 (Table 3.3) after pumping 750 L of cement. Mobility ratio 6.92; flow rate 15 L/s. A 100-m interval is simulated. The annulus is shown unwrapped. Mud (fluid in place) is shown in *grey*. Spacer (injected fluid) is shown in *black*. The flow direction is upwards
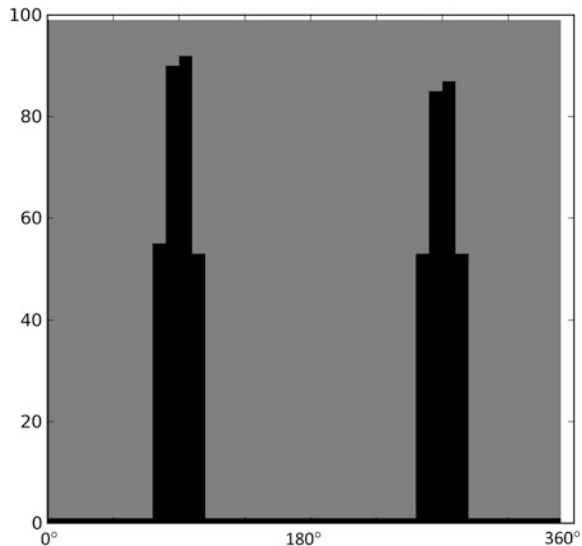
Fig. 3.30 Fluid distribution in the annulus in simulation B2 (Table 3.3) after pumping 750 L of cement. Mobility ratio 1.73; flow rate 15 L/s. A 100-m interval is simulated. The annulus is shown unwrapped. Mud (fluid in place) is shown in *grey*. Spacer (injected fluid) is shown in *black*. The flow direction is upwards
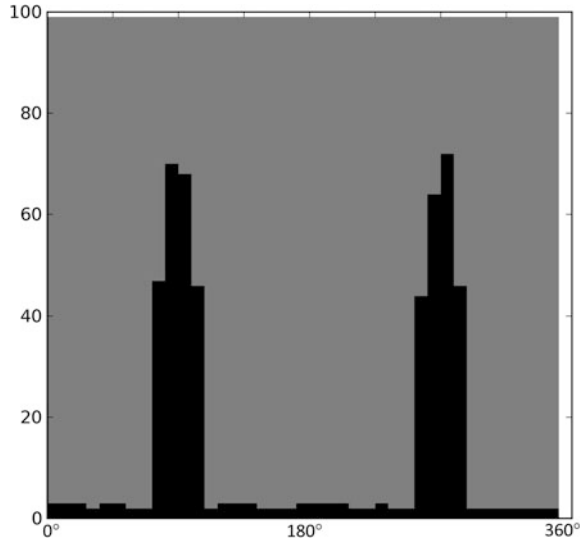
Fig. 3.31 Fluid distribution in the annulus in simulation B3 (Table 3.3) after pumping 750 L of cement. Mobility ratio 0.87; flow rate 15 L/s. A 100-m interval is simulated. The annulus is shown unwrapped. Mud (fluid in place) is shown in *grey*. Spacer (injected fluid) is shown in *black*. The flow direction is upwards
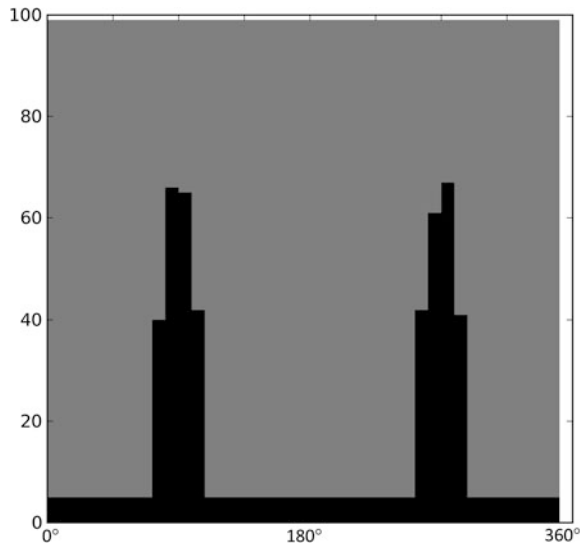
the case of a favorable mobility ratio (simulation B3, Fig. 3.31). The displacement front in the rest of the annulus is significantly delayed with respect to the displacement in the breakouts. Figures 3.29, 3.30 and 3.31 demonstrate how important it is to have an in-gauge hole without breakouts for a successful cementing job.

Washouts, i.e. local enlargements of the borehole caused by the drillstring action or by the erosion due to the drilling fluid flow in the annulus, reduce the quality of annular cementing [11]. Unlike breakouts, a washout will hardly cause significant

Fig. 3.32 Effect of a washout
on annular flow and
displacement. *Dashed lines*
indicate the boundaries of
unyielded regions. The fluid
has non-Newtonian,
yield-stress rheology
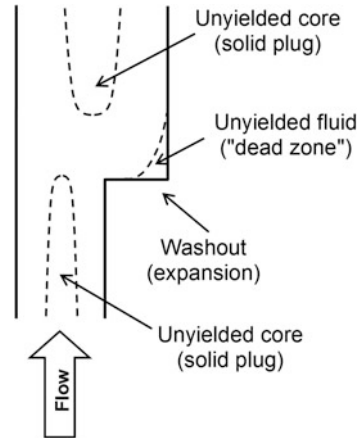
channelization of the displacing fluid through the mud. It is, however, difficult to fully displace mud (and possibly formation fluids) accumulated in a washout. As a result, pockets of undisplaced mud may be left in washouts. Even though such pockets might provide only a marginal contribution to hydraulic conductivity along the cemented well, they may nonetheless compromise well integrity by acting as stress concentrators during the subsequent life of the well (Chaps. 5 and 6). On top of that, mud located in a washout may be in gelled or dehydrated state. If such mud becomes mobilized during annular flow and displacement, it may contaminate the cement and thereby compromise the quality of well cementing.

The reason for poor displacement from a washout is that the annular velocity is reduced by the wellbore enlargement, which makes the displacement process locally less effective. Another factor contributing to poor displacement from a washout is non-Newtonian, yield-stress rheology of the fluid in place. This leads to the establishment of "dead zones" in the washout [16]. The fluid occupying these zones is not yielded (Fig. 3.32).

Interestingly, the size and shape of the flowing volume in the washout become virtually independent of the washout depth and shape if the washout is sufficiently deep (Fig. 3.33) [17]. As the washout depth increases, it becomes thus increasingly more difficult to mobilize the mud left in it. At the same time, the exact shape of the washout virtually does not affect the flow details in such deep washouts.

A washout may somewhat affect the frictional pressure loss in the annulus. In the presence of a washout, this pressure loss is smaller than it would otherwise be in an in-gauge well. However, since the bottomhole pressure in a cementing job is usually dominated by the hydrostatic pressure, the effect of a washout on the bottomhole pressure during well cementing is minor [17].

Fig. 3.33 Effect of the
washout depth on the
stationary ("dead") zone
inside the washout. See
Fig. 3.32 for labelling of the
different regions. The fluid
has non-Newtonian,
yield-stress rheology. Based
on the numerical results
reported in Ref. [17]
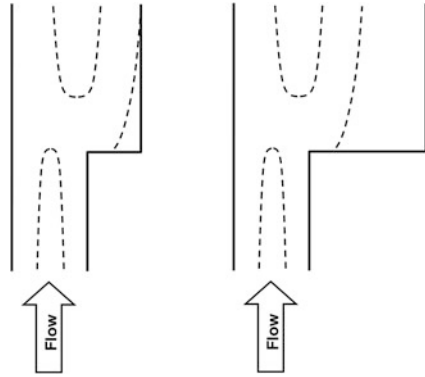
3.5   Lost Circulation

Bottomhole pressure (BHP) during a cementing job should stay below a certain
threshold, known as the *lost-circulation pressure* [18]. If BHP exceeds the
lost-circulation pressure, natural fractures crossed by the wellbore may open up and
start accepting cement. At sufficiently high BHP, new fractures can be induced
around the well that may accept cement, too, or may connect the wellbore to a
natural fracture network. The result in all these scenarios is that cement will be
partially lost into the formation instead of being placed in the annulus.

The lost-circulation pressure puts a limit on the maximum BHP and equivalent
circulating density (ECD) allowed in a well cementing job. As a result, even though
higher flow rates normally result in better mud displacement, the flow rate cannot be
increased indefinitely since at some point formation will fracture, and circulation
will be lost.

In order to prevent lost circulation during cementing jobs, all fractures exposed
or created during drilling should, ideally, be sealed by lost circulation material
(LCM) before cementing starts [2]. LCM is typically a particulate material that can
be pumped downhole and be deposited inside fractures, thereby reducing the
subsequent loss of mud, spacer, and cement into the fractures. Lost circulation
materials can also be added to cement in order to minimize cement losses if they
occur.

Lost circulation can be induced when running the casing pipe into the well. If the
casing is lowered into the wellbore too fast, the bottomhole pressure may increase
so much that it will exceed the lost-circulation pressure [3]. Pressure surges at the
bottomhole may also be induced by free fall of cement [19].

It should be clear from the above that avoiding lost circulation in well cementing
requires that the lost-circulation pressure is known and can be used when designing
the cement job. The lost-circulation pressure can be evaluated by performing an
extended leakoff test (XLOT). This test is performed after the casing has been set
and cemented. The results of the test, therefore, can only provide the lost-circulation
pressure for the next interval to be drilled, and only at one location, i.e., just below

the last casing shoe. The lost-circulation pressure (formation breakdown pressure; reopening pressure for natural fractures) in the interval to be cemented can therefore only be obtained by extrapolating the XLOT data available at the last casing point, by using information from offset wells, or by both.

In summary,

- acquiring reliable and accurate information about in situ stresses and lost-circulation pressure,
- plugging fractures induced or exposed during drilling, before cementing begins,
- keeping the bottomhole circulating pressure below the lost-circulation pressure, and
- reducing the bottomhole pressure surges caused, e.g., by running the casing pipe into the wellbore or by free fall of cement

will reduce the risk of lost circulation in primary well cementing jobs.

3.6   Effect of Well Inclination

High-angle wells (deviated or horizontal) are more difficult to cement than vertical wells. In particular, the issue of mud channels is exacerbated in deviated and horizontal wells. The following factors and mechanisms are responsible for poor cement jobs in deviated and horizontal wells:

- It is more difficult to centralize the pipe.
- Solid particles present in mud may settle onto the lower side of the annulus.
- Deviated and horizontal wells are usually more prone to breakouts.
- Wall erosion by the drill pipe action may lead to a keyhole-shaped cross-section in deviated and horizontal wells.

The inability to center the pipe leads to poor displacement efficiency. In laminar flow, it leads to channeling on the wider side and undisplaced mud left on the narrower side of the annulus. In turbulent flow, eccentricity leads to turbulence developing only on the wider side of the annulus, with poor or no displacement from the narrower side [5].

Settling of solid particles present in mud (primarily weighting agents, e.g. barite, and drill cuttings) results in thickening of the mud located at the lower side of the annulus (Fig. 3.34) [20]. It also increases the density of the mud in that part of the annulus [20]. Displacing thicker and heavier mud from the lower part of the annulus may require the rheological properties of preflushes and of cement to be higher than what normally would be required to displace the mud from the rest of the annulus.

The rate of accumulation of solid particles on the lower side of the annulus is proportional to $\mathbf{v}_\infty \sin i$, where $\mathbf{v}_\infty$ is the terminal settling velocity of the particles; i is the angle between the wellbore and the vertical direction [20]. Hence, the accumulation rate increases with the well angle, making a horizontal well most prone to mud channel formation by this mechanism.

Fig. 3.34 Schematic view of
solids settling and
accumulating in the lower part
of the annulus in a *deviated* or
horizontal well
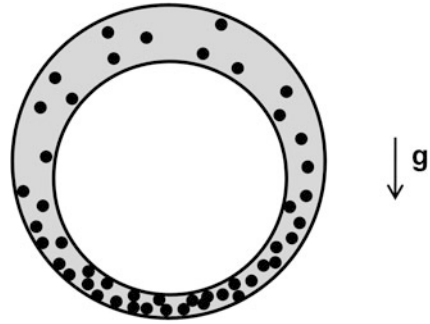
Breakouts are usually more common in deviated and horizontal wells since the
in situ-stress anisotropy in the plane normal to the wellbore axis is greater in such
wells (at least in an extensional tectonic environment). Breakouts result in cement
channeling through breakouts, as we saw in Sect. 3.4. A keyhole-shaped
cross-section, created by the drill pipe action, has a detrimental effect on cement-
ing quality, too.

An additional factor contributing to poor cementing in deviated and horizontal
wells is free-water breakout from cement during setting. Water then migrates
towards the upper part of the annulus, which results in an uncemented channel
running along the well [20]. Free-water breakout in high-angle wells has a more
detrimental effect on cement bonding than in vertical wells since in the latter case
the free water would simply migrate to the top of the cement column, while in the
former it creates an uncemented channel along the well [14].

Centering the pipe is one of the most effective measures available to improve the
mud removal in high-angle wells. The importance of casing centralization increases
in high-angle wells since casing tends to lean against the lower side of the annulus
in such wells. Using centralizers may have an additional positive effect on mud
removal since they create local disturbances to the flow, facilitating the displace-
ment process [21].

Reducing or preventing the mud channel formation in high-angle wells can be
achieved by increasing the mud circulation flow rate after casing has been run in
hole. It can also be achieved by increasing the yield strength and the gel strength of
the mud (thus improving its solids-suspending properties). Both methods do,
however, have a downside: both give rise to a higher bottomhole pressure, which
may inadvertently result in fracturing the formation and inducing lost circulation.
Losses caused by increased mud rheology may occur during mud conditioning (i.e.,
mud circulation performed before pumping preflushes and cement) or during
subsequent pumping of preflushes and cement (while trying to displace thicker and
heavier mud from the mud channel). In addition, thicker mud is more difficult to
displace from the narrow side of the annulus, as we saw earlier in this chapter.

Experimental studies by Crook et al. [21] demonstrated that there is a threshold value of the mud yield stress required to prevent solids from settling and channel formation. This threshold value increases with the well inclination, i.

It is conceived that the cement placement in a horizontal well proceeds as follows: After preflushing, the casing pipe (or the liner) is filled with cement. This reduces its buoyancy and, accordingly, the gap between the pipe and the wellbore wall on the lower side of the well cross-section decreases. As the cement exits the casing pipe, it therefore tends to flow on the upper side of the annulus, leaving an uncemented channel along the lower side. As cement exits the pipe, the pipe weight decreases, and its buoyancy improves. This increases the clearance at the lower side of the annulus. The cement can then gradually fill the lower side [14].

3.7 Example Case History: Primary Cementing in a Horizontal Well

The following field example is described by S.A. McPherson in SPE paper 62893 "Cementation of horizontal wells" [14].

An extended-reach well (vertical depth: 1,800 m) was drilled with oil-base mud. A carefully designed sequence of preflushes (washes and spacers) was pumped before cement in order to improve the mud displacement and the subsequent bonding of cement to the surfaces exposed in the annulus:

- 100 bbl (16 m^3) of a base-oil wash. This was a Newtonian fluid with dynamic viscosity 1–2 cP. It was pumped in turbulent regime. Turbulent flow improved the mud removal and the breakdown of the filter cake deposited in the annulus.
- 75 bbl (12 m^3) of a sea-water. This fluid, too, was pumped in turbulent regime.
- 75 bbl (12 m^3) of a water-base spacer containing a surfactant. This fluid, weighted with barite, had a density in between those of the mud and the cement slurry. The surfactant would improve the compatibility with the oil-base mud. The spacer had low yield-stress and was pumped in turbulent regime.
- 75 bbl (12 m^3) of sea-water, with the same surfactant as used in the spacer. The purpose of this flush was to reduce the bottomhole pressure during the subsequent cement placement.
- 75 bbl (12 m^3) of a water-base spacer containing a surfactant and a mutual solver. The mutual solver improved subsequent bonding of cement to the surfaces exposed in the annulus. The density of the spacer was between those of the mud and the cement slurry.

The fluid displacement was facilitated by liner rotation at 30 rpm.

3.8   Effect of Flow Regime

As mentioned at the beginning of this chapter, turbulent flow of preflushes (washes or spacers) is normally expected to improve the mud displacement efficiency. The fluid velocity profile is flatter in turbulent than in laminar flow. Moreover, the mud cake can be eroded more efficiently in turbulent flow since turbulent eddies and fluid pressure fluctuations are at play. Finally, in turbulent flow, the pressure gradient increases faster with the flow rate than it does in laminar flow. These features of turbulent flow make it easier to mobilize the mud in the narrow part of the (in general, eccentric and non-circular) annulus. If, however, turbulence is achieved by thinning the displacing fluid rather than by increasing the flow rate, it may induce channeling and thus reduce the displacement efficiency [7], as we saw earlier in this chapter. In addition, excessive thinning of a weighted spacer may reduce its ability to suspend the weighting solids. Weighting is needed in order for the spacer to have greater density than the mud, and thereby prevent gravity instabilities during displacement (Sect. 3.4).

Even though turbulent flow is the preferred regime in primary well cementing, it is not always achievable. The required flow rates and pressures may exceed the equipment capacity. In addition, excessive bottomhole pressures may fracture the formation. Newtonian fluid rheology is usually required to achieve turbulence without breaking the formation or exceeding the pumping capacity of the surface equipment. Thus, Newtonian washes (e.g. water, brine, base oil) are potential candidates for turbulent flow.

Cement pumping during cementing jobs is usually performed in laminar regime [20]. The preceding preflushes can be pumped either in laminar or turbulent regime. As recommended in Ref. [2], Newtonian washes such as water or base oil should be pumped at the highest possible flow rate, and, if possible, in turbulent regime. Improving the displacement efficiency by increasing the flow rate should, however, always be weighed against the risk of fracturing the formation or fluid escape into natural fractures (lost circulation). If a fracture has been created during preflush, it may serve as an escape route for cement during subsequent cement pumping. The pumping schedules should be designed so as to avoid lost-circulation problems with a safe margin.

Fluids pumped up the annulus during primary cementing have non-Newtonian, yield-stress rheology. Turbulence and transition to turbulence in such fluids have been studied considerably less than those in Newtonian fluids. A detailed review and discussion of transition to turbulence in non-Newtonian fluids can be found in Refs. [4, 22, 23]. As pointed out by Frigaard and Nouar [22], even the very definition of Reynolds number, Re, is not straightforward for yield-stress fluids. According to their approach, Re can be defined as follows:

$$\mathrm{Re} = \frac{\rho R u_0}{\mu_{\mathrm{pl}}} \tag{3.8}$$

where ρ and μ_{pl} are the density and the plastic viscosity of the fluid; u_0 is the mean fluid velocity (the flow rate divided by the conduit area); R is the characteristic size (pipe radius for pipe flow; half-width of the annular gap for annular flow). Transition to turbulence starts around the critical value of Re, Re_c. For yield-stress fluids, Re_c is a function of the *Bingham number*, Bi. The latter is defined as follows [22]:

$$\text{Bi} = \frac{\tau_Y R}{\mu_{pl} u_0} \tag{3.9}$$

The Bingham number is essentially the ratio of the yield stress to the viscous stress. The critical Reynolds number, Re_c, increases with Bi. A comparison of different transition criteria made by Frigaard and Nouar suggests that the most accurate one is the criterion of Ryan and Johnson (or, equivalently, the criterion due to Hanks). For plane-channel flow (approximating a narrow annulus), this criterion reads as follows:

$$\text{Re}_c = \frac{2100 y^*}{\text{Bi}(1 - y^*)^3} \tag{3.10}$$

where Re and Bi are defined in Eqs. (3.8) and (3.9), respectively. y^* in Eq. (3.10) is the width of the unyielded core normalized by the width of the annulus. Thus, $0 < y^* < 1$.

At high Bingham numbers, an asymptotic expression for Re_c is available given, for the Ryan and Johnson/ Hanks criterion in plane-channel geometry, by [22]:

$$\text{Re}_c \sim 1050 \sqrt{\text{Bi}/2} + O(1) \tag{3.11}$$

The critical Reynolds number thus increases with Bi, as schematically shown in Fig. 3.35. For Herschel-Bulkley fluids, Re_c also increases with the flow behavior index, n [4].

The issue of transition to turbulence becomes especially complicated in non-circular annulus geometry. In particular, in an eccentric annulus, the transition may occur in the wider part, while the flow remains laminar in the narrow part

Fig. 3.35 Schematic plot of critical Reynolds number as a function of Bingham number for a yield-stress fluid (in log-log coordinates). Based on the results presented in Ref. [22]
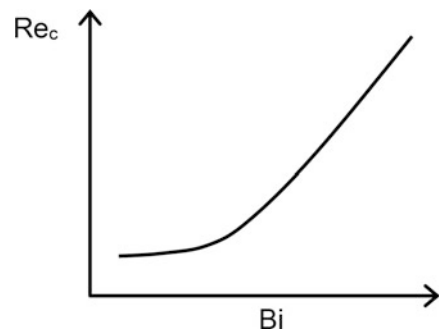
Fig. 3.36 Transition to
turbulence in an eccentric
annulus. *Dotted lines* indicate
the boundary between the
turbulent and the laminar
regions. Schematic plot based
on Ref. [9]
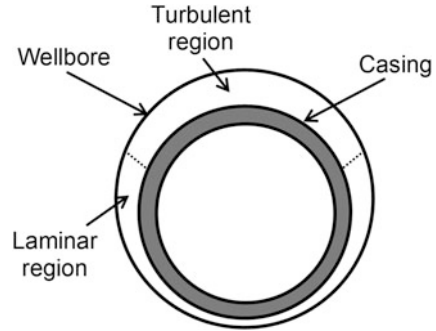
(Fig. 3.36). This will compromise mud displacement from the narrow side of the
annulus since the displacing fluid will create a channel on the wider side. Uneven
borehole walls and the presence of hardware in the annulus (centralizers, etc.) can
complicate the issue of flow regime even further.

Flow regimes in real wells may thus be quite complex because of changing
annular geometry along the well. As a result, laminar, turbulent, or transitional
regimes may coexist in different parts of the annulus [22]. Moreover, the very
definition of Reynolds number is not unambiguous for eccentric annuli [12].

Current industrial practices recommend that, in order to fully exploit the
advantages of turbulent flow, turbulence should be achieved around the whole
annulus, and the contact time of the displacing fluid with the walls in the annulus
must be sufficient to complete the cleaning [5]. Centering the casing pipe is
essential for achieving the first of these goals.

3.9 Effect of Pipe Movement

Two types of casing pipe movement are known to improve mud displacement in
primary cementing: reciprocation and rotation [21]. The improvement is due to the
drag, and thereby the shear stress, the pipe applies to the mud (Fig. 3.37). This
shearing action can break gel and reduce the flow resistance of the mud. In par-
ticular, it facilitates the mud flow in the narrow part of the annulus. It may also
improve the flow and displacement from washouts that would otherwise be left
unaffected during displacement (Sect. 3.4) [3]. Moreover, pipe movement removes
the filter cake (i.e., dehydrated mud) deposited on the borehole wall [14]. In
addition, pipe movement (either rotation or reciprocation) is known to cause earlier
transition to turbulence [9], which is beneficial for mud displacement.

Typical amplitudes and periods of casing reciprocation are 6–12 m and 1–5 min,
respectively [2]. Lateral movement of the pipe occurring during axial reciprocation
may improve the overall effect [7, 11]. Such secondary lateral movement is com-
mon e.g. in deviated wells [2]. Drawbacks of pipe reciprocation are surges and
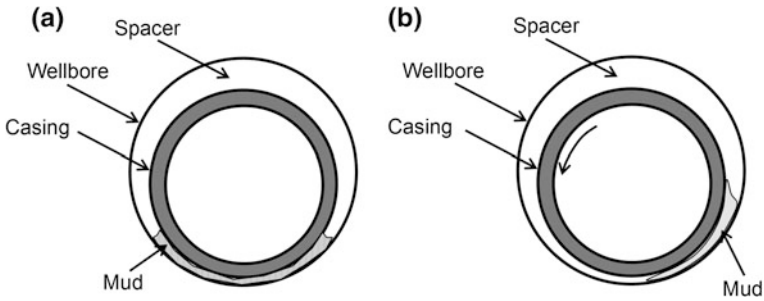
Fig. 3.37 Effect of pipe rotation on mud displacement in the annulus: **a** no rotation; **b** rotation facilitates mud removal from the narrow part of the annulus

swabs of the bottomhole pressure, which may lead to either borehole instabilities, formation fluid influxes, or fluid losses into the formation. Another drawback is the risk of the pipe getting stuck [2].

Pipe rotation is usually more effective than pure reciprocation [2, 7, 11]. It is free from the above-mentioned drawbacks. The rotation rate is typically 10–40 rpm [2]. The effect of pipe rotation is amplified by orbital movement of the pipe that may accompany rotation at high rpm [2].

3.10   Models of Cement Flow in the Annulus

A successful cementing job requires that the optimum fluid rheologies, pumping rates, and injection volumes are used. Such optimization can be achieved by numerical modeling of different cementing scenarios at design stage. Numerical models of well cementing can be subdivided into three classes:

1. Simple kinematic models, e.g. [6, 7, 24].
2. Two-dimensional models of Hele-Shaw-cell type, e.g. [25, 26].
3. Fully three-dimensional models, e.g. [27–29].

In kinematic models, the annulus is discretized into tubes arranged along the azimuth. The annulus is thereby effectively represented as a collection of sectors. Flow and displacement are calculated in each tube, whereby possible mass and momentum transfers between the tubes are neglected. In particular, assuming zero mass transfer between the tubes makes azimuthal flows impossible. The kinematic model of well cementing described in Sect. 3.2 is an example of this type of model. By neglecting azimuthal flows, kinematic models tend to deliver conservative predictions of the displacement efficiency.

In two-dimensional models, the annulus is discretized into computational cells along the wellbore axis and along the azimuthal direction, or along the wellbore axis and along the radial direction [2]. In the former case, the flow can be computed

as a flow in a Hele-Shaw cell. Azimuthal flow is then possible. Such two-dimensional models neglect the fluid velocity variation along the annular gap (in reality, the fluid velocity is maximum near the mid-plane of the conduit and is zero at the walls). Thus, some effects still cannot be accurately captured by these models, such as the slower displacement of mud at the walls than in the middle of the annular gap. In the other type of 2D models, i.e. those with discretization along the well and in the radial direction, the velocity profile across the annulus is captured correctly, which enables e.g. simulation of mud cake erosion. The flow is, however, considered at only one azimuthal location.

In fully-3D models, the annulus is discretized in all three dimensions, i.e. along the well, along the azimuth, and along the annular gap. Computational fluid dynamics (CFD) can be used to solve the problem with a full 3D discretization. Fully-3D models capture the underlying physics most accurately, but they do so at the expense of an increased computational cost.

Using numerical models to design well cementing jobs requires that many scenarios can be run and tested. Thus, computational efficiency is high on the list of priorities in well cementing modelling. Modelers are forced to find a reasonable compromise between accuracy and computational speed. Two-dimensional models often offer such a compromise.

3.11   Summary and Discussion

A sequence of fluids is pumped to displace the mud and prepare the annulus for cementing in a primary cement job. As a rule of thumb, each subsequent fluid in this fluids train should be thicker and heavier than the previous fluid, to ensure that the displacement is stable. If, however, the fluid is pumped in turbulent regime (e.g. Newtonian washes such as fresh water, base oil, or chemical wash), the fluid can be thinner than the previous fluid, in order to achieve turbulence without creating excessively high bottomhole pressure.

In addition to properly designing the fluid hierarchy and using turbulent regime with Newtonian preflushes, the quality of primary cementing can be improved by pipe motion, particularly the rotational one. Other factors that affect cement placement are the eccentricity of the casing positioning in the annulus, the geometry of the annulus (determined by the hardware and by the shape of the wellbore cross-section), and lost circulation. While some of these factors, e.g. breakouts and washouts in the well, can only be mitigated during drilling, others, e.g. lost circulation and casing eccentricity, can in many cases be controlled during the cement job fairly well. Often such control involves, however, an optimization strategy. For instance, reducing the risk of lost returns by reducing the bottomhole pressure requires that the flow rate of preflushes and cement be limited, which may reduce the displacement efficiency. Knowledge of cement and formation properties as well as availability of reliable, validated numerical models make for steady improvements in the quality of primary cementing jobs.

An important factor that may compromise the cement placement during a primary cementing job is fluids mixing on their way down the pipe. The hierarchy of fluid rheologies and densities that is beneficial for stable displacement in the annulus is disadvantageous for flow down the pipe since their sequence is then reversed. Therefore, mechanical plugs are often used to prevent hydrodynamic instabilities as well as contact and mixing of poorly compatible fluids on their journey towards the bottomhole. Even if such plugs are used, their wear may result in a fluid film remaining on the inner walls of the tubular [2]. This film may contaminate the fluids pumped subsequently.

Given the variability of downhole conditions (geometry of the annulus, formation temperature and permeability), it is all but impossible to design cement jobs such that perfect cementing is guaranteed in each and every well. After the set, the cement usually contains defects of different sizes, e.g. mud channels, gas-filled bubbles, delaminations along interfaces with casing and rock, etc. In the next chapter, we will take a closer look at defects in annular cement.

References

1. Shadravan A, Narvaez G, Alegria A, Carman P, Perez C, Erger P (2015) Engineering the mud-spacer-cement rheological hierarchy improves wellbore integrity. In: SPE paper 173534 presented at the SPE E&P Health, safety, Security and Environmental Conference-Americas held in Denver, CO, USA, 16–18 March 2015
2. Nelson EB, Guillot D (eds) (2006) Well cementing. Schlumberger
3. Sauer CW (1987) Mud displacement during cementing: a state of the art. J Petrol Technol 39(9):1091–1101
4. Brand F, Peixinho J, Nouar C (2001) A quantitative investigation of the laminar-to-turbulent transition: application to efficient mud cleaning. In: SPE paper 71375 presented at the 2001 SPE Annual Technical Conference and Exhibition held in New Orleans, LA, 30 Sept–3 Oct 2001
5. Khalilova P, Koons B, Woody D, Eihancha A (2013) Newtonian fluid in cementing operations in deepwater wells: friend or foe? In: SPE paper 166456 presented at the SPE annual technical conference and exhibition held in New Orleans, LA, USA, 30 Sep–2 Oct
6. Lavrov A (2016) Effect of eccentric annulus, washouts and breakouts on well cementing quality: laminar regime. Energy Procedia 86:391–400
7. McLean RH, Manry CW, Whitaker WW (1967) Displacement mechanics in primary cementing. J Petrol Technol 19(2):251–260
8. Luo Y, Peden JM (1990) Flow of non-Newtonian fluids through eccentric annuli. SPE Product Eng 5(1):91–96
9. Erge O, Ozbayoglu EM, Miska SZ, Yu M, Takach N, Saasen A, May R (2015) Laminar to turbulent transition of yield power law fluids in annuli. J Petrol Sci Eng 128:128–139
10. Laird WM (1957) Slurry and suspension transport—basic flow studies on bingham plastic fluids. Ind Eng Chem 49(1):138–141
11. Clark CR, Carter LG (1973) Mud displacement with cement slurries. J Petrol Technol 25(7):775–783
12. Kelessidis VC, Dalamarinis P, Maglione R (2011) Experimental study and predictions of pressure losses of fluids modeled as Herschel-Bulkley in concentric and eccentric annuli in laminar, transitional and turbulent flows. J Petrol Sci Eng 77(3–4):305–312

13. Tehrani MA, Bittleston SH, Long PJG (1993) Flow instabilities during annular displacement of one non-Newtonian fluid by another. Exp Fluids 14(4):246–256
14. McPherson SA (2000) Cementation of horizontal wellbores. In: SPE paper 62893 presented at the 2000 SPE annual technical conference and exhibition held in Dallas, TX, 1–4 Oct 2000
15. Fjær E, Holt RM, Horsrud P, Raaen AM, Risnes R (2008) Petroleum related rock mechanics, 2nd edn. Elsevier, Amsterdam
16. Mitsoulis E, Huilgol RR (2004) Entry flows of Bingham plastics in expansions. J Nonnewton Fluid Mech 122(1–3):45–54
17. Roustaei A, Gosselin A, Frigaard IA (2015) Residual drilling mud during conditioning of uneven boreholes in primary cementing. Part 1: Rheology and geometry effects in non-inertial flows. J Nonnewton Fluid Mech 220:87–98
18. Lavrov A (2016) Lost circulation: mechanisms and solutions. Elsevier, Oxford
19. Beirute RM (1984) The phenomenon of free fall during primary cementing. In: SPE paper 13045 presented at the 59th annual technical conference and exhibition held in Houston, TX, 16–19 Sept 1984
20. Keller SR, Crook RJ, Haut RC, D.S K (1987) Deviated-wellbore cementing: part 1—problems. J Petrol Technol 39(8):955–960
21. Crook RJ, Keller SR, Wilson MA (1987) Deviated wellbore cementing: part 2—solutions. J Petrol Technol 39(8):961–966
22. Frigaard IA, Nouar C (2003) Predicting transition to turbulence in well construction flows. In: SPE paper 81150 presented at the SPE Latin American and caribbean petroleum engineering conference held in Port-of-Spain, Trinidad, West Indies, 27–30 April 2003
23. Guillot DJ, Denis JH (1988) Prediction of laminar and turbulent friction pressures of cement slurries in pipes and centered annuli. In: SPE paper 18377 presented at the SPE European petroleum conference, London, UK, 16–19 Oct 1988
24. Graham HL (1972) Rheology-balanced cementing improves primary success. Oil Gas J 18:53–59
25. Bittleston SH, Ferguson J, Frigaard IA (2002) Mud removal and cement placement during primary cementing of an oil well. Laminar non-Newtonian displacements in an eccentric annular hele-Shaw cell. J Eng Math 43:229–253
26. Osayande V, Isgenderov I, Bogaerts M, Kurawle I, Florez P (2014) Beating the odds with channeling in ERD well cementing: solution to persistent channeling problems. In: SPE paper 171271 presented at the SPE Russian oil and gas exploration and production technical conference and exhibition held in Moscow, Russia, 14–16 Oct 2014
27. Savery MR, Chin W, Yerubandi KB (2008) Modeling cement placement using a new 3-D flow simulator. In: AADE-08-DF-HO-08 paper presented at the AADE fluids conference and exhibition held at the Wyndham Greenspoint Hotel, Houston, TX, April 8–9
28. Vefring EH, Bjørkevoll KS, Hansen SA, Sterri N, Sævareid O, Aas B, Merlo A (1997) Optimization of displacement efficiency during primary cementing. In: SPE paper 39009 presented at the Fifth Latin American and caribbean petroleum engineering conference and exhibition held in Rio de Janeiro, Brazil, 30 Aug–3 Sept 1997
29. Biezen E, van der Werff N, Ravi K (2000) Experimental and numerical study of drilling fluid removal from a horizontal wellbore. In: SPE paper 62887 presented at the 2000 SPE annual technical conference and exhibition held in Dallas, TX, 1–4 Oct 2000

Chapter 4
Heterogeneities in Cement

Abstract It is not possible to create a perfectly homogeneous annular cement sheath in a well. Defects will always be present at different scales, ranging from intergranular microcracks to bubbles and gas channels. Defects can be produced at all stages of primary cementing, i.e. during cement slurry mixing, placement, hardening, and subsequent loading. Defects have a strong impact on well integrity since they may provide leakage paths for formation fluids along the cemented annulus. In this chapter we discuss some important heterogeneities in cement (channels, pockets, cement porosity, slurry segregation issues, and interface defects). It is outlined how they can be studied by state-of-the-art imaging techniques, such as X-ray computed tomography. Special emphasis is given to the unavoidable interface transition zone (ITZ) forming along cement interfaces, and the debonding of cement from steel/rock. The chapter forms the basis for the further discussion of operation-induced defects in Chaps. 5 and 6.

Keywords Defects · Heterogeneities · Interfacial transition zone (ITZ) · Bonding · Debonding · Characterization · Tomography

Creating a perfect, flawless cement sheath in a well is rarely possible. Defects are introduced in the cement sheath at all stages. For instance, bubbles can be introduced into cement slurry during mixing. Gas channels and chimneys can be left in cement after placement. Micro- and macro-cracks can be induced during the life of the well. Defects may affect well integrity by increasing the porosity and permeability along the cemented casing. As we will see in subsequent chapters, they can also affect the mechanical robustness and stability of the annular cement sheath. In this chapter, we review different types of defects in well cement and why they appear.

4.1   Large-Scale Channels/Pockets

Defects arising as a result of improper cement mixing or placement have been discussed in Chap. 3. These include macro-scale channels or pockets of undisplaced preflushes or mud. The radial extent of such defects is typically on the same scale as the annular gap between the casing and the borehole wall, and their length along the well is on the meter-scale. Similar channels in the cement can occur if pressurized gas from the formation invades the slurry during solidification and creates so-called "chimneys".

4.2   Enhanced Cement Porosity

Well-formed cement typically has a relatively low porosity, on the order of 10–30 % when measured by helium pycnometry [1]. In some cases, however, the porosity can become significantly higher. An example is when cement is hardening adjacent to a gas-hydrate-bearing formation. In this case the slurry solidification, which releases heat to the surroundings, may thaw the formation and enable gases to invade the slurry [2]. Air bubbles can also be mixed into the cement slurry at the rig site, and in some cases bubbles are deliberately introduced to lower the slurry density. The latter is referred to as *foamed cement*.

The water-to-cement ratio is also important for set cement porosity. Even if this is optimal when the slurry is being pumped into the well, it can be reduced/enhanced upon interactions with the formations in the well. Water-bearing formations can add water to the cement slurry, while water can similarly be filtrated out of the slurry into porous formations. Control of the water-to-cement ratio during the whole cementing process is thus difficult, and several additives have been introduced to combat this problem in primary cementing.

The exact effect of different water-to-cement ratios on well cement porosity (and other properties) has not yet been fully explored. Some indications can, however, be drawn based on results from a recent study investigating in detail two cement slurries—one with high water content and one with low [3]. These had significant differences in pore size distributions and nano-porosity. The low-water cement slurry ended up with fewer but larger pores, while the high-water cement slurry had many but small (equal-size) pores. The absolute porosity, as determined by micro computed tomography (μ-CT), was, however, similar in both samples [3]. Micro computed tomography reconstructs a three-dimensional (3D) cement volume based on two-dimensional (2D) projections where the pores can be segmented and analysed. This is exemplified in Fig. 4.1. The technique is non-destructive, and resolutions down to the micrometer-range can be obtained. The drawbacks of this technique for visualizing cement porosity are the long acquisition time (meaning that porosity *changes* over time are difficult to monitor), the requirement for small
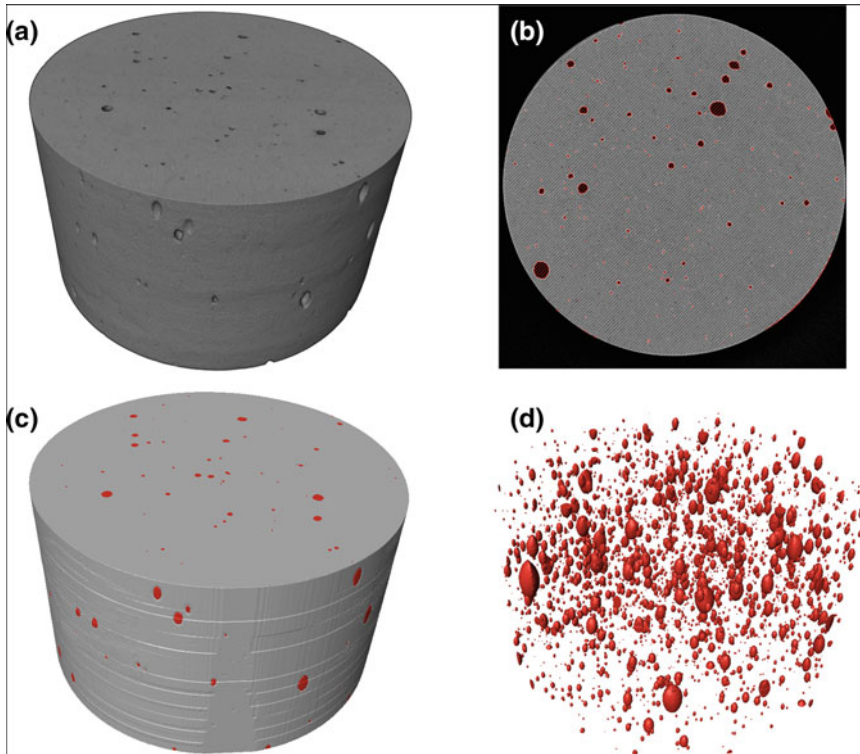
Fig. 4.1 3D cement volume imaged by X-ray micro computed tomography (CT). **a** A 3D visualization of the CT data, **b** cement pores are segmented and marked with *red color* in each of the stacked 2D images, **c** a 3D visualization of the segmented data, **d** a visualization of cement pores only. These type of 3D visualizations can be used to find sample porosity, pore size distributions, pore connectivity and pore morphology

samples sizes, and the inability to image the smallest cement pores (which are on the nanometre scale).

   A first attempt was made in the same study to investigate also the nano-porosity of cement. This was done by performing additional porosity investigations using Focused Ion Beam-Scanning Electron Microscopy (FIB-SEM), which is a type of SEM instrument allowing 3D analyses. It was found that even the smallest nano-pores in each of the cement samples could be analysed using this technique. The high-water cement slurry was found to have a porosity slightly higher than the low-water cement slurry at the very smallest scales. Both the pore size distribution differences and the nano porosity differences were used to explain why the mechanical properties of the two samples were different. The main drawbacks with using FIB-SEM for cement porosity analyses is that the sample is destroyed during analysis (meaning that the same volume can never be imaged twice), and that it is

difficult to know whether the very small volume under investigation is representative for the sample as a whole.

If it is desired to monitor *changes* in cement porosity over time, it is beneficial to make use of X-ray synchrotron radiation. This is similar to µ-CT, but enables quick acquisition of tomograms. It is non-destructive, and has high spatial and time resolutions.

4.3   Cement Slurry Settling

The cement slurry consists of particles of different sizes that are immersed in (and react with) water. There is a wide size distribution of the particles in the cement slurry. Some are large, others are small. Since solidification takes time, heavier particles can in some cases be slowly drawn towards the bottom section of the cement column, leaving lighter particles and fluid on top (see also the discussion of slurry segregation, slurry stability, and free fluid in Sects. 2.1 and 3.6). This results in density gradients along the cement sheath, and porosity differences. The environment in which the cement particles are hydrating is thus different at the top and bottom of the volume.

4.4   Interface Defects

Even if cement is perfectly mixed and placed in the well, the interface between cement and adjacent steel casing and drilled rock will be a weak link in well construction. A striking illustration of this is a field study done on sidecores (including casing, cement and caprock) retrieved from a well where CO_2 was used for enhanced oil recovery [4]. These cores show indications of CO_2 leakage along both the casing-cement and the cement-rock interfaces.

Such an annular-shaped leakage path at the casing-cement or cement-rock interface is referred to as a *microannulus*, and the process in which it is created is called *debonding*. Debonding can be caused e.g. by chemical interactions between cement and the casing/rock surfaces, but it can also be created by loading applied during the well life. The latter will be discussed in Chaps. 5 and 6.

Early studies of cement interfaces were made in the 1980s, when crack propagation in cement adjacent to steel was investigated [5]. It was found that cracks propagating towards the cement-steel contact were arrested and changed direction at a distance of about 10 µm from the contact zone. As seen in Fig. 4.2, the crack direction is changed by about 90° and the crack continues to propagate within a near-wall zone parallel to the interface. This zone in which the crack "prefers" to travel was found to be a weak and porous region of the cement referred to as the *interfacial transition zone (ITZ)*.
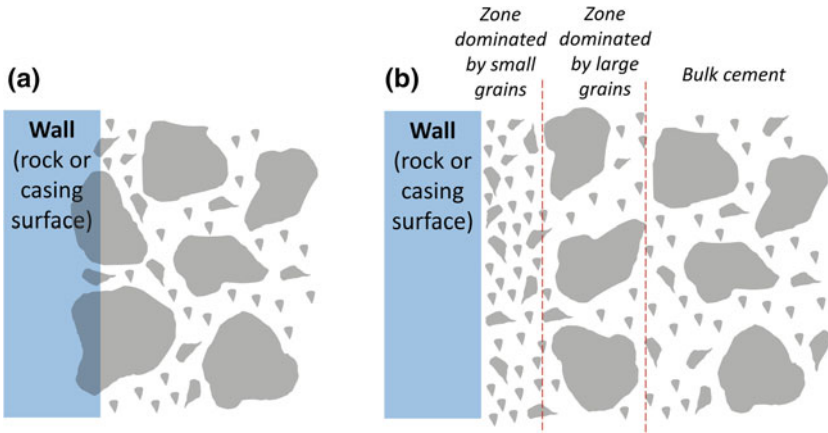
Fig. 4.2 Schematic illustration of a crack initiated in the cement and propagating upwards towards a steel wall. Instead of travelling directly to the cement-steel interface it is arrested and then propagates in a weak region parallel to the interface (about 10 μm from the cement-steel contact itself). This zone is known as the interfacial transition zone (ITZ). Based on the results presented in Ref. [5]
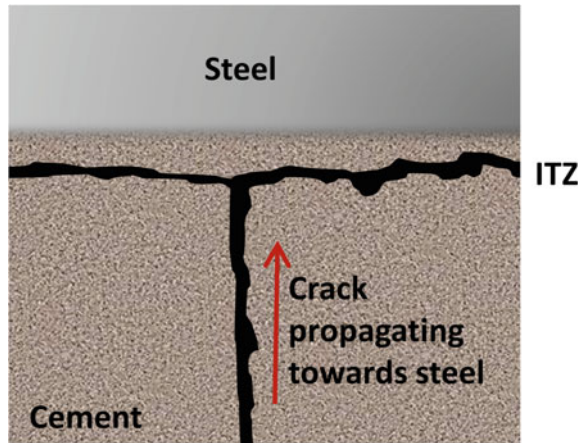
The ITZ develops when cement is allowed to harden next to a solid wall. The cement slurry consists of particles/grains ranging in size from smaller than 1 μm up to around 100 μm. When this mixture is placed near a wall, the optimal packing configuration of grains is disrupted. This is schematically depicted in Fig. 4.3. The wall cannot cut through cement grains, resulting in a "wall effect" where a region closest to the wall is depleted of larger cement grains. This region will be filled with water and small cement particles. The region adjacent to it will contain predominantly large grains, as smaller grains have been transported by water flow into the near-wall zone. These differences in particle size distribution adjacent to walls have been studied by plotting the volume fraction of unhydrated grains as a function of time [6]. Since small grains quickly hydrate, while larger grains remain unhydrated at their cores, this measure gives an indication of spatial particle size distribution.

The inability of large particles to approach the wall may be due to the *lubrication forces* acting on the particle in the direction opposite to the particle's velocity as the particle approaches the wall [7]. Large particles in Fig. 4.3 may be thought of as particles immersed in a suspension of small particles. As the gap between a large particle and the wall closes, it takes more and more energy to squeeze the suspension out of the gap. This is perceived as a repelling force acting on the large particle. In the limit of zero gap, this force increases towards infinity, keeping large particles away from the wall [8]. As a result, the near-wall region is depleted of large particles.

The ITZ in cement has long been a topic of interest for construction engineers working with concrete, which is a mixture of cement and large aggregate particles. By forcing Wood's metal into the pores of a concrete sample, it has been found that ITZ is present around aggregates (their size is so much bigger than cement particles that they act as "walls") [9]. The width of the ITZs displayed using Wood's metal ranges from 30 to 100 μm. Separate studies have found that the porosity in the ITZ is two to three times larger than in the bulk cement, and that the pores are coarser than in the bulk [10]. This suggests that ITZ porosity is significant, and that pores

Fig. 4.3 Schematic illustration of the "wall effect", where the wall can be either the steel casing or the drilled rock surface in wells, based on [6]. **a** Representation of unphysical packing, since the wall cannot cut through cement grains. **b** Cement grains will have to pack in a different way close to the wall, giving rise to the ITZ

Fig. 4.4 Schematic illustration of microstrength measurements in the ITZ based on the results reported in Ref. [11]. The weakest part of the ITZ was found to lie in the range 10–30 μm from the wall, and the total ITZ was found to stretch about 70 μm from the wall
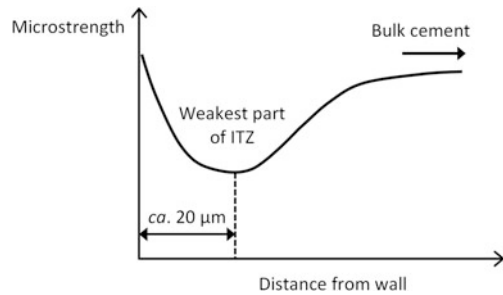
are interconnected in three dimensions. This will have an impact not only on leakage, but also on chemical interactions between well cement and its downhole environment.

Micro-mechanical properties (micro-hardness and elastic modulus) of the ITZ have been measured using a depth-sensing micro-indentation method [11]. This was done in a concrete mixture surrounding a steel reinforcement bar. It was found that mechanical properties were at a minimum around 10–30 μm from the steel bar. They then increased when indentation points moved towards the bulk concrete and became roughly constant at distances greater than 50–70 μm. The general trend of the measured samples is illustrated in Fig. 4.4.

The reason why the ITZ is so weak lies in the hydration behavior of cement. When cement hardens, two major hydrate phases are formed, namely calcium hydroxide (CH) and calcium silicate hydrate (C–S–H). The latter forms directly

around cement grains (since the concentration of silicate in solution is low), while CH forms in open voids and pores. The less than optimal grain packing in the ITZ, which gives rise to significant porosity, will thus favor CH formation close to the wall. Experiments show a strong correlation between the zone initially characterized by excess porosity and subsequent increased growth of the CH phase [6]. The CH phase is formed by layering of plate-shaped crystals. These crystals have been found to align with the plate normal perpendicular to the wall [10]. This well-packed CH region is relatively strong, but is likely to be easily cleavable in the plane parallel to the wall. Also the region adjacent to the CH-enriched region, namely that dominated by poorly cemented large grains, is likely to become mechanically weak and prone to fracturing. The weakest part of the ITZ it thus likely to be the transition between its small-grained and large-grained domains.

Since the development of ITZ is due to fundamental hydrodynamic, physical, and chemical mechanisms, the formation of such zones is difficult to prevent. ITZ is also a heterogeneous zone characterized by variations in porosity, permeability, and mechanical properties, and it is not always easy to distinguish ITZ from the bulk cement in microscopy images [12]. There is no sharp boundary between the ITZ and the bulk cement. The ITZ can stretch up to 100 μm from the wall. Hydration in the direct vicinity of the wall will be different from that in the bulk cement since the water-to-cement ratio is locally higher, and the growth and the nature of hydrate phases may be influenced by the surface and the chemical nature of the wall itself. This is related to the discussion of cement bonding to various surfaces in the next Section.

4.5   Measurements of Cement Bonding Quality

In addition to the weak near-wall ITZ region, the interface between cement and casing or rock can be a weak zone in well construction. After drilling, the wellbore wall is never smooth and clean. Rather it is a rough surface with leftovers of preflushes or mud. This affects the adhesion of the cement slurry as it solidifies downhole.

Early studies of cement bonding to steel pipes were performed by Carter and Evans [13]. They used a push-out test, similar to that described in Chap. 2, to evaluate the shear bond strength between cement and pipe. The finish of the pipe was varied in order to investigate its influence on the shear bond strength. It was found that the shear bond strength between cement and a new pipe with mill varnish was 74 psi (0.5 MPa). By chemically removing the varnish, a bond strength of 104 psi (0.7 MPa) was obtained, and by using a rusty pipe it became as high as 141 psi (1 MPa). The highest cement-pipe shear bond strength was measured with a pipe that was resin-sand coated. It was then 2400 psi (16.5 MPa). This study is a clear indication that the surface roughness impacts the shear bond strength to cement.

In the same study [13], Evans and Carter also investigated whether the presence of mud on the pipe impacted the cement-pipe shear bond strength. They found that

for a pipe with a thin film of water-base mud on the surface, the shear bond strength was 97 psi (0.7 MPa), while for oil-base mud it was 63 psi (0.4 MPa). This is clearly lower than the shear bond strength to a clean pipe quoted above. The presence of mud will, in other words, reduce the adhesion of cement to a steel pipe.

A follow-up study was done by Carpenter et al. using a purpose-made pressurized push-out tester [14]. They found that also in the pressurized environment, the shear bond strength was strongly dependent on the surface finish of the pipe. With a mill varnish coating the bonding strength was 57 psi (0.4 MPa), while for a pipe with a coarse sand blast it was 613 psi (4.2 MPa). They investigated several cement mixtures and found that the bonding could be improved further by using water-wetting surfactants or expansive additives.

A renewed interest in cement bonding has been awakened in recent years, following the petroleum industry's focus on well integrity and the discussions related to geological storage of CO_2 in subsurface reservoirs. Ladva et al. [15] studied the shear bond strength between cement and different rock types, again using the standard push-out test. An Oxford clay outcrop shale (17 % smectite) and a Cartoosa shale from Oklahoma (6 % smectite) were compared. After 1-day curing of the Portland G cement (85 °C), the cement-Oxford strength was 58 psi (0.4 MPa) while the cement-Cartoosa strength was 70 psi (0.48 MPa). This indicates that the amount of swelling clay affects cement shear bond strength to formation. Several curing times were also investigated, and it was found that the shear bond strength increased over time. For the Cartoosa shale, it was 116 psi (0.8 MPa) after 5 days of curing.

The formation impact on shear bond strength was further studied by Opedal et al. [16] using a push-out test. They tested several rock types in pristine state, with a film of water-base mud and with a film of oil-base mud at the interface. It was found that the presence of mud at the rock interface greatly affected cement adhesion. They also imaged the porosity at the interface using μ-CT for each sample in order to map the leakage potential. It was found that the interface voids were in a size range of ∼100 μm, that they were well-connected along the length of the sample, and that they had complex geometrical shapes. These studies underline the importance of mud removal before cementing to obtain good cement adhesion to the drilled rock surface.

All the studies discussed above have been measuring the shear bond strength between cement and rock. This is important in the case of vertical movement of casing/rock relative to the well cement. For predicting debonding as a result of well operations it is, however, necessary to measure the *tensile bonding strength* of cement to casing/rock. This has not been extensively studied so far, but Liu et al. [17] have proposed a methodology for measuring this. The concept is illustrated in Fig. 4.5, and involves performing a Brazilian test (see Chap. 2) on a composite, disc-shaped cement-rock sample. Using this setup they measured the tensile bond strength between Class H Portland cement and Colorado oil shale outcrop (no reactive clays, naturally oil-wet, 38 % quartz) to be 55 psi (0.38 MPa) with a standard deviation of 7 psi (0.05 MPa).

Fig. 4.5 Schematic illustration of the method for measuring tensile bond strength between cement and rock proposed by Liu et al. [17]
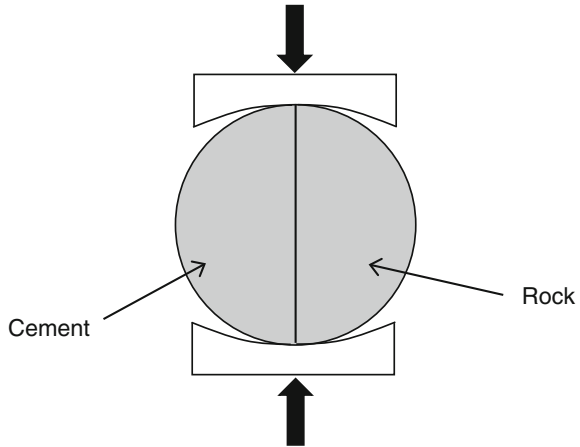
4.6 Operation-Induced Damage

The cement heterogeneities that have been discussed so far in this chapter are all related to the cement slurry and its placement and solidification. Over the life of a well, however, defects can be introduced also in the operational phase of the well or after abandonment. The de-bonding of annular cement discussed above can also be introduced by variations in casing diameter as a result of pressure and temperature variations. Furthermore, radial fractures, shear damage and disking can be introduced by casing/rock deformation. These issues will be discussed in detail in Chaps. 5 and 6.

An important observation on how defects affect the life of a well is that it is necessary to have information on *defect properties*. A finite-element study of a casing-cement-rock assembly containing heterogeneities showed that if the defects have a lower Young's modulus than the surrounding intact cement, the risk of tensile failure during heating or cooling will be reduced [18]. If the thermal conductivity of defects is lower than that of the surrounding intact cement, the risk of tensile failure will be enhanced. The thermal and mechanical properties of defects are thus important for determining a well's ability to handle temperature variations.

4.7 Summary and Discussion

Heterogeneities will always be present in an annular cement sheath, even when all recommendations are followed for cement mixing and placement. The defects discussed in this chapter can be summarized as follows:

- *Large-scale channels/pockets* Can be caused by poor mud displacement or influx of formation fluids into the solidifying slurry.

- *Enhanced cement porosity* Can be caused by gas influx into the slurry or by inferior water-to-cement ratio during hydration. The water content can be wrong from the pumping stage, or it may be altered upon encounter with the downhole formation.
- *Cement slurry settling* During a long solidification, the cement slurry can separate into a dense mass at the bottom and a lighter mass at the top. This is due to gravity drawing down heavier particles before solidification.
- *Interface defects* The casing and rock surfaces act as walls for the well cement, and during hardening they will introduce wall effects. The interfacial transition zone (ITZ) originates from the depletion of the near-wall region of large cement grains. This gives rise to an increased porosity in the near-wall region. If the casing/rock is covered with a film of preflush or mud, this will additionally reduce the bonding strength.
- *Operation-induced defects* Fracturing and de-bonding of annular cement can be caused by operations. This will be thoroughly discussed in Chaps. 5 and 6.

State-of-the-art imaging techniques, such as X-ray computed tomography and electron microscopy, can be used for studying microstructural details in cement. With use of modern synchrotron-based methods, the evolution of heterogeneities over time can also be studied.

Properties of defects are important. Little is so far known about their stiffness or their thermal properties, but in order to perform reliable simulations of wellbore systems, these issues should be resolved. In the next chapter, we will see how individual defects, e.g. an uncemented channel, can affect the stress state and failure in cement during the lifetime of the well.

References

1. Krus M, Hansen KK, Künzel HM (1997) Porosity and liquid absorption of cement paste. Mater Struct 30(7):394–398
2. Nelson E, Guillot D (2006) Well cementing, 2nd edn. Schlumberger, Sugar Land, Texas
3. Vralstad T, Vullum PE, Torsaeter M, Opedal NVDT (2013) A visual journey into the 3D chemical nanostructure of oilwell cement. In: SPE paper 164105 presented at the SPE international symposium on oilfield chemistry, 8–10 April, The Woodlands, Texas, USA
4. Carey JW, Wigand M, Chipera SJ, WoldeGabriel G, Pawar R, Lichtner PC, Wehner SC, Raines MA, Guthrie GD Jr (2007) Analysis and performance of oil well cement with 30 years of CO_2 exposure from the SACROC Unit, West Texas, USA. Int J Greenhouse Gas Control 1(1):75–85
5. Bentur A, Diamond S, Mindess S, The microstructure of the steel fibre-cement interface. J Mater Sci 20(10):3610–3620
6. Scrivener KL, Crumbie AK, Laugesen P, The interfacial transition zone (ITZ) between cement paste and aggregate in concrete. Interface Sci 12(4):411–421
7. Torsæter M, Todorovic J, Lavrov A (2015) Structure and debonding at cement–steel and cement–rock interfaces: effect of geometry and materials. Constr Build Mater 96:164–171

8. Lavrov A, Laux H (2007) DEM modeling of particle restitution coefficient versus Stokes number: the role of lubrication force. In: Paper No S2_Thu_C_54 presented at the 6th international conference on multiphase flow, ICMF 2007, Leipzig, Germany, 9–13 July 2007

9. Scrivener KL, Nemati KM (1996) The percolation of pore space in the cement paste/aggregate interfacial zone of concrete. Cem Concr Res 26(1):35–40

10. Ollivier JP, Maso JC, Bourdette B (1995) Interfacial transition zone in concrete. Adv Cem Based Mater 2(1):30–38

11. Zhu W, Bartos PJM (2000) Application of depth-sensing microindentation testing to study of interfacial transition zone in reinforced concrete. Cem Concr Res 30(8):1299–1304

12. Diamond S, Huang J (2001) The ITZ in concrete—a different view based on image analysis and SEM observations. Cement Concr Compos 23(2–3):179–188

13. Carter LG, Evans GW (1964) A study of cement-pipe bonding. J Petrol Technol 16(2): 157–160

14. Carpenter RB, Brady JL, Blount CG (1992) The effects of temperature and cement admixes on bond strength. J Petrol Technol 44(8):936–941

15. Ladva HKJ, Craster B, Jones TGJ, Goldsmith G, Scott D (2005) The cement-to-formation interface in zonal isolation. SPE Drill Completion 20(3):186–197

16. Opedal N, Todorovic J, Torsaeter M, Vralstad T, Mushtaq W (2014) Experimental study on the cement-formation bonding. In: SPE paper 168138 presented at the SPE international symposium and exhibition on formation damage control, Lafayette, LA, USA, 26–28 Feb

17. Liu X, Nair SD, Cowan M, van Oort E (2015) A novel method to evaluate cement-shale bond strength. In: SPE paper 173802 presented at the SPE international symposium on oilfield chemistry, The Woodlands, TX, USA, 13–15 April

18. Lavrov A, Torsæter M, Todorovic J (2015) Numerical study of thermal stresses in casing-cement-rock system with heterogeneity. In: ARMA paper 15–110 presented at the 49th US rock mechanics/ geomechanics symposium held in San Francisco, CA, USA, 28 June–1 July 2015

Chapter 5
Formation Stresses, Casing Pressure, and Annular Cement

Abstract Tensile hoop stresses in the cement sheath may induce radial cracks. Tensile radial stresses may cause debonding at cement-steel or cement-rock interfaces. Casing pressure changes and in situ stress variations (caused by production or injection) may cause tensile stresses in cement. Whether or not this occurs depends on the initial stresses in cement. The uncertainties involved in the evaluation of initial stresses in cement sheaths are discussed. Results of finite-element simulations of stress changes in cement caused by casing pressure changes and in situ stress changes are presented. The effect of uncemented channels (e.g. gas channel or mud channel) on stresses in the cement sheath is demonstrated. An uncemented channel acts as a stress amplifier, increasing the variations of cement stresses by a factor of 2–3, as compared to an intact cement sheath. The effects of anisotropic in situ stresses on the formation and shape of microannulus are discussed. Hysteresis of microannulus permeability during repeated loading/unloading of the cement-casing-rock system is outlined.

When a wellbore is drilled, the rock that originally occupied the borehole volume, is removed. This results in stress concentration around the hole since the rock that was supporting the formation is not there anymore. During drilling, mud exerts some pressure on the borehole wall, which reduces the stress concentration around the hole. It is, however, not possible to exactly restore the original state of stress around the hole by applying wellbore pressure (i.e. by varying the mud weight) unless the in situ stresses are isotropic in the plane normal to the wellbore axis, and deformations are linear elastic around the wellbore.

After setting casing and cementing the annulus, the disturbance to the stress field is still there. If the casing pressure is changed or the casing string is heated or cooled, the stress disturbance around the hole may be amplified, possibly leading to cracks developing in casing, cement or rock in the near-well area. Similarly, the near-well stresses may be affected by in situ stress changes in the reservoir caused

by depletion or by injection of fluids (e.g. during water flooding). In particular, the total horizontal stresses in the reservoir usually decrease during depletion, while the total horizontal stresses in the cap rock may slightly increase during depletion [1, 2]. Complex stress changes may occur around faults if these become reactivated during depletion or injection [3]. Shear displacements of faults intersected by the well may damage the casing string and the adjacent cement [4]. In situ stresses in the reservoir and, especially, around injectors may decrease because of the temperature reduction when a cold fluid is injected into the reservoir. This may happen on large scale during water flooding.

Five types of mechanical failure of annular cement are possible [5, 6]:

- debonding at the casing-cement interface;
- debonding at the cement-rock interface;
- radial fractures in cement;
- shear failure of cement;
- disking of the cement sheath.

The type of failure is controlled by the absolute and relative magnitudes of the principal stresses in cement. In the case of a circular wellbore and centered casing, these principal stresses are the *radial stress*, the *hoop stress* (also known as the *circumferential stress*), and the *axial stress*. The axial stress is directed along the wellbore axis. The directions of the other two principal stresses are shown in Fig. 5.1, for the most basic case of a circular wellbore and centered casing.
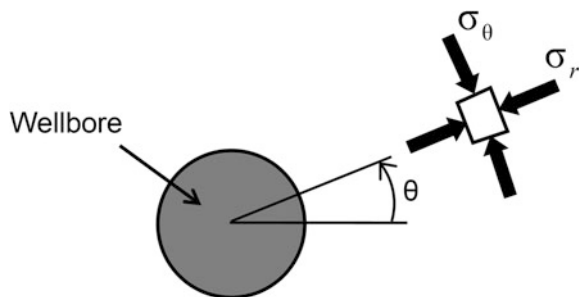
Debonding at the casing-cement interface occurs if the effective radial stress at the interface exceeds the tensile strength of the interface (the tensile bonding strength between steel and cement). This is schematically illustrated in Fig. 5.2.

Debonding at the cement-rock interface occurs if the effective radial stress at the interface exceeds the tensile strength of the interface (the tensile bonding strength between cement and rock). This is schematically illustrated in Fig. 5.3.

Both types of debonding may result in the development of a *microannulus* along the wellbore that may compromise zonal isolation.

Radial cracks in cement may appear if the effective hoop stress exceeds the tensile strength of cement (Fig. 5.4).
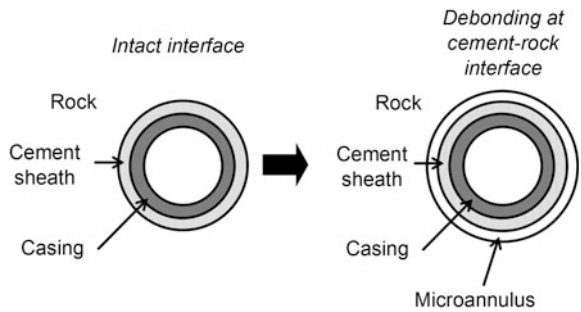

**Fig. 5.1** Orientation of radial stress, σ_r, and hoop stress, σ_θ, in the vicinity of the well

Fig. 5.2 Debonding at casing-cement interface (not to scale)

Intact interface

Debonding at casing-cement interface

Rock

Cement sheath

Casing

Rock

Cement sheath

Casing

Microannulus
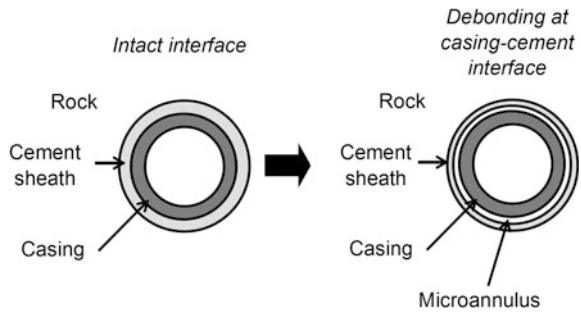
Fig. 5.3 Debonding at cement-rock interface (not to scale)

Intact interface

Debonding at cement-rock interface

Rock

Cement sheath

Casing

Rock

Cement sheath

Casing

Microannulus

Fig. 5.4 Radial fractures in cement sheath (schematic)

Rock

Cement sheath

Casing
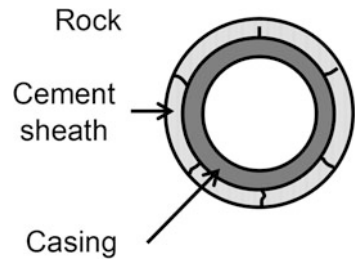
Shear failure of cement may develop if all the principal effective stresses are compressive and such that the shear strength of cement is exceeded. In theoretical analyses of cement failure, the Mohr-Coulomb failure criterion is often used to describe the shear strength, as discussed in Chap. 2. More complex failure criteria are available and have been used for well cement [5].

The last type of failure in the above list, i.e. the disking of the cement sheath, is a result of tensile effective stress acting along the wellbore axis.

In this and the next chapter, we shall take a closer look at what happens to stresses in cement during mechanical loading (variation of in situ stresses and casing pressure) and heating/cooling of the wellbore, and how these stress changes affect well integrity. Our primary focus will be on tensile failure of cement caused by tensile radial stress (Figs. 5.2 and 5.3) or tensile hoop stress (Fig. 5.4).

5.1 Initial Stresses in Annular Cement

Numerical calculation of stresses caused by casing pressure changes, thermal cycles, or in situ stress alteration requires that the initial stresses in annular cement are known. *Initial stresses* here mean the stresses that exist in cement right after it has hardened [7]. Although it might, in theory, be possible to measure these stresses (e.g. by installing pressure sensors in cement before it hardens), usually this is not done, and some assumptions about the initial stress values must be made in numerical models.

In a liquid cement slurry, the stresses are close to isotropic and are determined by the hydrostatic pressure of the cement column in the annulus (plus whatever is above that column). As the slurry sets, it may lose some water into the porous rock. Cement contraction may also be facilitated by cement shrinkage caused by hydration. As a result of cement contraction, the cement column tends to move downwards, which creates shear stresses between cement and the walls exposed in the annulus, i.e. the formation face and the casing outer surface. At the same time, the cement develops shear strength. The shear strength counteracts the downward movement of the cement column. The shear strength thereby reduces the hydrostatic pressure, as if the slurry were hanging on the walls exposed in the annulus (Fig. 5.5). In particular, if the yield stress (gel strength) of cement, τ_Y, were uniform along the entire height of the annular cement column, the bottomhole pressure in cement would be given by [8]

$$P_{\text{BHP}} = P_{\text{BHP},0} - \frac{2\tau_Y L}{R_w - R_c} \qquad (5.1)$$

where $P_{\text{BHP},0}$ is the initial bottomhole pressure right after the cement slurry has been placed in the annulus; P_{BHP} is the bottomhole pressure when the cement has built yield stress τ_Y; L is the length of the cemented interval; R_w and R_c are the radius of the wellbore and the outer radius of the casing, respectively.

In reality, the yield stress (gel strength) of cement does not change uniformly along the entire cemented interval since it is affected by pressure, temperature, and shear rate in different parts of the well. More elaborate models are available in the

Fig. 5.5 Reduction in the hydrostatic pressure in the cement sheath caused by shear strength development during solidification
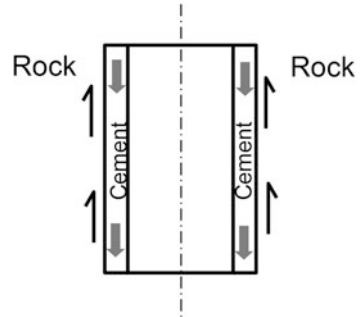
literature to predict the reduction in the bottomhole pressure due to the build-up of the yield stress (e.g. [9]).

As a result of this build-up, the vertical stress in the cement column at the bottomhole gradually decreases during setting. An additional reduction in the cement pressure can be due to the water disappearing from cement into the formation (fluid loss) during cement setting. This fluid loss may also cause a reduction in the pore pressure in set (and solidified) cement [8, 9]. Reductions in hydrostatic pressure in cement slurry and in the pore pressure in set cement are amongst the factors usually held responsible for gas influx from formation into the annulus during well cementing, the phenomenon known as *gas migration*.

The explanation of the hydrostatic pressure decrease in cement during setting laid out above is a brief summary of the current views on the subject [7–11]. Even this brief and qualitative exposition demonstrates how complex the issue of initial stresses in cement is. The initial stresses in cement are likely to depend not only on the properties of cement (rheology, strength build-up, fluid loss, expansion/contraction, capillary entry pressure, etc.) but also on the formation properties along the cemented section (formation permeability, formation temperature) [10, 12]. As pointed out by Chenevert and Jin, in order to minimize the pressure reduction during cement setting, it is necessary to minimize shrinkage and fluid loss into the formation [8].

Therefore, the evolution of the hoop stress, σ_θ, and the radial stress, σ_r, during setting is far from clear. It depends, in particular, on the properties of cement (density, rheology, fluid loss, expansion/contraction, etc.) and the properties of the formation (permeability). For instance, an expanding cement might develop significant compressive stresses in the radial and circumferential directions during setting since the formation and the casing represent constraints that reduce expansion. If, on the other hand, cement shrinks during setting, compressive stresses might not build up to the same extent.

The type of cement affects its strength, too, and, consequently, the effect the same stress magnitudes may have in a particular cement. In this and the next chapter, we will focus mostly on tensile stresses and tensile failure of cement, caused by the radial stress or the hoop stress. If the radial stress becomes tensile and in excess of the tensile strength of the interface between casing and cement or cement and formation, it may lead to debonding at those interfaces. If the hoop stress becomes tensile and in excess of the tensile strength of cement, it may induce radial cracks in cement. Both types of tensile failure will affect the permeability of cement in the direction along the well. In particular, if tensile fractures create a continuous flow path, the well integrity may be jeopardized. The elevated permeability of the near-well zone may persist even after the loads (mechanical or thermal) that caused it have been removed.

Tensile failure of cement is most relevant when the initial stresses in cement are low or zero. If these stresses are high and compressive, shear failure is likely to be the dominant failure mode when casing pressure or temperature is changed [13]. This underlines the essential role that initial stresses play in cement failure.

At present, there seems to be no consensus in the industry about the magnitude of the initial stresses in cement. Different modelers base their simulations on different assumptions. For instance, Gray et al. assumed that cement is in a hydrostatic compressive state of stress after hardening [14]. As a consequence, Gray et al. set the principal initial stresses equal to the hydrostatic pressure in the slurry column. Bosma et al. followed a different approach. Namely, they considered three types of cement: shrinking, zero-shrinkage, and expanding. They argued that the initial stresses in a shrinking cement could be set equal to zero; the initial stresses in a zero-shrinkage cement could be set equal to the hydrostatic pressure of the slurry; and the initial stresses in expanding cement could be set to the hydrostatic pressure plus some expansion-induced extra stress [13].

We will focus in this chapter mostly on tensile failure of cement since it is this failure that creates tensile fractures and interface discontinuities that can significantly increase the permeability along the well and thereby compromise zonal isolation. Since the initial stresses in cement are in practice unknown, it only makes sense to discuss *stress variations* caused, e.g., by temperature variation in the wellbore by 1 °C, or by in situ stress variation in the reservoir by 1 MPa, or by casing pressure variation by 1 MPa. We will follow this approach in this and the next chapter.

5.2   Effect of Casing Pressure Increase on Annular Cement

Casing pressure can increase during the following operations:

- well perforation;
- hydraulic fracturing;
- formation integrity test;
- casing pressure test;
- injection of fluids (water, steam, etc.) in oil and gas reservoirs;
- injection in gas storage wells.

Expansion of the casing caused by the casing pressure increase tends to expand the surrounding cement and rock. As a result, the hoop stress in cement and rock will become less compressive (i.e. more tensile), while the radial stress will become more compressive. We shall now study numerically how casing expansion affects the hoop stress in cement when the well is drilled in rock formations of different stiffness (Young's modulus). The properties of cement and casing are the same in all simulations discussed in this chapter. The properties of all the materials are given in Table 5.1. Three types of rock are considered: "soft rock" (with Young's modulus lower than that of cement), "medium-stiff rock" (with Young's modulus equal to that of cement), and "hard rock" (with Young's modulus higher than that of cement). From practical applications' point of view, the "medium rock" and the "hard rock" cases are the most interesting ones since, with modern well cement formulations, hardened cement is often softer than rock [10].

Table 5.1 Material properties used in the simulations

Property	Casing steel	Cement	Soft rock	Medium rock	Hard rock
Young's modulus (GPa)	200	10	1	10	100
Poisson's ratio	0.22	0.2	0.2	0.2	0.2

Fig. 5.6 Geometry of the model used in simulations of casing pressure effect on stresses in cement
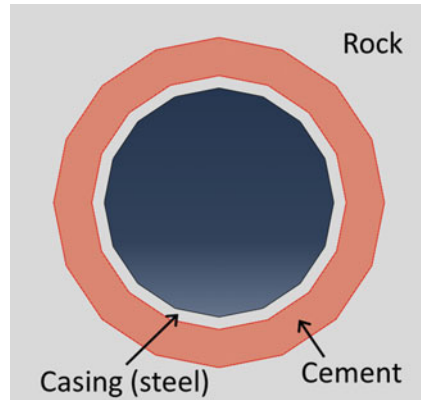
The geometry of the finite-element model is shown in Fig. 5.6. The model is 2D and has the size of 10 m × 10 m (only the near-well area is shown in Fig. 5.6). The wellbore has the diameter of 31.7 cm. The inner and outer diameters of the casing are 22.0 and 24.4 cm, respectively. The casing is assumed to be perfectly centered in the wellbore (standoff 100 %). Plane strain conditions are assumed, as it is frequently done in finite-element simulation of wellbore stability and annular-cement integrity (e.g. [15, 16]).

The results of the simulations are summarized in Table 5.2. These results suggest that the rock stiffness has significant effect on the stress variation in cement

Table 5.2 Simulation results: reduction in compressive hoop stress in cement per 1 MPa increase of the casing pressure

Formation stiffness	Reduction in compressive hoop stress (MPa) in cement caused by 1 MPa increase in the casing pressure	
	Near casing-cement interface	Near cement-rock interface
Soft (rock has Young's modulus 10 times lower than the cement does)	0.33	0.26
Medium-stiff (rock has the same Young's modulus as the cement does)	0.24	0.16
Hard (rock has Young's modulus 10 times higher than the cement does)	0.05	0.04

Positive figures mean decrease, the hoop stress becoming less compressive

caused by casing pressurization. In particular, the stiffer the rock, the less likely it is that the cement will experience tensile hoop stress during casing pressurization. If, however, the rock is sufficiently soft, and the initial stresses in cement are sufficiently low, the casing pressure increase may produce tensile hoop stress in cement sufficient to create tensile radial fractures [15]. For instance, in our example with the rock being 10 times softer than cement, an increase of casing pressure by 10 MPa would result in the hoop stress reduction in cement by 3.3 MPa near the casing-cement interface. If the initial hoop stress in the set cement was zero, this will result in the hoop stress becoming tensile and equal to 3.3 MPa upon casing pressurization. Such tensile stress may well be in excess of the tensile strength of a flexible or expanding cement, or even a neat cement.

The rock stiffness around the well may be substantially reduced if the rock has undergone plastic deformation upon drilling. In this case, the effective rock stiffness may be much lower than the Young's modulus of the undamaged rock. Subsequently, rock plasticity will further contribute to increase the tensile hoop stress in the cement sheath caused by casing pressurization.

The effect of rock stiffness on the development of tensile hoop stress in cement is intuitively clear. Indeed, the stiffer the rock is, the less the cement expansion will be as the casing expands and pushes the cement sheath outwards and against the rock. Less radial expansion means lower tensile hoop stress in cement.

The effect of rock stiffness on microcrack formation in well cement was investigated experimentally by Boukheilifa et al. [17]. The confining effect of the rock was modelled by using metal rings of different stiffness around the cement sheath. The experiments demonstrated that higher stiffness of the surrounding ring acted to suppress the development of microcracks in cement. This is consistent with the simulation findings presented in Table 5.2.

If the initial stresses in cement are compressive, the hoop stress changes in cement caused by casing pressurization might not be sufficient to make the stresses tensile. This underlines the importance of knowing the initial stresses in cement for meaningful predictions of its structural stability during the well life. The results described above suggest that it is advantageous to use expanding cements, so that tensile hoop stresses are not produced during casing pressurization. It should, however, be noted that such cements might have lower tensile (and compressive) strength. Therefore, if tensile stresses *are* produced, such cement might break easier.

5.3 Effect of Casing Pressure Decrease on Annular Cement

Casing pressure can decrease e.g. during hydrocarbon production from the reservoir, when the bottomhole pressure drops from the initial pore pressure to the production pressure. Another example of casing pressure decrease is found in gas storage wells where it is part of the well operation cycle.

Table 5.3 Simulation results: reduction in compressive radial stress in cement per 1 MPa decrease of the casing pressure

Formation stiffness	Reduction in compressive radial stress (MPa) in cement caused by 1 MPa decrease in the casing pressure	
	Near casing-cement interface	Near cement-rock interface
Soft (rock has Young's modulus 10 times lower than the cement does)	0.10	0.03
Medium-stiff (rock has the same Young's modulus as the cement does)	0.24	0.16
Hard (rock has Young's modulus 10 times higher than the cement does)	0.49	0.40

Positive figures mean decrease, the radial stress becoming less compressive

When the casing contracts, the surrounding cement and rock will tend to move radially towards the well axis. As a result, the hoop stress in cement and rock will become more compressive, while the radial stress will become less compressive, i.e. more tensile. We shall now investigate numerically how casing contraction affects the radial stress in cement when the well is drilled in rock formations of different stiffness (Young's modulus). The material properties used in the simulations are shown in Table 5.1. The geometry of the finite-element model near the well is shown in Fig. 5.6. The model is 2D and has the size of 10 m × 10 m. The wellbore has the diameter of 31.7 cm. The inner and outer diameters of the casing are 22.0 and 24.4 cm, respectively.

The results of the simulations are summarized in Table 5.3. It is evident from Table 5.3 that the radial-stress change is greater at the casing-cement interface than it is at the cement-rock interface. It is also evident that this change is greater in cement set against a stiffer rock (see also Ref. [5]). This is intuitively clear: a stiffer rock counteracts the "pulling" effect that the contracting casing has on cement. As a result, cement becomes more stretched in the radial direction, thus higher tensile radial stresses can be produced. Whether or not tensile radial stresses indeed occur during casing contraction, depends on the initial state of stress of cement. If the initial radial stress was zero, a decrease in the casing pressure by 10 MPa will produce a tensile radial stress of 2.4 MPa at the casing-cement interface, in the medium-stiff formation (Young's modulus of rock 10 GPa and equal to that of cement). Such tensile stress is likely to cause debonding between cement and casing. If, on the other hand, the initial radial stress in cement was higher than 2.4 MPa, no tensile stresses will be produced in the same scenario. In any event, as Table 5.3 indicates, the risk of debonding caused by casing pressure decrease is higher in a stiffer formation. Another factor affecting debonding and pointed out e.g. by Gray et al. is the compressive strength of the formation: If the compressive strength of the rock is lower, the rock may deform plastically, and the radial displacements may thus be accommodated without debonding at the casing-cement interface [14].

The stiffness of cement itself is of importance, too. In particular, as pointed out by Bois et al. [5], more flexible (i.e. less stiff) cement develops lower tensile stresses during casing depressurization.

Consequences of having tensile stresses at the casing-cement or cement-rock interfaces for well integrity will ultimately depend on the tensile strength of the interface. As discussed in Chap. 2, while the shear strength of interfaces between cement and materials such as steel or rock is routinely measured in the so-called push-out test, there prevails significant uncertainty about the magnitude of the interface tensile strength.

5.4   Effect of an Uncemented Channel on Stresses in Annular Cement Caused by Casing Pressure Changes

As discussed in Chap. 3, uncemented channels are sometimes left in cement after a cement job. During subsequent life of the well, such channels may serve as stress concentrators, i.e. they amplify the stress variations that otherwise would occur in the intact cement [16, 18, 19].

Let us have a look at how large the effect of such a channel might be in practice. To this end, we set up a simulation of a cased and cemented well in which part of the cement has been removed. The so obtained channel is filled with gas having negligible bulk modulus compared to the surrounding cement (Fig. 5.7). The diameter of the channel is equal to 1.2 cm. The other dimensions in the model are the same as in the previous simulations in this chapter. The channel runs along the well (the direction normal to page in Fig. 5.7). Only one simulation, with the rock's Young's modulus equal to 10 GPa, is performed to investigate the effect of the channel. This corresponds to the rock designated as "medium-stiff" earlier in this chapter.
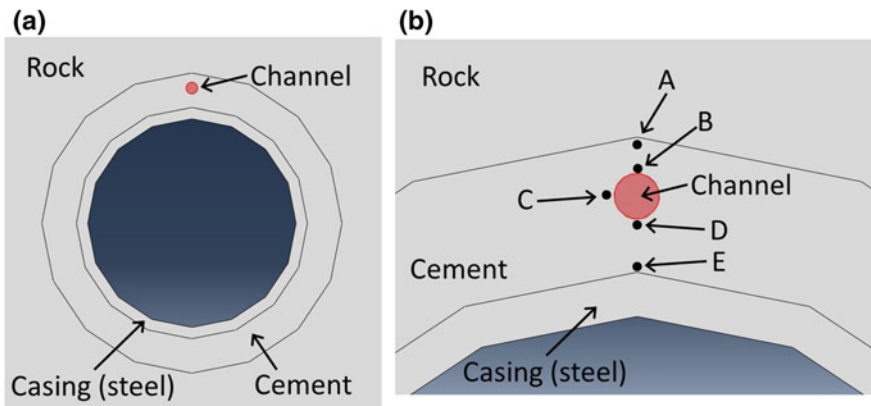

Fig. 5.7 Geometry of a cased and cemented well with a void channel *left* in cement

Table 5.4 Simulation results: changes of hoop stress and radial stress around the channel in cement per 1 MPa variation in the casing pressure

Location (cf. Fig. 5.2)	Change of compressive stress (MPa) caused by 1 MPa increase in the casing pressure		Change of compressive stress (MPa) caused by 1 MPa decrease in the casing pressure	
	Hoop stress	Radial stress	Hoop stress	Radial stress
A	+0.16	(−0.02)	(−0.16)	+0.02
B	**+0.45**	+0.07	(−0.45)	(−0.07)
C	(−0.02)	(−0.41)	0.02	**+0.41**
D	**+0.45**	+0.02	(−0.45)	(−0.02)
E	+0.25	−0.1	(−0.25)	+0.1

Positive figures mean decrease, the stresses becoming less compressive. Negative figures mean increase, the stresses becoming more compressive

The results are shown in Table 5.4. It is evident from Table 5.4 that *the channel amplifies the stress variation caused by casing expansion/contraction*. In particular, the reduction in the hoop stress at locations B and D near the channel caused by a 1-MPa casing pressure increase are much higher than the increase of the hoop stress anywhere in cement without the channel, under the same loading conditions (0.45 MPa in Table 5.4 vs. 0.16–0.24 MPa in Table 5.2). The reduction in the radial stress at location C caused by a 1-MPa casing pressure decrease are much higher than the reduction of the radial stress anywhere in cement without the channel, under the same loading conditions (0.41 MPa in Table 5.4 vs. 0.16–0.24 MPa in Table 5.3).

The results presented in Table 5.4 suggest that channels, bubbles, and other types of voids left in cement may represent a serious problem in terms of cement integrity. The size of the stress alteration zone around such a defect increases with the defect's size and will be larger for a large uncemented channel than for a small bubble.

Amplified tensile hoop stress at locations B and D in Fig. 5.7 may lead to a radial crack nucleation from the channel during casing pressurization. Such a crack may then propagate through the cement, creating a communication pathway between the formation and the casing. This will compromise one of the functions of annular cement, i.e. insulation of the casing from aggressive formation fluids.

5.5 Effect of Formation Stress Changes on Annular Cement

In situ stresses in the reservoir and the cap rock are not constant and may change during production and injection. In particular, total in situ stresses in the reservoir somewhat decrease during production [1, 2, 20]. In this section, we shall see how

Table 5.5 Simulation results: changes of compressive stresses in cement per 1 MPa decrease of in situ stresses normal to the wellbore axis

Formation stiffness	Change of compressive stress (MPa) in cement caused by 1 MPa decrease in the casing pressure			
	Near casing-cement interface		Near cement-rock interface	
	Hoop stress	Radial stress	Hoop stress	Radial stress
Soft (rock has Young's modulus 10 times lower than the cement does)	1.2	1.6	1.3	1.5
Medium-stiff (rock has the same Young's modulus as the cement does)	0.82	1.4	0.9	1.1
Hard (rock has Young's modulus 10 times higher than the cement does)	0.22	0.3	0.22	0.3

Positive figures mean decrease, the stresses becoming less compressive. Negative figures mean increase, the stresses becoming more compressive

reduction in the in situ stresses normal to the wellbore axis affects stresses in the cement. The geometry of the problem is the same as was used earlier (Fig. 5.6). In the finite-element simulations presented in this section, the casing pressure is held constant, while the far-field in situ stresses applied at the outer boundaries of the model (not shown in Fig. 5.6) are decreased, i.e. they become less compressive. Both principal in situ stresses normal to the wellbore axis are decreased by the same amount.

The results are summarized in Table 5.5. It is evident from Table 5.5 that both hoop stress and radial stress in cement become less compressive as the in situ stresses decrease. Moreover, this effect is stronger in softer rock formations. In a stiffer formation, the cement is shielded by the stiffer rock from the in situ stress changes. This phenomenon is usually referred to as *arching effect*. In an infinitely stiff rock, changes of the in situ far-field stresses would have no influence on the stress state in the annular cement.

5.6   From Stresses to Well Integrity: Microannulus, Cracks, and Permeability Hysteresis

If the effective radial stress at the cement-casing or cement-rock interface exceeds the tensile strength of the interface, debonding will occur. The two material surfaces then become separated from each other, and a gap is introduced between them. Likewise, if the effective hoop stress exceeds the tensile strength of cement, a radial crack (or cracks) will appear. The extent to which debonding or radial cracks affect well integrity depends on several factors. In particular, a thoroughgoing crack or

debonding developing along a substantial length of the well will have more detrimental effect than a small localized defect of the same type. The permeability of a thoroughgoing crack or debonding is determined by their aperture, i.e. the distance between the crack faces or between the cement-casing or cement-rock surfaces separated by debonding. It is difficult to quantify the effect of debonding on the permeability along the well because of the heterogeneity of materials such as rocks and cement which affects the aperture of the defects. In addition, the aperture between the debonded interfaces is not constant even at a given location along the well. Anisotropy of in situ stresses leads to the aperture being smaller at the locations along the wellbore circumference where the maximum in situ stress normal to well is perpendicular to the interface (Fig. 5.8) [14].
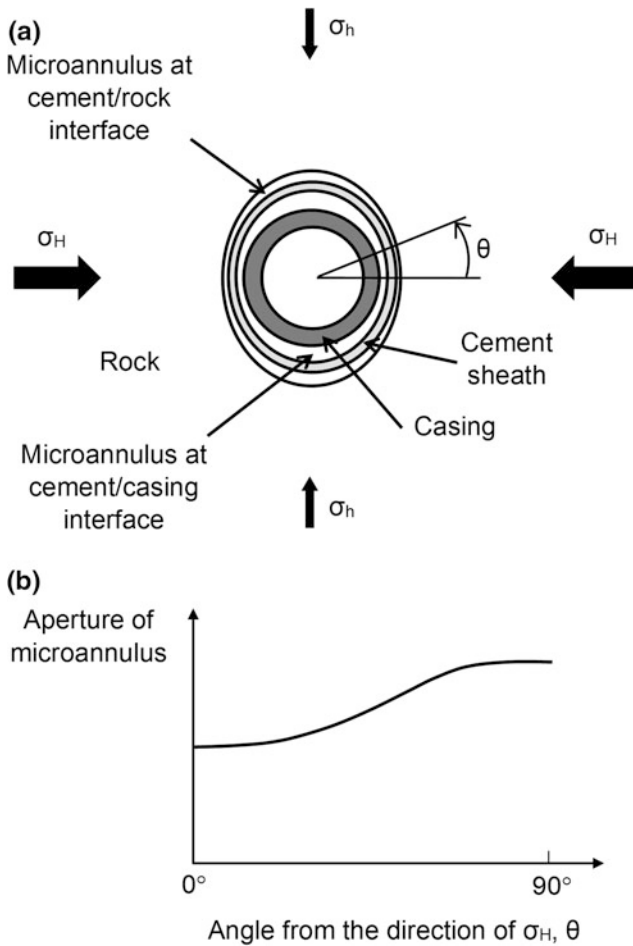
Fig. 5.8 Effect of in situ stress anisotropy on the aperture of microannuli around a vertical well. σ_H and σ_h are the maximum and minimum *horizontal* in situ stresses, respectively. Based on the simulation results by Gray et al. [14]

Fig. 5.9 Hysteresis of
microannular permeability
due to mismatch of the faces
caused by asperities and by
shear displacement between
casing and cement in casing
contraction/expansion cycles
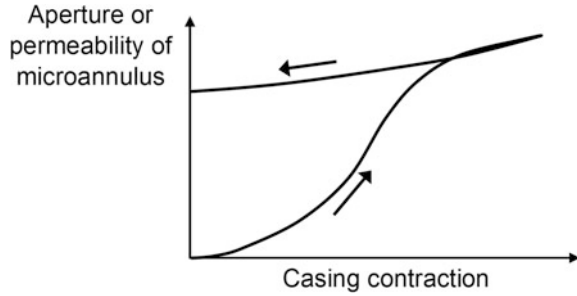
A well may experience a complex history of mechanical and thermal loading
during its lifetime. As a result, a microannulus, once created, may persist even after
its original cause has been removed. Consider, for instance, a microannulus
between casing and cement created by casing pressure reduction. The surfaces
exposed in such a microannulus may have some roughness (asperities) since the
fracture making the microannulus rarely creates a clean, smooth separation of
cement from steel (cf. interfacial transition zone, Chap. 4). Originally the asperities
on the opposite sides of the microannulus are matching. However, if afterwards
there is a shear displacement between casing and cement, the asperities on the two
faces will be displaced relatively to each other. As a result, if the casing pressure is
then restored, the microannulus will not be able to close. Therefore, the perme-
ability of the microannulus might not return to its original value after the casing
pressure is restored (Fig. 5.9). This type of hysteresis is well known in natural
fractures (see e.g. [3] and references therein), and has also been experimentally
observed in cement during repeated loading/unloading of laboratory models of
cemented wells [17].

The complexity of microannulus development and the uncertainties about the
major factors involved make it inherently difficult to predict numerically the per-
meability created by debonding. The same argument applies to the annular per-
meability caused by radial cracks. To complicate things even further, the
propagation of radial cracks along the well is facilitated if cement-rock or
casing-cement interfaces are debonded [15]. Other factors affecting propagation of
radial cracks along the wellbore include the Young's modulus and the Poisson's
ratio of cement: Cements with lower Young's modulus and higher Poisson's ratio
are more resistant against propagation of radial cracks along the well [10].

5.7   Summary and Discussion

Simulations presented in this chapter are intended to give some qualitative ideas
about the effect of casing pressure variation and in situ stress alterations on cement
integrity. In particular, we chose to focus on tensile failure only. In reality, cement can
break also in compression, if the shear stresses generated in cement become

sufficiently high (cf. the Mohr-Coulomb failure criterion discussed in Chap. 2). Moreover, poroelastic effects in cement and rock were neglected in all calculations presented in this chapter. Poroelastic change of pore pressure caused by a total stress change may, in reality, affect the change of the effective stresses in cement [5].

For instance, during casing expansion caused by an increase in the casing pressure, the pore pressure in cement will increase. This will make the effective hoop stress even less compressive (i.e. even more tensile) than it otherwise would be. Since, in a poroelastic material like cement it is the effective rather than total stress that effects failure, the poroelastic effects will in this case act so as to facilitate the development of radial cracks in cement.

On the other hand, during casing contraction caused by a reduction in the casing pressure, the pore pressure in cement will drop, and this will mitigate the reduction in the compressive effective radial stress that would be observed otherwise. This will mitigate the development of failure in form of debonding.

Depending on the loading rate, i.e. the speed of casing pressure increase/decrease in our case, the poroelastic effects may be more pronounced (rapid loading, close to undrained regime) or less pronounced (slow loading, close to drained regime). The analyses presented in this chapter can be considered as a limiting case of very slow load application, whereby the pore pressure does not change (or, more precisely, any change of the pore pressure is dissipated by pore pressure diffusion). This is known as *drained regime*.

A more elaborate approach to evaluating the initial stresses in cement involves using poromechanics, as exemplified by the work of Saint-Marc et al. [7].

In addition to poroelastic effects, two major uncertainties will always affect numerical evaluation of stresses and failure in annular cement:

- unknown initial stresses in cement;
- unknown tensile strength of cement-steel and cement-rock interfaces.

The first of these two uncertainties will persist unless some stress sensors are installed in cement before hardening, and the readings from these sensors are used as initial conditions in numerical models. Alternatively, advanced poromechanical models can be used to evaluate the initial stresses in the cement sheath numerically, provided that the required cement and formation properties downhole are available [21–23].

The second of the uncertainties requires that reliable techniques for measuring the tensile strength of cement-steel and cement-rock interfaces in laboratory or in the field be developed and used in the industry.

We have seen throughout this chapter that, in many cases, it is beneficial to have cement formulations that result in lower Young's modulus and higher tensile strength of cement upon hardening. Unfortunately, these two requirements are often mutually exclusive: softer cements are often weaker than their stiffer counterparts. This conundrum partially explains why new well cement formulations are introduced to the market every year.

In summary, the factors affecting cement failure caused by casing pressure changes and in situ stress variations are as follows:

- elastic properties of cement;
- elastic properties of the rock
- tensile and compressive strengths of cement;
- cement-rock and casing-cement bond strengths;
- cement shrinkage;
- initial stresses in the cement sheath;
- channels and voids left in cement;

In particular, the initial stresses in the cement affect the failure mode: tensile failure is more likely in cements with low or zero initial stresses, while compressive (shear) failure is more likely if the initial stresses were sufficiently high (and compressive). This suggests that too much of expansion may be just as bad as shrinkage: excessive expansion creates elevated initial compressive stresses that may bring the cement closer to the failure envelope and thus facilitate shear failure during the subsequent life of the well [13].

In laboratory setups used to study the effect of thermal stresses on annular cement (e.g. [24]), the model boundaries are often stress-free during thermal cycling. Even though, in reality, rocks are subject to in situ stresses even in the initial state, the annular cement might be almost stress-free initially, if the cement did not expand sufficiently to generate initial stresses. Thus, a stress-free laboratory setup might still be relevant for modelling what is happening in cement during temperature changes. Thermal stresses in cement induced by heating or cooling of the casing string are the main focus of the next chapter.

References

1. Fjær E, Holt RM, Horsrud P, Raaen AM, Risnes R (2008) Petroleum related rock mechanics, 2nd edn. Elsevier, Amsterdam
2. Lavrov A (2016) Dynamics of Stresses and Fractures in Reservoir and Cap Rock under Production and Injection. Energy Procedia 86:381–390
3. Holt RM, Gheibi S, Lavrov A (2016) Where does the stress path lead? Irreversibility and hysteresis in reservoir geomechanics. In: Paper ARMA 16–496 presented at the 50th US rock mechanics/geomechanics symposium held in Houston, Texas, USA, 26–29 June 2016
4. Dusseault MB, Bruno MS, Barrera J (2001) Casing shear: causes, cases, cures. SPE Drill Completion 16(2):98–107
5. Bois A-P, Garnier A, Rodot F, Saint-Marc J, Aimard N (2011) How to prevent loss of zonal isolation through a comprehensive analysis of microannulus formation. SPE Drill Completion 26(1):13–31
6. Shadravan A, Schubert J, Amani M, Teodoriu C (2015) Using fatigue-failure envelope for cement-sheath-integrity evaluation. SPE Drill Completion 30(1):68–75
7. Saint-Marc J, Garnier A, Bois A-P (2008) Initial state of stress: the key to achieving long-term cement-sheath integrity. In: SPE paper 116651 presented at the 2008 SPE annual technical conference and exhibition held in Denver, Colorado, USA, 21–24 Sept

8. Chenevert ME, Jin L (1989) Model for predicting wellbore pressures in cement columns. In: SPE paper 19521 presented at the 64th annual technical conference and exhibition of the society of petroleum engineers held in San Antonio, TX, 8–11 Oct 1989

9. Prohaska M, Ogbe DO, Economides MJ (1993) Dtermining wellbore pressures in cement slurry columns. In: SPE paper 26070 presented at the western regional meeting held in Anchorage, Alaska, USA, 26–28 May 1993

10. Zhou D, Wojtanowicz AK (2000) New model of pressure reduction to annulus during primary cementing. In: IADC/SPE paper 59137 presented at the 2000 IADC/SPE drilling conference held in New Orleans, Louisiana, 23–25 Feb 2000

11. Chenevert ME, Shrestha BK (1991) Chemical shrinkage properties of oilfield cements. SPE Drill Eng 6(1):37–43

12. Backe KP, Lile OB, Lyomov SK, Elvebakk H, Skalle P (1999) Characterizing curing-cement slurries by permeability, tensile strength, and shrinkage. SPE Drill Completion 14(3):162–167

13. Bosma M, Ravi K, van Driel W, Schreppers GJ (1999) Design approach to sealant selection for the life of the well. In: SPE paper 56536 presented at the 1999 SPE annual technical conference and exhibition held in Houston, Texas, 3–6 Oct 1999

14. Gray KE, Podnos E, B E (2009) Finite-element studies of near-wellbore region during cementing operations: Part I. SPE Drill Completion 24(1):127–136

15. Wang Z, Lou Y, Suo Z (2016) Crack tunneling in cement sheath of hydrocarbon well. J Appl Mech 83(1)

16. Pattillo PD, Kristiansen TG (2002) Analysis of horizontal casing integrity in the Valhall field. SPE/ISRM paper 78204 presented at the SPE/ISRM rock mechanics conference held in Irving, Texas, 20–23 Oct 2002

17. Boukhelifa L, Moroni N, James SG, Le Roy-Delage S, Thiercelin MJ, Lemaire G (2005) Evaluation of cement systems for oil and gas well zonal isolation in a full-scale annular geometry. SPE Drill Completion 20(1):44–53

18. Lavrov A, Todorovic J, Torsæter M (2016) Impact of voids on mechanical stability of well cement. Energy Procedia 86:401–410

19. Lavrov A, Torsæter M (2016) Effect of rheology on annular sealing: from placement to failure. In: SPE paper 180028 presented at the SPE bergen one day seminar held in Bergen, Norway, 20 April 2016

20. Zoback MD (2007) Reservoir geomechanics. Cambridge University Press, Cambridge

21. Bois A-P, Vu M-H, Ghabezloo S, Sulem J, Garnier A, Laudet J-B (2013) Cement sheath integrity for CO_2 Storage—An integrated perspective. Energy Procedia 37:5628–5641

22. Ghabezloo S (2010) Association of macroscopic laboratory testing and micromechanics modelling for the evaluation of the poroelastic parameters of a hardened cement paste. Cem Concr Res 40(8):1197–1210

23. Ghabezloo S (2011) Micromechanics analysis of thermal expansion and thermal pressurization of a hardened cement paste. Cem Concr Res 41(5):520–532

24. Todorovic J, Gawel K, Lavrov A, Torsæter M (2016) Integrity of downscaled well models subject to cooling. In: SPE paper 180025 presented at the SPE Bergen one day seminar held in Bergen, Norway, 20 April 2016

Chapter 6
Thermal Stresses in Annular Cement

Abstract Heating of casing, e.g. by the drilling fluid returning to surface, expands the casing string. This results in the hoop stress in the cement sheath becoming less compressive (more tensile). Similarly, cooling of casing, e.g. by injecting cold water down the well, makes the casing contract. This results in the radial stress in cement sheath becoming less compressive (more tensile). These stress changes may induce radial cracks or debonding at cement-casing and cement-rock interfaces. Finite-element simulations are performed in order to estimate the magnitude of the stress variations in cement sheath caused by the temperature variation at the inner side of the casing. Simulations are performed for different combinations of thermal expansion coefficients of cement, steel, and rock. It is shown that, at least in some cases, it is beneficial to have cement formulations that result in lower Young's modulus and higher tensile strength of cement upon hardening. The role of initial stresses in cement sheath for practical evaluation of cement sheath stability during wellbore heating/cooling is discussed.

Keywords Cement · Stress · Temperature · Thermal stresses · Radial fracture · Crack · Fracture · Debonding · Tensile strength

Expansion and contraction of casing can be caused not only by casing pressure variations (Chap. 5), but also by temperature changes in the well. This is particularly relevant for the following types of wells:

- high-pressure, high-temperature (HPHT) wells;
- steam injection wells;
- geothermal wells;
- CO_2-injection wells.

As the temperature of the casing changes, the casing expands (when temperature increases) or contracts (when temperature decreases). Inevitably, these mechanical deformations will affect the near-well area and, in the first instance, the annular cement. Furthermore, as the temperature change propagates into the cement and the rock, these materials might expand or contract, too. The thermal stresses produced as

a result of such contraction or expansion will be determined by the relationship between coefficients of thermal expansion and elastic properties of casing, cement and rock. Similarly to the stresses and failure caused by casing pressure changes considered in Chap. 5, the eventual effect of thermal stresses depends on the initial stresses in cement. If significant compressive initial stresses are induced in the cement sheath during hardening (e.g. an expanding cement), the predominant mode of failure during subsequent thermal loading may be compressive (shear). If the initial stresses are not very high or are zero, tensile cracks and debonding may occur. Similarly to the previous chapter, we will focus in this chapter mostly on tensile failure of cement since it is this failure that creates tensile fractures and interface discontinuities that can significantly increase the permeability along the well. Tensile failure implies that the initial compressive stresses in cement were not very high, so that the stress increments caused by heating or cooling can result in tensile effective stresses in cement. Tensile radial stresses would then induce debonding, while tensile hoop stresses would induce radial cracks. Both these types of failure may jeopardize the well integrity if they propagate over a large distance along the well.

6.1   Effect of Casing Temperature Increase on Well Cement

In this chapter, we shall look into the effects that casing heating and casing cooling have on stresses in cement and, thus, on cement failure and debonding. Since the initial state of stress in cement is, in most cases, unknown (see Sect. 5.1), we will follow the same approach as in Chap. 5 by looking only at the variation of cement stresses per 1 °C variation in the casing temperature.

   The magnitudes of thermal stresses in cement (as well as in rock) depend largely on the absolute and relative magnitudes of elastic properties and thermal expansion coefficients of the materials, i.e. cement, rock, and casing, as well as on the magnitude of temperature variation in the well. We will assume in this chapter that the Young's modulus of cement is lower than the Young's modulus of the rock. This assumption is relevant for some popular well cement formulations currently used in the industry [1, 2]. When it comes to the relative values of the thermal expansion coefficient, there is more uncertainty. In total, six types of combinations are possible, as exemplified in Table 6.1. We shall study the effect of heating and cooling on thermal stresses for each of these combinations. The remaining thermal and mechanical properties are listed in Table 6.2. The simulations will be plane strain 2D, as in Chap. 5. We will use both transient and steady state models. The steady state, in this case, is a limit case of a transient model, whereby the time is so large that there are no more temperature changes in the system.

Table 6.1 Combinations of thermal expansion coefficients used in the simulations

Combination ID	Thermal expansion coefficient of steel (casing) (10^{-6}/K)	Thermal expansion coefficient of cement (10^{-6}/K)	Thermal expansion coefficient of rock (10^{-6}/K)
A	10	12	14
B	10	14	12
C	12	10	14
D	12	14	10
E	14	10	12
F	14	12	10

Table 6.2 Material properties used in the simulations

Property	Steel	Cement	Rock
Young's modulus (GPa)	200	5	20
Poisson's ratio	0.22	0.2	0.3
Specific heat capacity (J/(kg K))	500	1500	1000
Thermal conductivity (W/(m K))	15	1	1
Density (kg/m^3)	8000	2000	2100

The outer dimensions of the model are the same as in Chap. 5, i.e. 10 m × 10 m. The wellbore has the diameter of 31.7 cm. The inner and outer diameters of the casing are 22 and 24.4 cm, respectively. The effect of different combinations of the thermal expansion coefficient will be studied with a smooth-walled wellbore. The casing is assumed to be perfectly centered in the wellbore (standoff 100 %) in these simulations.

The outer boundary of the model is maintained at a constant (far-field) temperature. The temperature of the inner surface of the casing is increased by 1 °C instantaneously at the initial moment and is then kept constant.

The results of the simulations with casing heated by 1 °C are summed up in Table 6.3. Stress values at two locations in cement are reported in Table 6.3: near the cement-casing interface and near the cement-rock interface. Two stresses are monitored at each location: the radial stress and the hoop stress. Positive figures entering the Table signify that the respective stress becomes more tensile during heating.

It is evident from Table 6.3 that, with the chosen combinations of elastic and thermal properties, both hoop stresses and radial stresses in cement become more compressive as the casing is heated. In particular, the radial stress always becomes more compressive. The reason for this is that the rock is stiffer than the cement. Thus, the cement sheath is effectively pressed against the stiffer rock by the expanding casing (which is stiffer than both cement and rock). Thus, debonding cannot happen in any of the models A through F under heating, given the combinations of properties listed in Tables 6.1 and 6.2.

Table 6.3 Results of simulations with casing heating

Combination of thermal expansion coefficients (Ref. Table 6.1)	Time	Change of compressive σ_r in cement near cement-casing interface (MPa)	Change of compressive σ_θ in cement near cement-casing interface (MPa)	Change of compressive σ_r in cement near cement-rock interface (MPa)	Change of compressive σ_θ in cement near cement-rock interface (MPa)
A	6 min	(−0.076)	(−0.027)	(−0.063)	**0.003**
	1 h	(−0.089)	(−0.050)	(−0.079)	(−0.027)
	∞ (steady state)	(−0.078)	(−0.050)	(−0.073)	(−0.051)
B	6 min	(−0.062)	(−0.036)	(−0.064)	**0.003**
	1 h	(−0.073)	(−0.062)	(−0.083)	(−0.032)
	∞ (steady state)	(−0.084)	(−0.065)	(−0.081)	(−0.064)
C	6 min	(−0.088)	(−0.015)	(−0.072)	**0.005**
	1 h	(−0.101)	(−0.033)	(−0.088)	(−0.019)
	∞ (steady state)	(−0.089)	(−0.032)	(−0.079)	(−0.038)
D	6 min	(−0.091)	(−0.031)	(−0.075)	**0.005**
	1 h	(−0.106)	(−0.057)	(−0.095)	(−0.031)
	∞ (steady state)	(−0.102)	(−0.062)	(−0.095)	(−0.064)
E	6 min	(−0.102)	(−0.011)	(−0.083)	**0.066**
	1 h	(−0.085)	(−0.028)	(−0.099)	(−0.018)
	∞ (steady state)	(−0.107)	(−0.028)	(−0.093)	(−0.038)
F	6 min	(−0.104)	(−0.019)	(−0.084)	**0.006**
	1 h	(−0.119)	(−0.041)	(−0.102)	(−0.024)
	∞ (steady state)	(−0.113)	(−0.043)	(−0.101)	(−0.051)

Positive entries mean that the stress becomes less compressive (more tensile), which may lead to tensile failure of cement. Negative entries mean that the stress becomes more compressive

The hoop stress in cement near the cement-rock boundary becomes more tensile at the very beginning of heating, but then becomes more compressive as the temperature front propagates into the near-well area. This behavior has been previously noticed in numerical simulations by Thiercelin et al. [3]. They pointed out that, with a stiffer cement, higher tensile hoop stress (more exactly, its increment with regard to the initial hoop stress) is generated at the cement-rock boundary than with a softer cement. It also takes longer time for this tensile stress increment to become compressive. This is schematically illustrated in Fig. 6.1. The difference between stiffer and softer cements is evident from Fig. 6.1. This difference is another reason why softer cements are preferred in wells, in addition to their better performance under casing pressure changes discussed in Chap. 5.
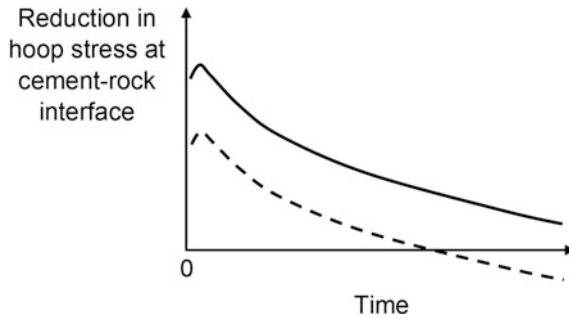
Fig. 6.1 Reduction in compressive hoop stress in cement near cement-rock interface for cements with different Young's modulus. *Solid line* stiffer cement. *Dashed line* softer cement. The Young's modulus of the rock is the same in both cases. Positive values of reduction mean that the hoop stress becomes more tensile

One interesting observation from Table 6.3 is the remarkably large tensile stress at the cement-rock interface obtained with material combination E: The hoop stress reduction after 6 min is an order of magnitude larger in case E than in the other five simulations. This result is consistent with the material properties used in simulation E. The thermal expansion coefficient of cement is in this case lower than those of steel and rock. As a result, cement expands less than the other two materials. The adjacent casing thus tends to stretch the cement sheath in the circumferential direction, thereby reducing the compressive stress in cement and possibly inducing tension.

With our choice of material properties, case E is the only one where realistic temperature increments may lead to tensile cracks in cement. For instance, heating by 100 °C will in case E reduce the compressive hoop stress near the cement-rock interface by 6.6 MPa which, if the initial hoop stress was close to zero, may fracture cement. Other cases (A to D and F) will experience a reduction in the compressive hoop stress by less than 1 MPa under 100 °C heating.

As mentioned previously, we focus on tensile failure in this study. However, the data shown in Table 6.3 suggest that compressive failure of cement under heating cannot be excluded if the initial stresses in cement were sufficiently high (and compressive). It is evident from Table 6.3 that an increase of casing temperature by 100 °C will result in the increase of the compressive radial stress in cement by *ca.* 10 MPa in many cases. The hoop stress increases less. If the initial stresses in cement were close to zero, such an increase in compressive stresses is unlikely to induce failure. If, however, the initial stresses were already high (e.g. in an expanding cement), and the cement thus was close to shear failure, the moderate increase of the radial stress might be sufficient to trigger such failure.[1]

---

[1]Provided that the internal friction coefficient of cement is low, and thus the strengthening effect of increasing σ_θ is small.

6.2   Effect of Casing Temperature Decrease on Well Cement

Cooling results in both radial stress and hoop stress becoming less compressive (Table 6.4). Particularly the radial stress reduction is significant: not only is it greater than the corresponding reduction in the hoop stress in all simulations, but the tensile strengths of cement interfaces with rock and casing are most likely lower than the tensile strength of the bulk cement itself. Thus, for instance, cooling the casing by 40 °C in case D will reduce the compressive radial stress by 4 MPa. If the initial radial stress was close to zero, this reduction will most probably be sufficient to break the cement-casing bonding in the well.

Table 6.4   Results of simulations with casing cooling

Combination of thermal expansion coefficients (Ref. Table 6.1)	Time	Change of compressive σ_r in cement near cement-casing interface (MPa)	Change of compressive σ_θ in cement near cement-casing interface (MPa)	Change of compressive σ_r in cement near cement-rock interface (MPa)	Change of compressive σ_θ in cement near cement-rock interface (MPa)
A	6 min	**0.076**	**0.027**	**0.063**	(−0.003)
	1 h	**0.089**	**0.050**	**0.079**	**0.027**
	∞ (steady state)	**0.078**	**0.050**	**0.073**	**0.051**
B	6 min	**0.062**	**0.036**	**0.064**	(−0.003)
	1 h	**0.073**	**0.062**	**0.083**	**0.032**
	∞ (steady state)	**0.084**	**0.065**	**0.081**	**0.064**
C	6 min	**0.088**	**0.015**	**0.072**	(−0.005)
	1 h	**0.101**	**0.033**	**0.088**	**0.019**
	∞ (steady state)	**0.089**	**0.032**	**0.079**	**0.038**
D	6 min	**0.091**	**0.031**	**0.075**	(−0.005)
	1 h	**0.106**	**0.057**	**0.095**	**0.031**
	∞ (steady state)	**0.102**	**0.062**	**0.095**	**0.064**
E	6 min	**0.102**	**0.011**	**0.083**	(−0.066)
	1 h	**0.085**	**0.028**	**0.099**	**0.018**
	∞ (steady state)	**0.107**	**0.028**	**0.093**	**0.038**
F	6 min	**0.104**	**0.019**	**0.084**	(−0.006)
	1 h	**0.119**	**0.041**	**0.102**	**0.024**
	∞ (steady state)	**0.113**	**0.043**	**0.101**	**0.051**

Positive entries mean that the stress becomes less compressive (more tensile), which may lead to tensile failure of cement. Negative entries mean that the stress becomes more compressive

The maximum reductions in the radial stress are observed in cases E and F, i.e. when the thermal expansion coefficient of casing is larger than those of cement and rock. This is understandable since steel is much stiffer than cement and rock. Thus, if the casing contracts more than cement and rock do, it will tend to pull the cement inwards, thereby creating tensile stresses at the casing-cement and cement-rock interfaces.

6.3   Effect of Eccentric Casing Positioning

We saw in Chap. 3 that eccentric casing position, i.e. standoff less than 100 %, has a detrimental effect on mud displacement during primary cementing. The negative consequences of eccentric casing do not end there. During subsequent life of the well, eccentric casing will affect the stress distribution in cement, even if no mud channels or other types of voids have been left in the annulus.

In order to demonstrate how eccentric casing positioning affects tensile stresses in cement, the simulation A from Table 6.4 is rerun, now with the casing shifted by 2 cm to the left (Fig. 6.2). The standoff is thus equal to 55 %. Only a transient simulation is performed, with the casing cooled by 1 °C at time zero.

The stresses are monitored near the casing-cement interface, at two points, L and R, located opposite to each other (Fig. 6.2). The cement sheath is thinnest at location L and thickest at location R. The results are summarized in Table 6.5.

It is evident from Table 6.5 that, given the values of cement and rock properties used in this simulation, the thermal-induced stress reduction is larger where the cement is thinner. Thus, cooling-induced tensile failure in form of debonding or radial cracking of cement is more likely on the thinner side of the cement sheath. On the other hand, the difference, even with the standoff 55 %, is not that large: the values of the radial stress change are only approximately 10 % larger on the thinner side than on the thicker side of the sheath. Given the notoriously large variability of

Fig. 6.2 Model with eccentric casing positioning. Stresses are monitored near the casing-cement interface at locations *L* and *R*
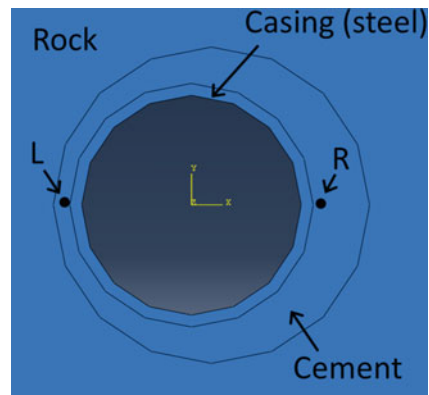
Table 6.5 Results of transient simulation of casing cooling by 1 °C with eccentric casing (standoff 55 %)

Location in Fig. 6.2	Monitored quantity	After 6 min	After 1 h
L (thinnest cement)	Change of compressive radial stress, σ_r (MPa)	0.084	0.095
	Change of compressive hoop stress, σ_θ (MPa)	0.039	0.056
R (thickest cement)	Change of compressive radial stress, σ_r (MPa)	0.072	0.085
	Change of compressive hoop stress, σ_θ (MPa)	0.032	0.049

Material properties are the same as in simulation A (Table 6.1). Positive entries mean that the stress becomes less compressive (more tensile), which may lead to tensile failure of cement

material properties in casing-cement-rock systems, it is not certain that a 10 % difference between stress increments would necessarily result in a preferential failure of the cement sheath at its thinner side.

6.4 Summary and Discussion

The factors affecting cement failure caused by temperature changes in the well may be summarized as follows:

- coefficients of thermal expansion of cement and rock;
- thermal properties of cement and rock;
- elastic properties of cement and rock;
- tensile and compressive strengths of cement;
- cement-rock and casing-cement bond strengths;
- cement shrinkage during setting;
- initial stresses in the cement sheath;
- channels and voids left in cement.

In particular, the initial stresses in cement affect the failure mode: tensile failure is more likely in cement sheaths with low or zero initial stresses, while compressive (shear) failure is more likely if the initial stresses were sufficiently high (and compressive).

Cement is a porous material. Poromechanical effects were neglected in this chapter. More advanced models, based on the theory of thermo-poroelasticity are available and have been used to study thermal effects in cement [4].

We have seen throughout this chapter that, at least in some cases, it is beneficial to have cement formulations that result in lower Young's modulus and higher tensile strength of cement upon hardening. Unfortunately, these two requirements are often mutually exclusive: softer cements are often weaker than their stiffer counterparts. This conundrum partially explains why new well cement formulations are introduced to the market every year.

We have seen in this and the preceding three chapters that considerable progress has been made in the studies of annular cement placement and its behavior during the subsequent well life. Despite this progress, some knowledge gaps and unresolved problems persist. Moreover, new challenges in primary well cementing keep emerging as more difficult wells (e.g., HPHT and deepwater wells) are drilled. This trend will continue in the future. In the next chapter, we will take a closer look at the most important challenges within physics and mechanics of primary well cementing.

References

1. Dusseault MB, Gray MN, Nawrocki PA (2000) Why oilwells leak: cement behavior and long-term consequences. In: SPE paper 64733 presented at the SPE international oil and gas conference and exhibition in China held in Beijing, China, 7–10 Nov 2000
2. Wang Z, Lou Y, Suo Z (2016) Crack tunneling in cement sheath of hydrocarbon well. J Appl Mech 83(1)
3. Thiercelin MJ, Dargaud B, Baret JF, Rodriguez WJ (1998) Cement design based on cement mechanical response. SPE Drill Completion 13(4):266–273
4. Ghabezloo S, Sulem J, Saint-Marc J (2009) The effect of undrained heating on a fluid-saturated hardened cement paste. Cem Concr Res 39(1):54–64

Chapter 7
Knowledge Gaps and Outstanding Issues

Abstract Despite substantial progress made in research and development of cement formulations, preflush engineering, cementing technologies, and numerical modelling over the past decades, several knowledge gaps and unresolved problems still exist. These problems are likely to persist in the future as more complicated cementing conditions are encountered, e.g. in deepwater wells, HPHT wells, geothermal wells, and during underground CO_2 storage. New challenges are due either to harsh downhole conditions (e.g. HPHT) or more stringent environmental and safety regulations (e.g. geothermal and CO_2 wells). Challenges are found in the design, where perfect mud displacement and cement placement are still rare. Numerical models used to design cementing jobs are still often either too complicated (i.e. too slow) or inaccurate. Uncertainties about the formation properties (permeability, temperature, etc) and about the behavior of cement at downhole conditions reduce the practical value of even the most promising models. Despite these knowledge gaps, continuous progress over the past decades suggests that, in the years to come, the technology of primary cementing will continue to improve, based on our steadily improving knowledge of its physics and mechanics.

Even though cementing of the annulus has been used for decades, there are still many issues that make a perfect cement job all but impossible. As the depths increase and well trajectories become more complicated, the solutions that have been found viable in vertical wells stop working. Other complications are due to high pressures and high temperatures (HPHT conditions). In particular, primary cementing of HPHT wells is exacerbated by several factors such as:

- narrow pressure window (the difference between the lost-circulation pressure and the pore pressure);
- incompatibility of oil-base or synthetic-base muds, used in HPHT wells, with cement;
- the dependence of rheological properties on downhole pressures and temperatures;

A. Lavrov and M. Torsæter, *Physics and Mechanics of Primary Well Cementing*,
SpringerBriefs in Petroleum Geoscience & Engineering,
DOI 10.1007/978-3-319-43165-9_7

- the extended distance the fluid train must travel down the pipe (thereby increasing the risk of fluid mixing).

Other challenging cementing operations are found in geothermal wells, where high temperatures and pressures and safety policies call for longer cemented intervals and more demanding requirements with regard to cement behavior and properties. CO_2 injection wells used for carbon storage are another example of a technology where well integrity is essential and is determined by the quality of the annular cement sheath, amongst other factors.

Several unresolved and unexplored issues pertain to mud displacement, even in conventional wells in the oil and gas industry. In particular, as noted by Kelessidis et al. [1], experimental data on flow of yield-stress fluids in concentric and eccentric annular geometries are scarce, and so are the data on transition to turbulence for such fluids. Several different criteria for laminar-to-turbulent transition of yield-stress fluids have been proposed over the past two decades, and there are often discrepancies between the criteria. This makes design and optimization of primary well cementing even a greater challenge than it otherwise would be. Other outstanding problems in placement design include the following:

- modeling of the effects of casing movement on the annular flow;
- modeling of chemical interactions during displacement;
- incorporation of mud thixotropy in the flow models;
- mechanisms of mud-cake and solids-bed erosion in turbulent flow (shear stresses as compared to pressure fluctuations);
- numerical models of mud-cake and solids-bed erosion both in turbulent and in laminar flow;
- proper account for instabilities and possible mixing of fluids during their downward journey inside the pipe [2];
- flow instabilities in the annulus [3].

An inherent difficulty in modeling mud displacement and cement placement in the annulus is due to the multiscale nature of the problem. Namely, the dimension along the wellbore is about four orders of magnitude greater than the size of the annular gap. This impedes the development and application of three-dimensional models, while the computationally less demanding 2D models suffer from low accuracy and from not being able to capture the essential physics.

Predictions delivered even by the most accurate and sophisticated numerical models of well cementing are only as good as the input data are. The properties of mud, preflushes, and cement depend on pressure and temperature. Therefore, they are, in general, different at the downhole conditions from those measured at laboratory pressure and temperature. Systematic use of realistic P,T-conditions in laboratory tests may significantly improve the predictive capabilities of the models. An example is the use of a high-temperature spacer surfactant screening test to evaluate the water-wetting capacity of spacers at downhole temperatures and pressures, i.e. up to 400 °F (204 °C) and 3,000 psi (20.7 MPa) [4].

Experimental validation of numerical models of mud displacement under realistic P,T-conditions and flow regimes is often lacking. This reduces the applicability and value of the models.

The performance of solid cement during the life of the well, e.g. under casing pressurization/depressurization cycles or during wellbore heating/cooling, is currently not completely understood either. In particular, as pointed out by Bois et al. [5], currently used theoretical models cannot always explain the results of laboratory experiments. The problem of modelling well integrity is exacerbated by frequently insufficient information about the properties of cement and rocks downhole.

Despite the knowledge gaps and unresolved issues discussed above, significant (and steady) progress has been made in primary well cementing over the last decades. This development suggests that, in the years to come, the technology of primary cementing will continue to improve, based on our steadily improving grasp of its physics and mechanics.

References

1. Kelessidis VC, Dalamarinis P, Maglione R (2011) Experimental study and predictions of pressure losses of fluids modeled as Herschel-Bulkley in concentric and eccentric annuli in laminar, transitional and turbulent flows. J Petrol Sci Eng 77(3–4):305–312
2. Khalilova P, Koons B, Woody D, Eihancha A (2013) Newtonian fluid in cementing operations in deepwater wells: friend or foe? In: SPE paper 166456 presented at the SPE annual technical conference and exhibition held in New Orleans, Louisiana, USA, 30 Sept–2 Oct
3. Nelson E, Guillot D (2006) Well cementing, 2nd edn. Schlumberger, Sugar Land, Texas
4. Shadravan A, Narvaez G, Alegria A, carman P, Perez C, Erger P (2015) Engineering the mud-spacer-cement rheological hierarchy improves wellbore integrity. In: SPE paper 173534 presented at the SPE E&P Health, safety, security and environmental conference-Americas held in Denver, Colorado, USA, 16–18 March 2015
5. Bois A-P, Garnier A, Rodot F, Saint-Marc J, Aimard N (2011) How to prevent loss of zonal isolation through a comprehensive analysis of microannulus formation. SPE Drill Completion 26(1):13–31

Index